A New Approach for Slope Stability Analysis

Combining the limit equilibirum method and finite element method

T.A. Nguyen

TU Delft

Deltares

Enabling Delta Life

A New Approach for Slope Stability Analysis

Combining the limit equilibrium method and finite element method

by

Thy Anh Nguyen

Student number:	4308239	
Project duration:	September, 2020 – July, 2021	
Thesis committee:	dr.ir. C. Zwanenburg	Deltares/TU Delft
	dr.ir. R. Lanzafame	TU Delft
	dr. P.J. Vardon	TU Delft
	dr.ir. J.A.M. Teunissen	Deltares

Picture cover page from fietzfotos, Albrecht Fietz

TU Delft Delft University of Technology

Deltares Enabling Delta Life

Executive Summary

To protect the Netherlands against flooding, approximately 3800 kilometres of primary flood protection structures, including dikes, dams and dunes, are built. There are multiple causes for these flood protections to fail, one of them being macro instability. High water levels or excessive rainfall can cause for the dikes to be unstable. Therefore different methods have been developed to assess the stability of dikes.

Two main approaches which have been applied to analyse slope stability are the Limit Equilibrium Method (LEM) and the Finite Element Method (FEM). The LEM uses a set of predefined slip surfaces to compare the available shear strength with the required shear strength, this ratio gives the factor of safety against sliding. The slip surface which gives the lowest safety factor is then chosen as the most critical one. There are various limit equilibrium, which all require the dike to be divided into slices, but have different assumptions on the forces between the slices. A finite element analysis can be used to model the soil behaviour of the dike and also assess its safety. This method gives a good representation of the stress distribution in the profile and does not assume a predefined failure surface. These are great advantages compared to the LEM. However, the method uses the shear strength reduction method (SSRM) to determine the safety factor. The SSRM simply decreases the strength parameters of the soil until failure occurs. Furthermore, the SSRM only gives the critical slip surface, the strength of other slip surfaces cannot be examined. Due to these drawbacks of the FEM a new method is introduced which combines concepts of both the LEM and FEM, namely the Enhanced Limit Method (ELM).

In this report a method is proposed to evaluate slope stability using the stress analysis from a finite element program and a safety factor definition based on the concepts of the limit equilibrium methods. The finite element program PLAXIS is used to obtain the stress distribution of the slope of interest. The genetic algorithm is implemented to search for the critical slip surface. This algorithm starts with creating a number of initial slip surfaces. Bounds should be given on the entry and exit point of the slip surface and the algorithm ensures that the created slip surfaces are kinematically accepted. The safety factor is defined as the ratio of the total maximum available shear strength along the slip surface to the total mobilised shear stress. With this definition the genetic algorithm is able to score the slip surfaces. Slip surfaces with a low safety factor are of interest for the optimisation process and will therefore get a high score. The algorithm uses a select number of the initial slip surfaces to produce new slip surfaces, called the offspring. With the crossover and mutation process, the proposed method is able to find slip surfaces which are more critical compared to the initial solutions. This optimisation process is performed a number of times and the final result is the critical slip surface.

The proposed method has proven to give reliable results compared to other analysis methods: LEM, FEM and other optimisation methods proposed in literature. Multiple case studies are performed in this research and the genetic algorithm is able to find a reasonable critical slip surface and safety factor in every example. However, the safety factor found by the algorithm is very dependent on the number of iterations in the optimisation process (the creation of an offspring population). Allowing the algorithm to run for an excessively long time (allowing for many iterations in the generation of new populations) ensures that the algorithm is able to find safety factors which are similar to the values obtained from the LEM and FEM analysis as well as the the methods proposed in literature.

The computation time of the genetic algorithm is heavily influenced by the genetic algorithm parameters: initial population size, selection size and the number of generations. The long computation time is the biggest drawback of the method. The advantages of the proposed method are its straightforwardness and adaptability. No use is made of doubtful methods such as the shear strength reduction technique, moreover, the method uses a well found stress distribution from the finite element analysis and the definition of the safety factor is very clear. Furthermore, the method requires bounds for the entry- and exit point of the slip surface, which ensures that only the slip surfaces of interest are considered. Different stress strain relationships can be used in the finite element analysis and different definitions of the maximum shear strength can be implemented, allowing for the method to investigate every soil type in all conditions.

Preface

This report marks the final chapter to obtain the degree Master of Science at Delft University of Technology and the end of my time as a student in Delft. My long time fascination with big (hydraulic) structures has caused me to start the bachelor Civil Engineering in Delft. However, being introduced to logistics and other mathematical problems have lead me to make a detour which entailed completing a second master at Erasmus University. But of course, my interest in the fascinating hydraulic structures had not faded and I still had to become an engineer, therefore this study has been performed for the faculty of Civil Engineering and Geosciences, Hydraulic Structures. Over the course of the last 9 months I have worked on the topic of slope stability assessment. In this project I got to combine two things that I enjoy: understanding the mechanical part of slope stability and implementing an optimisation algorithm.

Hereby I would like to thank all the supervisors that guided me through the process of this thesis with their feedback, expertise and enthusiasm. In the first place, I would like to thank my daily supervisors Hans and Cor. Their knowledge on the topic is incredible and our discussions throughout the project have forced me to find the challenges in the study and helped me find the solutions for these challenges. Cor has guided me through the completion of this thesis from the first day, also ensuring that I performed the work in a decent time frame. He always took time to read my preliminary reports and give detailed feedback. Hans has constantly motivated me to deeply understand the soil mechanics behind all my coding. Hans immediately recognised every paper that I have presented during our discussions and he could regularly recommend me other relevant works as well. In addition to this, I would like to express my gratitude Robert, who also gave me extensive feedback on my preliminary reports, including a proper check on my readability and writing, and was always up for a brainstorm session. Furthermore, I would like to thank Phil as the chair of the thesis committee. His comments and feedback were very to the point and helped me make concrete goals for every following meeting.

Even though I wasn't able to come to the office of Deltares, and the first meetings with some colleagues was online, I would also like to thanks those who took their time to help me in the process and explain me the the know-hows in their field of knowledge.

At last, I would like to thank my parents, sister and friends, who have always supported me, in not only this research time, but throughout my studies. To my parents, who have always supported my ambitions, even the prolongation of my student time by achieving a double master's degree. To my friends who have made my student time very enjoyable and memorable. Without you I would not have become the person I am today.

Thy Anh Nguyen
Delft, July 2021

Contents

List of Figures

List of Tables

Nomenclature

Abbreviations

CSSM	Critical State Soil Mechanics
ELM	Enhanced Limit Method
FEM	Finite Element Method
FoS	Factor of Safety
GA	Genetic Algorithm
LEM	Limit Equilibrium Method
MCC	Modified Cam-Clay
OCR	Overconsolidation Ratio
SSRM	Shear Strength Reduction Method

Symbols

γ	volumetric weight [kN/m^2]
κ	swelling index [-]
λ	isotropic logarithmic compression index [-]
ν	Poisson's ratio [-]
ϕ	friction angle [°]
σ	stress [kPa]
τ	shear stress [kPa]
θ	Lode's angle [°]
c	cohesion [kN/m^2]
E	elasticity modulus [kN/m^2]
e	void ratio
M	friction constant [-]
M	selection size in genetic algorithm
m	strength increase component
M_{init}	size of initial population in genetic algorithm
N	number of vertices in genetic algorithm
n_p	isotropic overconsolidation ratio [-]
OCR	overconsolidation ratio
p	mean stress [kPa]
p_i	initial mean effective stress [kN/m^2]
q	deviator stress [kPa]
r	pressure ratio [-]
S	normally consolidated undrained shear strength ratio [-]
v	specific volume

1 Introduction

1.1. Introduction to Flood Protection in the Netherlands

Two-thirds of the surface area of the Netherlands is at risk of flooding. These flood threats are due to the combination of the its low elevation and the large discharges in rivers. Needless to say that flood protection is an important issue for this country. It should not come as a surprise that the Dutch have become specialists in the development of water defences. Beaches and sand dunes absorb the forces of the rising sea water level, whilst dikes and levees keep the land dry that we are currently living on and so on.

Flood prone areas are protected by approximately 3800 kilometres of primary flood protection structures such as dikes, dams and dunes. The majority of these structures are managed by regional water authorities whilst the remainder is managed by the national water authority, Rijkswaterstaat. The protection against flooding is regulated by law in the Dutch Water Act, a law which specifies the standards for the safety of primary flood defences. Since the beginning of 2017, a new approach is used to determine the safety standards. Before 2017, the safety standards for primary flood defences were set as the probability of exceedance of a certain hydraulic load, which could be a high water level or wave. These standards are thus focused on overflow and overtopping of the flood defences. A maximum tolerated probability is still given in the new standards, however, this probability is not solely the probability of occurrence of overtopping or overflow, but is now defined as the probability of failure. The use of a failure probability allows for the inclusion of different failure mechanisms of a flood defence, not only overtopping or overflow. To determine the failure probability of the flood defences, guidelines have been developed by the government (Rijkswaterstaat [58]).

1.2. Introduction to Macro Stability of Dikes

As stated in the previous section, all flood defences have a maximum tolerated failure probability. There are multiple failure mechanisms which can cause dike failure. An overview of the most common failure mechanisms of dikes is given in Figure 1.1. The failure probability assessment should consider all relevant failure mechanisms.

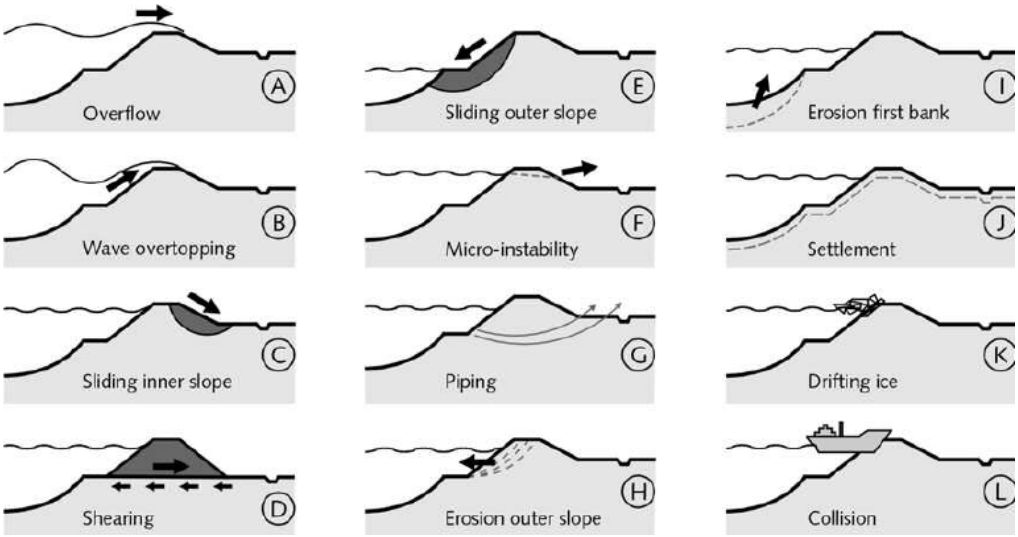

Figure 1.1: Important Failure Modes of Dikes (Schiereck [66])

In this research the failure mechanism 'sliding inner slope', also referred to as macrostability or slope stability, of flood defences will be investigated. However, the method is also applicable for other stability problems, such as the raising and levelling of structures or areas. An impression of an inner slope instability is shown in Figure 1.2. Sliding of the outer slope can also occur, although, this occurs due to a different mechanism and failure of the outer slope is less critical than inner slope instability. Sliding of the inner slope is also the most common failure mechanism that leads to breaching of dikes besides wave overtopping (Jonkman et al. [30]).

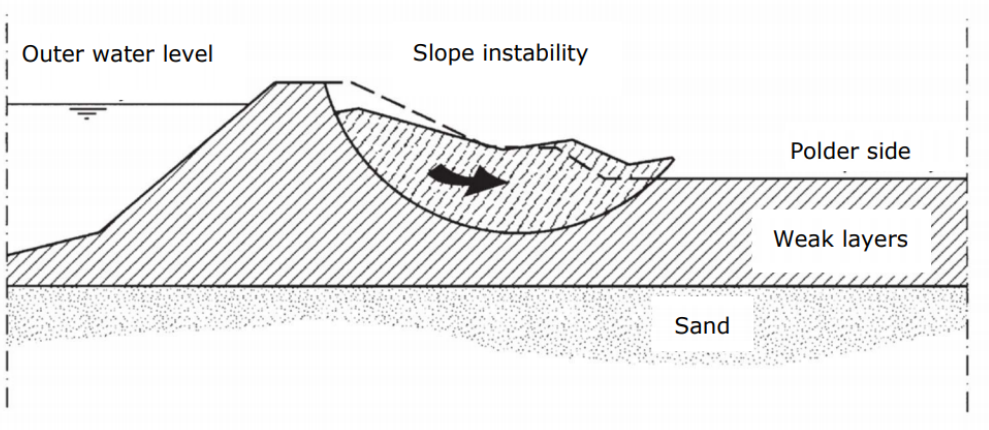

Figure 1.2: Macro-Instability (Rijkswaterstaat [58])

A brief description of this mechanism is given as follows: due to rainfall or water level rise on the outside of the dike, water infiltrates in the dike body, resulting in a saturated dike body and increasing pore pressures. The effective stresses reduce and therefore the shear strength of the soil reduces as well. During long-lasting floods, this can cause sliding planes in the slope. Sliding of the slope is generally an issue for river dikes, lake dikes and polder dikes, since the flood durations are long and the high water levels can reach the crest level. Nevertheless, sea dikes also have to meet safety standards against instability. There are mainly two approaches used to assess the stability of dikes, these approaches will discussed shortly in the next section and in more detail in the next chapter.

1.3. Problem Statement

Traditionally, slope stability is analysed with the Limit Equilibrium Method (LEM) in which a predefined slip circle is used to compare the available shear strength with the required shear strength. This gives a factor of safety for the slope against sliding. This analysis is performed on a bunch of predefined slip surfaces and the slip surface which gives the lowest safety factor is then chosen as the most critical solution. In general these type of methods require the soil mass to be divided into slices. For every slice the driving moment as well as the resisting moment is calculated. There are various limit equilibrium methods. Differences between these methods include the assumption on the forces between slices. These methods are widely used due to its simplicity, but have quite some drawbacks. One of those drawbacks are the strong simplifications of material behaviour, therefore the computed stress distributions are often unrealistic.

Alternatively, the Finite Element Method (FEM) can be used to model material behaviour and to determine the factor of safety. This method gives a good representation of the stresses in the soil and does not assume a predefined failure surface. These are great advantages compared to the limit equilibrium method. Nonetheless, the finite element method has one great disadvantage. This is the calculation of the safety factor with the Shear Strength Reduction Method (SSRM), also named the $\phi - c$ reduction method. This method does not make use of the advanced soil models, which can be present in the finite element program, to model the strength, but the shear strength strength parameters ϕ and c are simply reduced until the soil collapses. Another disadvantage of the SSRM is that only one critical slip surface is given, other slip surfaces cannot be examined with this method.

Both models, with their advantages and limitations, will be discussed in more detail in Sections 2.1 and 2.2.

1.4. Research Motivation

In the previous section two methods have shortly been described which can be used to analyse slope stability. Both the LEM and FEM have been applied in many case studies, which have shown the advantages and limitations. The finite element method has great advantages compared to traditional limit equilibrium methods. No assumptions are made on the shape or location of the failure surface and the computed stresses are closer to reality compared to the LEM. However, the shear strength reduction method is used to determine the safety factor and this method has quite some drawbacks. Soil models are highly nonlinear and the SSRM adjusts these soil parameters. The reduction of the strength parameters does not represent the real behaviour of the soil characteristics, since these do not have to decrease in an actual situation. Furthermore, even though the stress analysis has been performed using an advanced soil model, the SSRM does not take this model into account, but will reduce the strength of the soil by only adjusting the ϕ and c parameters of the material. Especially in an undrained analysis, the SSRM does not represent the undrained behaviour of the soil appropriately. Another disadvantage of the SSRM is that an irrelevant failure surface can be given, since only the slip surface is given with the lowest safety factor and other potential slip surfaces are not considered. In that case manual adjustments have to be made to the soil properties to acquire a relevant slip surface. However, these adjustments can influence the generation of the next slip surface again, which is undesirable.

Due to this limitation of the FEM, Deltares has initiated a new study that will develop a new approach which combines both methods; From the FEM the initial stress conditions are calculated and the safety factor is based on limit equilibrium concepts. The advantage of this new approach is that it makes use of the realistic initial stress conditions obtained from a finite element analysis and will therefore be more accurate than LEM. A safety factor definition based on limit equilibrium concepts is implemented, such that no use has to be made of the shear strength reduction method. This definition can be applied on any particular given slip surface. This approach is similar to the the Enhanced Limit Method (ELM), which will be discussed in the next chapter. The advantages of the proposed method will be elaborated on in the next chapter as well.

1.5. Research Goal

The goal of this research is to further develop the new approach to analyse slope stability as suggested by Deltares, such that a better understanding is gained on the process of slope (in)stability in soil dikes. The research objective is given as:

Improve the analysis of slope stability by developing a new method which combines concepts of both the Limit Equilibrium Method and Finite Element Method.

The following hypotheses are formulated which can be used to measure the objective:

The new approach is able to give a reasonable factor of safety in accordance with classical methods.

The new approach gives a better representation of the soil mechanics and is able to use non-linear assumptions to determine the (critical) soil strength and slip surface.

The new approach can be applied to different (complex) geometries to capture different loading conditions of embankments.

1.6. Research Framework and Supporting Research Questions

In this section the research framework is stated, which shows the steps to undertake to achieve the research goal. The steps for this research are based on the main research question, which is formulated as:

How can a new approach use both LEM and FEM concepts to analyse the stability of slopes?

The main research question is split up in sub-questions that should be answered to reach the research goal. These sub-questions also give a guide on the different processes which should be undertaken to answer the main research question. The sub-research questions are formulated as follows:

1. How should a stress analysis be performed by a finite element approach in PLAXIS?
   (a) Which soil models should be used in drained or undrained situations?
2. How can the critical slip surface be determined using the stress analysis obtained from the FEM?
   (a) What optimisation problems can be used to acquire the critical slip surface?
   (b) How is the critical soil strength determined?
   (c) Is it possible to determine the critical slip surface by implementing the stress analysis obtained with a FEM in a LEM program, such as D-Stability?
3. How is the performance of the new method compared to other, more classical, methods in analysing the slope stability?
   (a) On which grounds are differences found?

1.7. Research Strategy

The initial phase of the project can be seen as a qualitative study. In this phase information is gathered from experts at the Geo-engineering department of Deltares and from the literature study. This gives insight into the characteristics of both slope stability analysis methods that have been applied in research. This information is used in the second phase to develop the new approach which uses the stress distribution from a finite element method programme to calculate the critical slip surface. This new approach should be made independent of the used finite element program. To verify the new model, multiple case studies will be performed in which the results of the new approach will be compared to traditional methods.

1.8. Thesis Roadmap

The remainder of this thesis is as follows: Firstly, in Chapter 2 some theoretical background is given on the currently applied methods to assess slope stability, as well as on constitutive models to represent the behaviour of soil. Secondly, Chapter 3 elaborates on the new method which is implemented to answer the research question. This new method will be used to investigate different dike profiles and will be compared the more traditional methods, these results are given in Chapter 4. In Chapter 5 a sensitivity analysis is performed and the discussion is given in Chapter 6. Lastly, this research is wrapped up with a conclusion and recommendations, stated in Chapter 7.

2
Theoretical Background

In the introduction the motivation for this study has been explained. This motivation is based on the limitations of both the limit equilibrium and finite element method. Both methods will be discussed in more detail in this chapter, such that their limitations will also be featured. Furthermore, to apply a new method to determine the safety factor, the maximum available shear strength of the soil has to be defined. Different soil models are therefore discussed in this chapter as well, which can be used to determine the maximum shear strength of the soil in the slope.

2.1. Limit Equilibrium Methods

There are several methods to analyse slope stability published in literature. The stability of a slope is determined by the safety factor, which essentially is the ratio between the maximum available shear strength and the acting mobilised shear stress. Duncan [14] has given a detailed overview on equilibrium methods which are able to analyse slope stability. These methods in general compare the driving moments of a potential slip plane with the resisting moment. This gives the factor of safety. These methods require the soil mass to be divided into slices and the directions of the forces acting on each slice in the slope are assumed (Rabie [57]). Very importantly, the factor of safety is assumed to be constant along the complete slip surface. Failure is defined as the loads exceeding the maximum resistance for either vertical force, horizontal force or moment equilibrium for any potential sliding plane (Jonkman et al. [30]).

A limit equilibrium method can be used to determine the factor of safety of a predefined slip surface, this is only one part in the stability analysis. The second part consists of finding the slip surface which is the most critical. Search algorithms can be used to find the slip surface with the least safety (lowest factor of safety). One (very basic search) method is to calculate the safety factor for many (tens of thousands) slip surfaces to find the most critical one. Though with some ingenuity the search for the critical slip surface can be done much more efficient.

Fellenius [18] introduced the first limit equilibrium method, which is the Ordinary method, for a circular slip surface. Bishop [5] followed up on this version by introducing a new relationship for the base normal force. Therefore the equation for the factor of safety became non-linear. Janbu [28] developed a method for non-circular failure surfaces where the potential slip surface is divided into several vertical slices. The generalised procedure of slices is hereafter developed as an extension of the simplified method (Janbu [29]). Morgenstern and Price [50], Spencer [69] and Sarma [63] further developed the limit equilibrium methods by using different assumptions on the interslice forces. The General Limit Equilibrium method was developed by Chugh [12] as an extension on the Spencer and Morgenstern-Price methods, such that both moment and force equilibrium is satisfied. These are just some of the developed limit equilibrium methods.

There are quite some differences between the methods as mentioned above. These differences arise due to the assumptions made for the interslice normal (E) and shear (T) forces as well as the shape of the assumed slip surface. A summary of these assumptions is given in the following table.

Table 2.1: Summary of Different LEM (Aryal [1])

Methods	Circular	Non-cir.	$\sum M = 0$	$\sum F = 0$	Assumptions
Ordinary	⋆	–	⋆	–	Neglects both E and T
Bishop	⋆	–	⋆	–	Considers E, neglects T
Janbu simplified	⋆	⋆	–	⋆	Considers E, neglects T
Sarma	⋆	⋆	⋆	⋆	Interslice shear
Spencer	⋆	⋆	⋆	⋆	Constant inclination of slope of T
Morgenstern-Price	⋆	⋆	⋆	⋆	Slope of T is defined by $f(x)$

Some of the methods with their basic principles will be briefly described. The most applied method to analyse the slope stability is the Bishop method. Bishop [5] uses an assumed slip circle to check its moment equilibrium. The driving moment M_s is determined by the soil weight on the active side of the centre point. The resisting moment M_r consists of the soil weight on the land-side of the centre point as well as the shear capacity of the soil along the bottom of the sliding surface. The factor of safety is determined as the ratio of the two: $FoS = \frac{M_r}{M_s}$. Bishop's method also ensures that vertical equilibrium is met, meaning that the vertical forces between the slices are balanced.

In case the critical sliding surface is not circular shaped, Bishop's method fails to analyse this slip plane. This is typically the case in uplift conditions. This method is also unsuitable for non-horizontal soil layers or the inner toe of drainage ditches. In case of a long-lasting flood situation, the phreatic surface in the dike body rises. Water can infiltrate into the aquifer which results in increasing pore pressures, creating uplift pressure under the dike. This can result in a significant decrease of the effective stresses under the blanket, where a decrease to zero is also possible. This is called uplift, which results in zero shear stress capacity at the bottom of the blanket. These uplift conditions are shown in Figure 2.1. In this case the critical sliding surface is typically an elongated one, which covers the uplifted area.

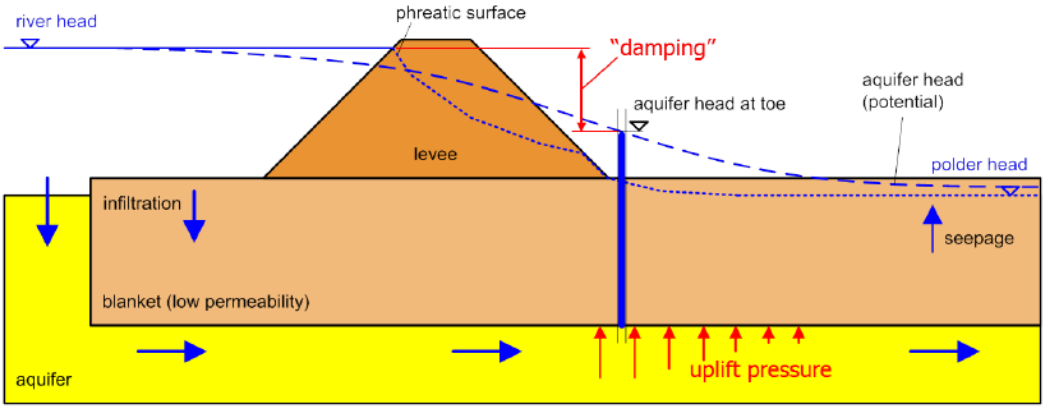

Figure 2.1: Uplift Conditions (Jonkman et al. [30])

For these conditions, the Uplift-Van model, as shown in Figure 2.2 was developed. Instead of a circular slip plane, the sliding surface consists of a horizontal plane with two circular parts on the active and passive side. The method becomes equal to Bishop's method if there is no horizontal part present and the radius of the active and passive circle are equal. To determine the stability of the slip plane, the Uplift-Van method determines the horizontal forces acting on the horizontal area between the active and passive circles. It divides the compressed area into slices and checks the horizontal forces transferred from the active to passive side. Since this method takes care of the horizontal force balance, also horizontal sliding planes can be analysed. For more detailed information on this method the reader is referred to Van [71].

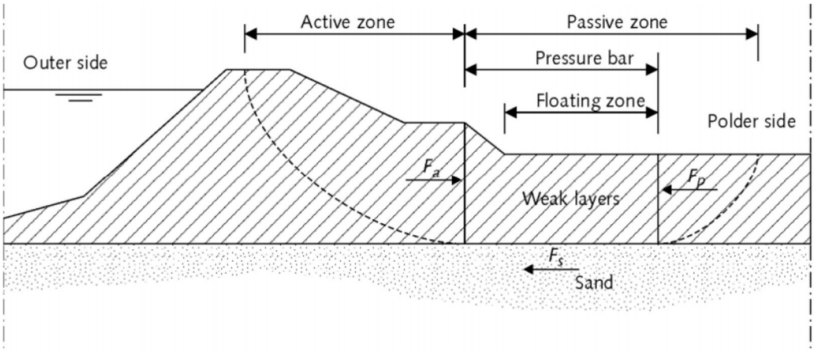

Figure 2.2: Uplift-Van Model (Rijkswaterstaat [58])

The last method which will be elaborated on is the method proposed by Spencer [69]. Spencer's method is not constrained to a circular plane and therefore any shape type can be analysed. Figure 2.3 shows a schematic representation of the model with piece-wise linear elements. Like Uplift-Van, Spencer's method also satisfies moment, horizontal and vertical equilibrium (Jonkman et al. [30]). Until recently, the use of this model was limited, because the search for the critical slip plane was difficult to work with. Both Bishop and Uplift-Van have the advantage that the critical slip plane could be found automated within pre-defined search grids. However, recently genetic algorithms have been able to find the critical slip plane within pre-defined bounds in Spencer's method.

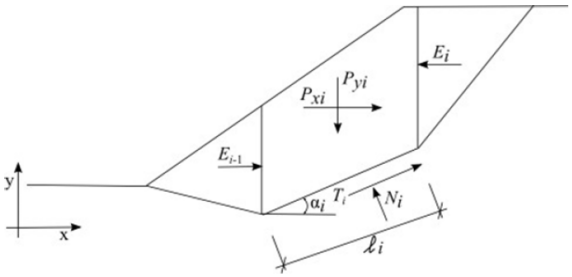

Figure 2.3: Spencer Model (Jonkman et al. [30])

In this section various limit equilibrium methods have been discussed. The limitations of the LEM have been demonstrated by Krahn [33] and are also discussed by Fredlund et al. [19]. The advantages and limitations of LEM are both summarised in Table 2.2.

Table 2.2: Summary LEM

Advantages	Limitations
Quick analysis	Assumption on location of critical slip surface
Most common method	Assumption that slip surface can be divided into slices
Relatively simple formulation	Assumption that FoS is the same for each slice
Can calculate the safety factor for every slip surface which is given	Works with static pore pressure field, deformation and groundwater flow are therefore not coupled
Minimal material input parameters required	Does not use the stress versus strain characteristics of the soils and therefore does not provide information on strains and deformations
Useful for evaluating sensitivity of failure to input parameters	Does not satisfy displacement compatibility. Computed stress distributions are often unrealistic
	Does not take slope history into account, nor initial state of stress before excavation or fill placement
	Finding lowest factor of safety can be challenging

2.2. Finite Element Methods

In the previous section various limit equilibrium methods have been discussed, including the limitations. If a stability analysis has to be performed, but these limitations pose a problem for the application of a LEM, numerical models such as a finite element method can provide an alternative. The most common reason for a LEM to be insufficient is when a correct display of the initial stresses is needed or if the stability of a slope in combination with a construction (such as a sheet pile) is examined.

There are multiple advantages to using the finite element method. FEM requires fewer a priori assumptions regarding the failure mechanism. Failure occurs at the zones in which the shear strength of the soil is insufficient to resist the shear stress, instead of at predefined slip planes. Therefore no assumption is needed on the shape or location of the critical failure surface. Secondly, since the soil mass is not divided into slices, there is no assumption on the direction of the forces in these slices. The method provides global equilibrium until failure is reached. Furthermore, if sufficient soil data is available, the finite element method can also provide information on deformations at working stress level. This method can easily be used to calculate stresses, movements, pore pressures in embankments and seepage, which is especially of importance in the safety assessment of a dike in combination with a construction. Lastly, the FEM is able to monitor progressive failure up to and including overall shear failure (Griffiths and Lane [24]).

To determine the slope stability using the finite element method, two approaches can be applied: the gravity increasing approach or the shear strength reduction method. The shear strength reduction method has been used as early as 1975 to analyse slope stability by Zienkiewicz et al. [78] and is applied in multiple case studies (Griffiths and Lane [24], Lane and Griffiths [42], Hammouri et al. [25], Rabie [57], Moni and Sazzad [49]). The SSRM reduces the strength characteristics of the soil mass until failure of the slope occurs. The critical slip surface will follow naturally from the analysis. The safety factor is defined as the number by which the original shear strength parameters are divided by in order to cause failure. When the standard Mohr-Coulomb criterion is used, the safety factor can be formalised as follows:

$$FoS = \frac{c - \sigma_n \tan\phi}{c_r - \sigma_n \tan\phi_r} \tag{2.1}$$

where c and ϕ are the actual input parameters and σ_n is the actual normal stress component. c_r and ϕ_r are the reduced strength parameters which just satisfy the strength equilibrium.

An advantage of the SSRM compared to the classical LEM is that the calculation of the safety factor is linear, since the stresses at the base of the slip surface are known from the stress analysis. In the LEM, starting with Bishop, an estimated factor of safety is used to compute the forces at the slices. The final safety factor of the critical slip surface is found through an iterative process. A disadvantage of the SSRM is that it does not make use of the more advanced soil models. These models can be used to attain the stresses in the dike profile and estimate the shear strength, but the safety factor is simply calculated by decreasing the strength parameters ϕ and c of the soil.

As mentioned before, many researchers have applied the LEM and FEM to analyse slope stability. Griffiths and Lane [24] have shown that FEM is a good alternative method to analyse slope stability, which is accurate and requires fewer assumptions compared to LEM. The safety factor is obtained naturally from the analysis without assuming a particular form of the failure mechanism a priori. Lane and Griffiths [42] assess the stability of slopes under different drawdown conditions with the FEM. The FEM is used to analyse critical cases of partial submergence and rapid drawdown, which traditional methods cannot produce. Hammouri et al. [25] use both a LEM and FEM to analyse (in)homogeneous slopes. The effects of rapid drawdown, undrained clay soils and crack locations were taken into consideration. The differences in the obtained safety factors were found to be small, whereas the critical slip surfaces found by both methods coincide. Due to the (small) differences in the safety factors obtained, the researchers recommend to use both methods to analyse critical slopes. Rabie [57] presents a comparison study between the LEM and FEM which analyses the stability of slopes under heavy rainfall. The main conclusion is that the classical methods are highly conservative compared to the FEM. Moni and Sazzad [49] analyse the stability of slopes with surcharge with both LEM and FEM. The effects of the mesh on the safety factor is investigated and they have stated that a finer mesh gives a more conservative result than a coarser mesh. In this analysis the factor of safety given by the Mohr-Coulomb model is lower than of Drucker-Prager, irrespective of the slope angle, type and position of the surcharge.

In this section the finite element method has been explained and various applications of this method to analyse slope stability have been presented. Overall can be said that the method is a promising alternative to the classical methods for analysing slopes. A summary of the advantages and limitations of the finite element method in combination with the shear strength reduction technique is given in Table 2.3.

Table 2.3: Summary FEM

Advantages	Limitations
No concept of slices needed	Deformation is limited to nodes in the mesh grid
No assumptions on shape or location of failure surface	Difficult to obtain good result for soft band with frictional soil input parameters
Displacement compatibility is satisfied	Difficulty with finding convergence as system approaches failure when nonlinear constitutive relationships are used to model displacement
Able to monitor progressive failure up to and including overall shear failure	Results SSRM sensitive to design of mesh and other input parameters
Computed stresses are closer to reality compared to LEM	SSRM calculates the safety factor by decreasing the strength, no use is made of the more advanced soil models in this calculation
If soil compressibility data is available, able to give information about deformations at working stress levels	SSRM only finds one critical solution, while other local minima may differ only slightly from the critical solution. The critical slip solution does not have to be the most dangerous one as well.

2.3. Enhanced Limit Method: Combination of LEM and FEM

As described in Sections 2.1 and 2.2 both the LEM and FEM have some limitations in their usage. Therefore a different method is proposed by Fredlund et al. [19], based on the work of Kulhawy [34], called the enhanced limit method. In Figure 2.4 the basic idea presented by Fredlund et al. [19] is shown. The first step in the enhanced limit method is to obtain the stresses from a single finite element analyses. These stresses are then used to calculate the safety factor of a predefined slip surface, as described by Kim and Lee [32] and Fredlund et al. [19]. The factor of safety of a slip surface can be defined as the resisting shear strength of the soil divided by the mobilised shear stresses. This way no use has to be made of the SSRM to acquire a safety factor. The second step is to search for the most critical slip surface using a search algorithm.

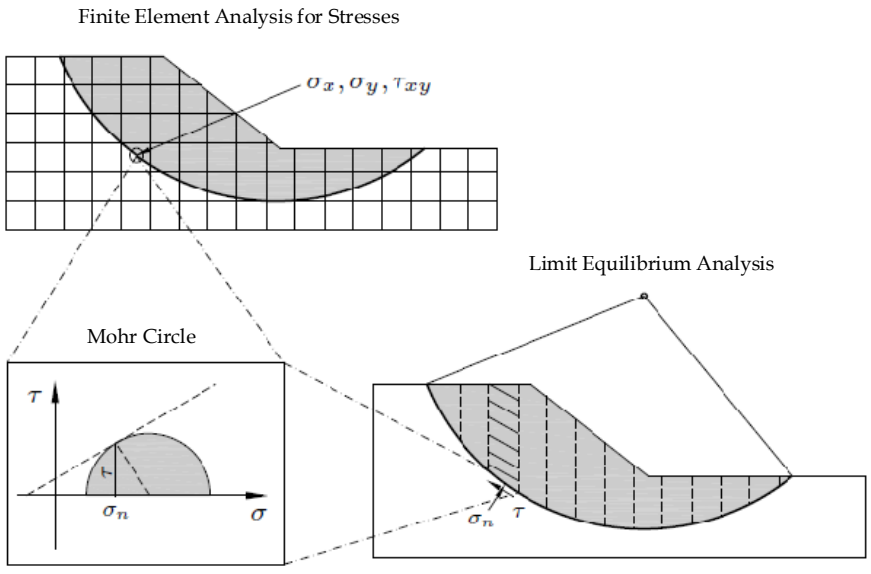

Figure 2.4: Enhanced Limit Method (Fredlund et al. [19])

Fredlund et al. [19] has given three definitions for the factor of safety, namely the strength, stress and strength-stress level approach. The safety factor in a strength analysis is given as:

$$\text{FoS} = \frac{\sum \left(c + \sigma_n \tan\phi\right) \Delta L}{\sum \tau \Delta L}, \tag{2.2}$$

which can be rewritten into:

$$\text{FoS} = \frac{\sum_{i=1}^{n} \tau_{fi} \Delta L_i}{\sum_{i=1}^{n} \tau_i \Delta L_i}, \tag{2.3}$$

where τ is the mobilised shear stress and ΔL is the length of a section of the slip surface. A stress level analysis as performed by Zienkiewicz et al. [78] uses the following factor of safety:

$$\text{FoS} = \frac{\sum(\Delta L)}{\sum \left[\frac{(\sigma_1 - \sigma_3)}{(\sigma_1 - \sigma_3)_f} \right] \Delta L}. \tag{2.4}$$

The last definition described by Fredlund et al. [19] uses the strength-stress level approach and is defined as:

$$\text{FoS} = \frac{\sum(S \Delta L)}{\sum \left[\frac{(\sigma_1 - \sigma_3)}{(\sigma_1 - \sigma_3)_f} \right] S \Delta L}, \tag{2.5}$$

where S is given as $S = \left(c + \sigma_n \tan(\phi)\right)$. With this definition, the safety factor of any slip surface can be calculated. A search algorithm is then needed to find the most critical slip surface. In Figure 2.5 an overview is given of the different possibilities in a finite element slope stability analysis.

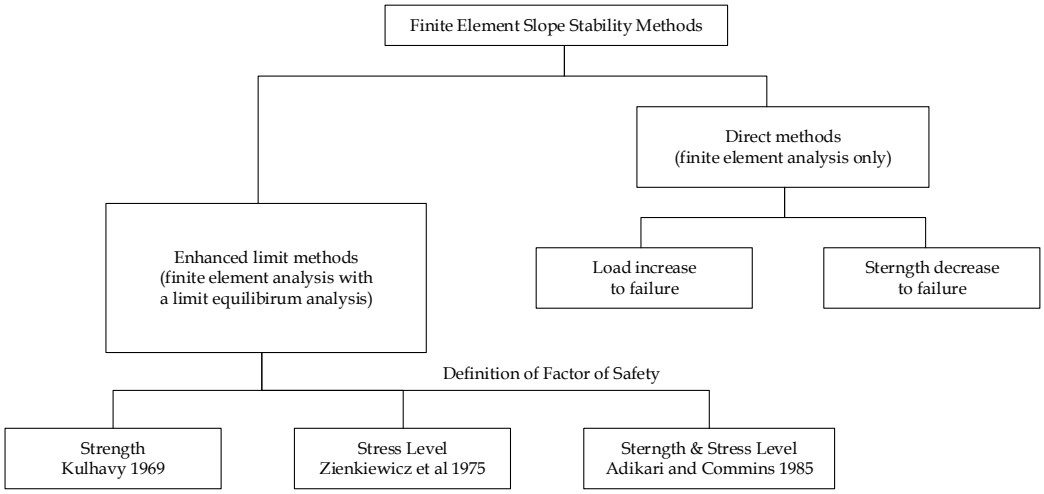

Figure 2.5: Finite Element Approaches for a Slope Stability Analysis (Fredlund et al. [19])

The enhanced limit method, in which the normal and shear stresses are obtained from a finite-element-based stress analysis (Yamagami and Veta [76], Farias and Naylor [17], Fredlund et al. [19], Pham and Fredlund [53]) has drawn much more attention, because the assumption relating to the inter-slice forces is not needed and the calculation of the safety factor is linear (Li et al. [43]). Both advantages also hold for the finite element method, however, the ELM is able to overcome the problem of finding an irrelevant critical slip surface. The normal and shear stresses along the slip surface can be calculated from the stress distribution which is found using a linear or non-linear stress analysis. Furthermore, any definition for the maximum available shear strength can be applied in Equation 2.3.

To summarise, the main idea of the enhanced limit method is that first, a finite element analysis, with a linear elastic or elasto-plastic soil model, is performed once. Then, the state of stress of the slope is exported into a limit equilibrium analysis. The primary task of the ELM is to locate the critical slip surface using mathematical optimisation. Using a specified definition for the factor of safety, the optimisation module finds the slip circle which gives the lowest safety factor.

2.4. Optimisation Methods

Baker [2] is the first to investigate the use of optimisation methods in the analysis of slope stability. In his paper he presents a dynamic programming minimisation procedure to find the minimal safety factor and the corresponding slip surface. In this procedure the minimisation procedure is coupled to Spencer's method. After Baker's findings, many more optimisation methods are proposed in literature to identify the critical slip surface, these are: the simplex method (Nguyen [51]), Davidon-Fletcher-Powell method (Yamagami and Veta [76]), Monte Carlo (Malkawi et al. [46]), dynamic programming (Pham and Fredlund [53]), genetic algorithm (Sabhahit et al. [62], Zolfaghari et al. [79], Li et al. [43]) and (Adaptive) Particle Swarm Optimisation (Cheng et al. [11], Liu et al. [45]), to name a few.

Finding the location of the critical slip surface with the minimum safety factor of a slope is a difficult NP-hard optimisation problem, meaning that the problem is very complex. The main difficulties in finding the location of the critical non-circular failure surface are described by Cheng et al. [11]:

1. The objective function of the safety factor is usually non-smooth, non-convex and may be non continuous over the complete solution domain. This can result in non-convergence if gradient type optimisation methods are applied.
2. Chen and Shao [8] have found that multiple minima can exist and that many solution methods will be trapped in a local minimum. The initial trial has great consequence on which solution will be found.
3. A good initial trial is often necessary to find the global minimum in many methods. However, estimating a good initial trial can be very difficult.

Especially classical (calculus-based) optimisation methods are prone to identifying a false critical slip surface due to the multiple minima over the solution domain (Li et al. [43]). According to Goh [23], the main shortcoming of these algorithms is that the robustness to find the global minimum instead of the local minimum is rather uncertain. The classical optimisation methods need a proper preliminary solution to converge to a valid slip surface. Metaheuristic optimisation algorithms do not face the limitation of getting trapped in a local minima and are therefore widely used in slope stability problems (Gandomi et al. [20]).

One of these metaheuristic optimisation methods applied in slope stability analyses is the genetic algorithm by Barricelli [4] and Holland [27]. Holland [27] has developed the genetic algorithm to investigate the adaptiveness in processes of natural systems. This algorithm is based on the biological evolutionary theory, where in a population of solutions the 'fittest' solution is more likely to be chosen as the final solution. Due to the use of this population, and mimicking biological mechanisms such as selection, crossover and mutation, it is less likely to get stuck in a local minimum. However, the speed of GA can be low due to the random crossover process. Genetic algorithms are suitable to solve complex optimisation problems, such as the minimisation problem in localising the critical slip surface.

Various applications of optimisation methods in a slope stability analysis have been found in literature. Goh [23] uses a genetic-based evolution algorithm to locate the critical slip surface whilst only circular slip surfaces are considered. The search strategy is used in accordance with Bishop's method to determine the factor of safety. Zolfaghari et al. [79] present a simple genetic algorithm for the search of a critical non-circular failure surface, in which the safety factor is defined by the Morgenstern-Price method. Li et al. [43] has developed a search approach for locating a non-circular critical slip surface by employing a real-coded genetic algorithm. In their research, different methods are used to determine the factor of safety, such as Spencer, Morgenstern-Price and a finite-element-based method. Zhu and Chen [77] have incorporated a local improvement procedure based on tabu search into a basic genetic algorithm. This hybrid genetic algorithm is used to search for both circular and non-circular slip surfaces associated with their minimum safety factors. To find the safety factor, both the Bishop method as the improved Morgenstern-Price method are implemented. Pasik and van der Meij [52] present a tailored genetic algorithm, which proves to be an efficient method to find circular and unconstrained slip surfaces. For the circular slip surface, Bishop's method is used to determine the safety factor. For the unconstrained slip surface Spencer's method is applied. Cheng et al. [11] use a modified particle swarm optimisation method with a termination criterion to find the critical slip surface. They have shown that the algorithm is effective and efficient in solving complicated slope problems.

2.5. Shear Strength

One of the main interests in this research is the selection of soil models and its influence on the identification of the critical slip surface. Most finite element analysis programs contain many constitutive models, though every model has its own assumptions and limitations. A disadvantage of the more advanced soil models is that they require more geotechnical parameters compared to simple models. As described in Section 2.2, the FEM determines the safety factor against instability of a slope with the shear strength reduction technique. Consequently, even though many soil models are applicable, the program does not make use of the expressions for the (undrained) shear strength from advanced soil models to determine the strength of the slip surface. This limitation is the main motivation for this study.

To overcome the disadvantage of the shear strength reduction method, a different approach will be used to find the safety factor of the slip surfaces. In accordance with the enhanced limit method, Fredlund et al. [19] has given three definitions for the factor of safety as given in Section 2.3. In this research the safety factor will be calculated by taking the ratio of the total maximum available shear strength to the total mobilised shear stress along a slip surface, which is equivalent to the strength level approach as given by Equation 2.6:

$$\text{FoS} = \frac{\sum \left(c + \sigma_n \tan\phi\right) \Delta L}{\sum \tau \Delta L}, \tag{2.6}$$

which can be rewritten into:

$$\text{FoS} = \frac{\sum_{i=1}^{n} \tau_{fi} \Delta L_i}{\sum_{i=1}^{n} \tau_i \Delta L_i}. \tag{2.7}$$

Using this type of safety factor, the full potential of the finite element analysis is used. This definition of the safety factor does not rely on extra assumptions or simplifications, but solely uses the current stresses in the soil and an expression for the maximum available shear strength.

The advantage of using a finite element analysis program for the stress analysis is that the initial stress conditions are realistically modelled. Therefore this approach has the potential to be more accurate than a LEM. The finite element analysis is able to accurately represent the behaviour of the soil. The maximum available shear strength will be defined using constitutive models. There are many models which can be used to define the maximum available shear strength and extra attention should be paid to whether the soil is drained or undrained. Especially for the undrained case it is not apparent how the shear strength should be defined. This undrained case will be discussed in the next section.

To summarise, the method has an advantage compared to LEM since it uses a realistic representation of the initial stresses. The advantage compared to FEM is that it makes no use of the shear strength reduction method. The shear strength reduction method makes a prediction for the shear strength at failure, whilst the proposed method makes a prediction for the maximum available shear strength. This way the 'reserve' strength in the soil is determined. Another difference is that the SSRM only reduces the shear strength parameters c and ϕ until failure occurs, consequently no use is made of the advanced constitutive models to search for the shear strength at failure. In the proposed method these models are used to define the maximum available shear strength, hence expressions for this strength are properly theoretically derived. Another advantage of the proposed method compared to the FEM is that the safety factor definition as given in Equation 2.6 can be applied to any slip surface of interest. Therefore not only the safety factor of the most critical slip surface is given by the method, the method is also able to give the safety factor of any intermediate result.

2.5.1. Undrained Analysis

A drained analysis can be performed if the excess pore pressures caused by loading or unloading have dissipated completely due to a slow rate of construction or because the phase that is being analysed is at a sufficient time after construction. Additionally, the shear induced pore pressures are also zero due to a slow rate of shearing. Sand and gravel with high permeabilities are typically drained. In Figure 2.6 this type of analysis is indicated with the ESA (effective stress analysis) arrow. Due to the absence of excess pore pressures, the effective normal stress σ'_{vc} is seen as the effective normal stress at failure σ'_{ff}. In other words, this type of analysis assumes a slow failure with complete dissipation of the shear induced pore pressures.

Contrarily, if considerable excess pore pressures are built up during the deformation process which cannot drain away quickly, this soil type is viewed as undrained. Clay is typically undrained due to its low permeability. Undrained shear of clay will develop positive shear induced pore pressures, which results in a lower effective normal stress at failure ($\sigma_{ff} < \sigma'_{vc}$), as indicated by the USA (undrained strength analysis) arrow in Figure 2.6. An undrained analysis inherently assumes a rapid failure, in which the excess pore pressures do not have the time to dissipate. If an impermeable soil, thus showing undrained behaviour, is analysed in a drained approach, the soil strength of the soil will be overpredicted. It is therefore very important to include these shear induced pore pressures, which reduce the effective normal stress, in an undrained analysis.

Figure 2.6 will be discussed in a bit more detail. In this figure the stresses are shown which act on an element of a horizontal failure surface as found by Ladd [36]. The vertical consolidation stress σ'_{vc} is determined from the total vertical stress and from measurements of the pore pressure. A conventional effective stress analysis computes the available shear strength $s_d = \tau_{ff}$ using the effective strength parameters c' and ϕ' as defined in the Coulomb criterion $\tau_{ff} = c' + \sigma'_{ff} \tan\phi'$. This conventional analysis assumes no excess pore pressure during loading. Therefore, the effective normal stress is treated as the effective normal stress at failure, thus $\sigma'_{vc} = \sigma'_{ff}$.

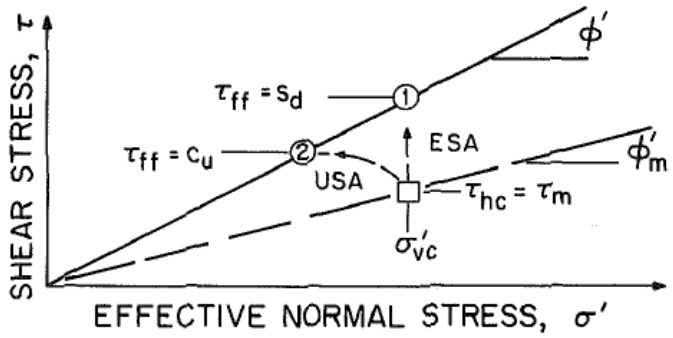

Figure 2.6: Comparison of Effective Stress and Undrained Strength Analysis (Ladd [36])

In an undrained stress analysis, a rapid failure corresponding to the consolidated-undrained case is assumed. In this case the undrained shearing of clay will develop positive shear induced pore pressures, which results in a lower effective normal stress at failure. The undrained shear strength will therefore be smaller than s_d at point c_u, as shown in Figure 2.6. The definition of c_u is given as $c_u = \tau_{ff} = q_f \cos(\phi)'$ by Ladd [36], where $q_f = \frac{1}{2}(\sigma_1 - \sigma_3)$. If the assumption $c_u = q_f \cos(\phi')$ is incorrect, the error will be on the safe side by 10-15% for typical values of $\cos(\phi')$ according to Ladd [36].

To summarise, Ladd [36] presents two options to represent the undrained shear strength of clay: (1) Using the effective stress strength parameters c' and ϕ', where extra care has to be taken to the pore pressure development and its influence on the normal effective stress and (2) Using the undrained shear strength parameters where the cohesion is set equal to the undrained shear strength: $c' \rightarrow q_f$ and $\phi = 0$. In the latter of this report, the undrained shear strength will be denoted with s_u instead of c_u.

Critical State Soil Mechanics (CSSM)

The shear strength of soil can in general terms be described by the concept of critical state. The Critical State Soil Mechanics (CSSM) model is introduced by Schofield and Wroth [67]. The critical state concept is an idealised description of the behaviour of saturated remoulded clays in triaxial compression test and is assumed to apply in undisturbed soils. It states that in case a soil sample is sheared, it will eventually lead to a state in which further shearing will not result in changes in the effective or yield stress as well as the specific volume, this is called the critical state. This is equivalent to the soil reaching constant plastic volumetric strains, whilst the deviatoric plastic strains increase steadily.

There are three distinguishes made in this method, between normally and over-consolidated behaviour of the soil, drained or undrained behaviour and between peak strength and critical state strength. The critical state strength of the soil can be used as a measure for the resistance against sliding. In the formulation of the critical state, cohesion does not play a role. In this framework cohesion is a result of overconsolidation. In case overconsolidation increases, the cohesion will increase as well.

Pore Pressure Development

Figure 2.7 gives a representation of a saturated specimen of clay that has been isotropically normally consolidated to the stress point A. In an undrained triaxial compression test, the effective stress path will be given as the curve AB, where B represents the critical state. The total stress path is the line AD. The excess pore pressure is given as the difference between the mean total and effective pressure, line BD. This excess pore pressure is split into two components: (1) due to the response of the clay to the shearing BC and (2) due to the change in mean total stress applied to the specimen, line CD.

This figure also shows that the magnitude of the excess pore pressure is not only dependent on the soil behaviour, but also on the mean total stress (Δp) which is applied. In case a different test had been conducted such as AE, the effective stress path would not have changed. However, BE is greater than BD. This is due to the difference in mean total stress (Δp) which is applied. Only BC is a unique property of the soil and can be correlated with other properties of the soil such as the overconsolidation ratio. The line CD/CE does not give information about the soil.

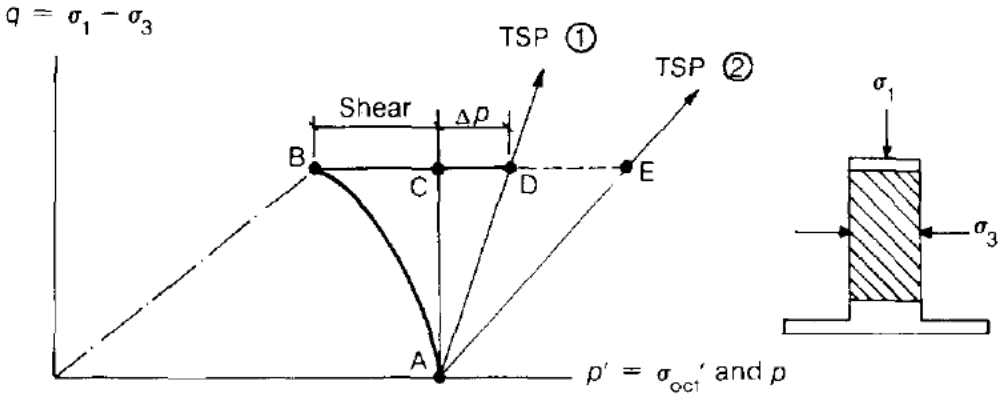

Figure 2.7: Interpretation of the Excess Pore Pressure in Triaxial Compression Tests (Wroth [75])

To express the pore-pressure change Δu in an undrained analysis, Skempton [68] has given the equation:

$$\Delta u = B\left[\Delta\sigma_3 + A\left(\Delta\sigma_1 - \Delta\sigma_3\right)\right], \tag{2.8}$$

where A and B are pore-pressure coefficients. These coefficients are measured experimentally in the undrained triaxial test. Skempton [68] found that the parameter B is dependent on the degree of saturation of the soil. A saturated soil gives the value 1, whereas for a dry soil B equals 0. Ladd [36] has shown that the pore-pressure coefficient A can be correlated to the overconsolidation ratio (OCR).

2.6. Soil Mechanics

Constitutive models describe the material responses to various loading conditions, which provide the stress-strain relations to formulate governing equations. There exist numerous constitutive models to represent the stress-strain and failure behaviour of soils. In this research some constitutive models are used to find definitions for the shear strength in the drained and undrained case.

If soil would be an isotropic linear elastic material, then its behaviour could be fully determined by two parameters, Young's modulus E and Poisson's ratio ν. However, the response to loading of soil is much more complicated. Most soil models are therefore elastic-plastic. In this research the undrained behaviour of clays, with its shear induced pore pressures, is of importance. Brinkgreve [6] has discussed different aspects of soil behaviour, including factors influencing the soil. A selection of the elasto-plastic models will be discussed briefly in the following sections. Lade [38] has given an overview of constitutive models including the principles and main characteristic functions. In Table 2.4 some very basic components of soil models are summarised, with examples of corresponding parameters for three different soil models.

Table 2.4: Elasto-Plastic Models obtained from Lade [38]

	Component	Function	Parameters for Simple Elastic-Perfectly Plastic Approach (Mohr-Coulomb)	Parameters for Modified Cam-Clay Model	Parameters for Single Hardening Model
Elastic Behaviour	Hooke's Law	Produces elastic strains whenever the stresses change	ν, E	κ, G	ν, M, λ
Plastic Behaviour	Failure Criterion	Imposes limits on stress states that can be reached	c, ϕ	M	η_1, m, a
Plastic Behaviour	Plastic Potential Function	Produces relative magnitudes of plastic strain increments (similar function as Poisson's ratio for elastic strains		-	μ, Ψ_2
Plastic Behaviour	Yield Criterion	Determines when plastic strain increments occur: Only when yield surface is pushed out/in (hardening/softening)		-	h, α
Plastic Behaviour	Hardening/Softening Relation	Determines magnitudes of plastic strain increments (similar function as Young's modulus for elastic strains)		Λ, λ	C, p

2.6.1. Mohr-Coulomb Model

The Mohr-Coulomb model is an elastic-perfectly plastic model as shown in Figure 2.8. The linear elastic part is based on Hooke's law of isotropic elasticity, whilst the perfectly plastic part is based on the Mohr-Coulomb failure criterion. When implementing the Mohr-Coulomb model, attention has to be given to the transition between the yield surfaces as shown in Figure 2.10. The yield surface is shaped as a hexagon which consists of six contours. In the finite element analysis program PLAXIS the exact form of the model is implemented, using a sharp transition between the sections of the yield surfaces. The parameters required by the Mohr-Coulomb model are listed in Table 2.5.

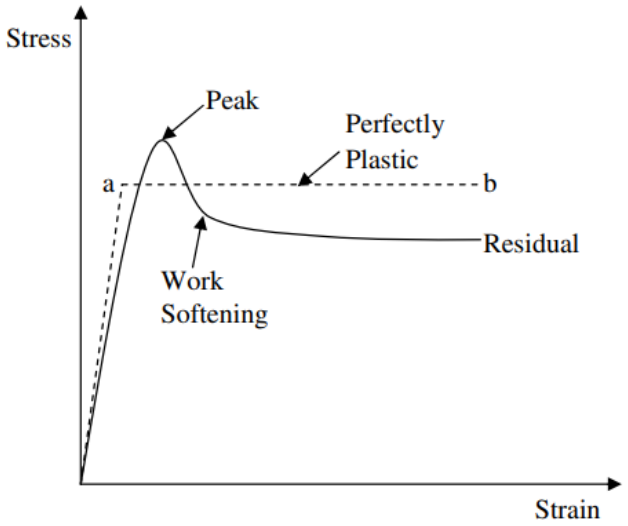

Figure 2.8: Elastic-Perfectly Plastic Assumption of Mohr-Coulomb Model (Prasad and Sai [56])

Table 2.5: Model Parameters Mohr-Coulomb Model

c'	(effective) cohesion	[kN/m^2]
ϕ'	(effective) internal friction angle	[°]
Ψ	Dilatancy angle	[°]
E	Elasticity modulus	[kN/m^2]
ν	Poisson's ratio	[-]
γ	Volumetric weight of the soil	[kN/m^2]

Charles-Augustin de Coulomb used the analogy of a sliding block to propose a relationship of the maximum possible shear stress in a soil body, according to Heyman and Coulomb [26]. This criterion can be written as

$$\tau_f = c' + \sigma' \tan\phi', \tag{2.9}$$

where c' is the cohesion, σ' the effective stress and ϕ the angle of shearing resistance. The Coulomb criterion thus relates the shear strength of the material to the cohesion, normal stress and angle of internal friction of the material. This definition for the shear strength will be used in this research in the drained analysis.

For a certain plane in Mohr's circle, the criterion in Equation 2.9 can be met. In Figure 2.9 these critical planes are indicated by C and D. On all other planes the shear stress remains below the critical value. The ratio between τ/σ is maximal when Mohr's circle touches the Coulomb envelope, this is where failure will start to occur. This is called the Mohr-Coulomb failure criterion. For this criterion the mathematical formulation is given as:

$$f = \frac{1}{2}\left|\sigma'_1 - \sigma'_3\right| + \frac{1}{2}\left(\sigma'_1 + \sigma'_3\right)\sin(\phi) - c\cos(\phi) \tag{2.10}$$

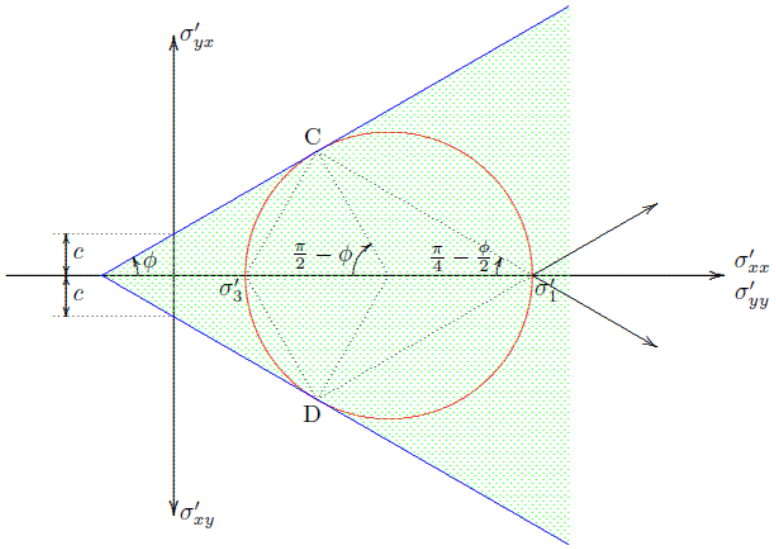

Figure 2.9: Mohr-Coulomb Failure Criterion (Verruijt [73])

A summary of the main characteristics of the Mohr-Coulomb model are given in Table 2.6. For a more detailed description of the Mohr-Coulomb model the reader is referred to Section A.1 in the Appendix.

Table 2.6: Advantages and Limitations Mohr-Coulomb Model

Advantages	Limitations
Simple and clear	Isotropic and homogeneous behaviour
Limited number and well defined parameters	Until failure linear elastic behaviour
Dilatancy can be included	No stress-dependent stiffness
Good representation of drained failure behaviour	Dilatancy continues forever (no critical state)
	No distinction between primary loading, unloading or reloading
	Undrained behaviour not always realistic
	Not able to model shear induced pore pressure
	No time-dependency (creep)
	No anisotropy

2.6.2. Matsuoka-Nakai Failure Criterion

In the previous section the Mohr-Coulomb model has shortly been introduced. The Mohr-Coulomb failure criterion as given in Equation 2.10 has been criticised according to Griffiths and Lane [24], considering that this failure criterion does not take account of the intermediate principal stress σ_2. One way to express the influence of the intermediate principal stress σ'_2 relative to the major σ'_1 and minor σ'_3 principal stresses is in terms of the parameter b:

$$b = \frac{\sigma'_2 - \sigma'_3}{\sigma'_1 - \sigma'_3} \tag{2.11}$$

For values of b other than 0, it has been found that the peak strength is generally greater than that given by the Mohr-Coulomb failure criterion. Georgiadis et al. [22] also confirm that the magnitude of the intermediate principal stress σ'_2 influences the shear strength of soil. Therefore in this research, the criterion of Matsuoka and Nakai [47] will be implemented, besides Coulomb, which considers the intermediate principal.

The Coulomb criterion assumes a constant value of ϕ', which is independent of b. This criterion is the hexagon in the deviatoric plane as shown in Figure 2.10. Matsuoka and Nakai [47] and Lade and Duncan [39] imply varying values of the friction angle with Lode's angle. Lode's angle is a different expression for the relative magnitude of the intermediate principal stress, given as:

$$\theta = \tan^{-1}\left[\frac{1}{\sqrt{3}}\left(2\frac{\sigma'_2 - \sigma'_3}{\sigma'_1 - \sigma'_3} - 1\right)\right] \tag{2.12}$$

Both fail surfaces have been drawn in such a way that they pass through the vertices of the Mohr-Coulomb hexagon which lie on the positive stress axes. For the shape of both failure surfaces it also holds that it varies with the friction angle; the shape becomes more circular with a decreasing ϕ.

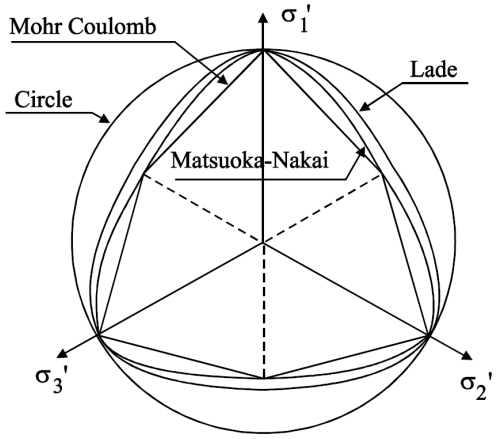

Figure 2.10: Failure Surfaces in the Deviatoric Plane (Georgiadis et al. [22])

Wroth [75] has attempted to relate different failure conditions to the friction angle ϕ, based on the work of Satake [64]. He adopted Matsuoka-Nakai's failure criterion to take proper account of the effect of the intermediate principal stress σ_2. Satake [64] has shown that if an associated flow rule is applied and Matsuoka-Nakai's failure criterion is used as the yield criterion, then plane strain conditions will give the maximum value that ϕ can have. Lagioia and Panteghini [41] also propose a method to find the equivalent Mohr-Coulomb friction angle ϕ^* using other failure criteria. In their derivation they use the failure criterion as proposed by Lagioia and Panteghini [40]. Their proposed formulation offers the possibility of rounding the corners of the Tresca and Mohr-Coulomb criteria in the deviatoric plane. Their failure criterion is given as:

$$f(p,q,\theta) = -M_c p + g_L \Gamma(\theta) = 0, \tag{2.13}$$

where

$$\Gamma(\theta) = \frac{1}{g_L(\theta)} = \alpha \cos\left[\frac{\arccos(\beta \sin(3\theta))}{3} - \gamma\frac{\pi}{6}\right] \tag{2.14}$$

The parameters α, β and γ are different for the classical criteria, and expressions can be found in Lagioia and Panteghini [41]. Equation 2.13 can be used to find (q/p) at any failure criteria and for any θ. Figure 2.11 shows that an equivalent Mohr-Coulomb criterion can be constructed which has the same value for q/p as Matsuoka-Nakai's criterion, if θ is between 0 and θ_f. The angle of shearing resistance ϕ^* is then given for Matsuoka-Nakai by:

$$\phi^* = \arcsin\left(\frac{\sqrt{3}\sin(\phi)\cos(\theta_f)}{\cos\left(\frac{1}{3}\arccos\left[\left(8+\cos^2(\phi)\right)\sin(\phi)\sin(\theta_f)/\left(4-\cos^2(\phi)\right)^2\right]\right)\sqrt{4-\cos^2(\phi)}-\sin(\theta_f)\sin(\phi)}\right) \tag{2.15}$$

Based on the work of Satake [64], Wroth [75] and Lagioia and Panteghini [40], Lode's angle will be set at plane strain failure. The derivation of this value for θ_f will be given below, but first an important remark should be made. Both Lagioia and Panteghini [40] and Lagioia and Panteghini [41] assume an associated flow rule, such that the yield surface is coincident with the plastic potential ($\Psi = \phi$). Substituting the value obtained from Equation 2.15 in Coulomb's criterion will therefore give an estimation of the maximum available shear strength. However, in reality it is not expected that this maximum shear strength will occur at the same time along the complete surface.

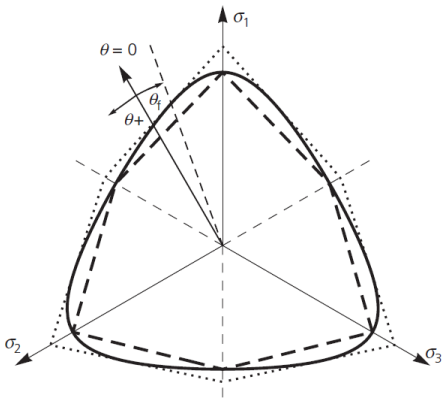

Figure 2.11: Expanded Mohr-Coulomb Hexagon (Dotted Line) having the same q/p of the Matsuoka-Nakai Criterion (Full Line) for θ = 0 - θ_f (Lagioia and Panteghini [41])

The importance of the shape of the plastic potential in the deviatoric plane in plane strain conditions was already recognised by Potts and Gens [54]. Plane strain is defined to be a state of strain in which the strain normal to the x-y plane ϵ_z and the shear strain γ_{xz} and γ_{yz} are assumed to be zero. In plane strain, a situation occurs in which the dimension of the structure in one direction, say the z-coordinate direction, is very large in comparison with the dimensions of the structure in the other two directions. The applied forces act in the x-y plane and do not vary in the z direction.

When investigating the plane strain failure of soils, the kinematic constraint controls the failure of the soil element and therefore the plastic potential plays an important role in investigating the failure condition. The derivation of the kinematic constraint will be elaborated on right now. The incremental strain component ϵ_i at failure can be expressed in an elastic and plastic part:

$$\dot{\epsilon_i} = \dot{\epsilon_i}^e + \dot{\epsilon_i}^p = \dot{\epsilon_i}^p \qquad i = 1,2,3 \tag{2.16}$$

The elastic incremental strain component is not considered, since only plastic flow takes place at failure. If failure occurs in plane strain conditions, then the out of plane incremental strain is equal to zero. The plastic strain tensor is evaluated by means of the plastic potential function $g(\sigma) = 0$, leading to:

$$\dot{\epsilon_{ij}}^p = \dot{\lambda}\frac{\delta g}{\delta \sigma_{ij}} \tag{2.17}$$

where $\dot{\lambda}$ is the plastic multiplier. Since the incremental out of plane strain is equal to zero in plane strain conditions, the following kinematic constraint is found:

$$\frac{\delta g}{\delta \sigma_{i*}} = 0 \tag{2.18}$$

The failure criterion of the Mohr-Coulomb model can be expressed in terms of invariants as

$$f = g = \sqrt{J_{2D}} - (c\cot\phi + p)\Gamma(\theta) = 0 \tag{2.19}$$

where

$$\Gamma(\theta) = \frac{\sin(\phi)}{\cos(\theta) + \frac{\sin(\theta)\sin(\phi)}{\sqrt{3}}} \tag{2.20}$$

In Equation 2.19 the plastic potential function is set equal to the yield function, therefore assuming an associated flow rule. This assumption will result in an expression that gives the maximum available shear strength along the complete slip surface. Deriving Equation 2.19 with respect to σ_i yields

$$\begin{aligned} \frac{\delta g}{\delta \sigma_1} &= 1 - \sin(\phi) \\ \frac{\delta g}{\delta \sigma_2} &= 0 \\ \frac{\delta g}{\delta \sigma_3} &= 1 - \sin(\phi) \end{aligned} \tag{2.21}$$

From Equation 2.21 it is clear that plane strain failure requires the out-of-plane direction to coincide with the intermediate one, assuming that $\phi < 90°$. Furthermore, since the derivative is independent on θ, the plane strain failure condition as given by Equation 2.18 is satisfied when the yield surface is attained, indicating that failure will always coincide with yield.

Instead of considering the Mohr-Coulomb model, another failure criterion could be implemented which derivative does not become zero for one of the principal directions, such as the Matsuoka-Nakai criterion. The elastic-perfectly plastic model uses the following criterion for both the yield and plastic potential surfaces, since an associated flow rule is assumed.

$$f = g = I_1 I_2 - k I_3 = 0 \tag{2.22}$$

where I_1, I_2, I_3 are the first, second and third stress invariant. In case a non-associated flow rule is applied, ϕ is replaced by Ψ in Equation 2.24 in the plastic potential surface. This failure criterion can be rewritten using Lode's angle θ and the generalised stress obliquity $M(\theta)$ to:

$$f = \frac{2}{\sqrt{27}} k \sin(3\theta) M(\theta)^3 + (k-3) M(\theta)^2 - (k-9) = 0 \tag{2.23}$$

where

$$k = \frac{9 - \sin^2(\phi)}{1 - \sin^2(\phi)} \tag{2.24}$$

Taking the derivative of the plastic potential of the Matsuoka-Nakai function (Equation 2.22) with respect to the principal stresses gives:

$$\frac{\delta g}{\delta \sigma_i} = \frac{k}{I_1} - \frac{I_1}{\sigma_i^2} \tag{2.25}$$

Equation 2.18 can only be satisfied when the principal out-of-plane direction is $i = 2$:

$$\frac{\delta g}{\delta \sigma_2} = \frac{k}{I_1} - \frac{I_1}{\sigma_2^2} = \frac{k\sigma_2^2 - I_1^2}{\sigma_2^2 I_1} = 0 \tag{2.26}$$

which is satisfied by

$$\sigma_2 = \frac{I_1}{\sqrt{k}} \tag{2.27}$$

The principal stresses can also be expressed as a function of the mean pressure p, second invariant of the deviatoric stress J_{2D}:

$$J_{2D} = \frac{1}{6}\left[(\sigma_1-\sigma_2)^2+(\sigma_2-\sigma_3)^2+(\sigma_3-\sigma_1)^2\right], \tag{2.28}$$

and Lode's angle θ as:

$$\begin{aligned}\sigma_1 &= p+\frac{2}{\sqrt{3}}\sqrt{J_{2D}}\sin\left(\theta+\frac{2}{3}\pi\right)\\ \sigma_2 &= p+\frac{2}{\sqrt{3}}\sqrt{J_{2D}}\sin(\theta)\\ \sigma_3 &= p+\frac{2}{\sqrt{3}}\sqrt{J_{2D}}\sin\left(\theta-\frac{2}{3}\pi\right)\end{aligned} \tag{2.29}$$

Using Equations 2.23, 2.27 and 2.29, the following expression is found for Lode's angle at plane strain collapse:

$$\theta_f = -\arcsin\sqrt{\frac{3k+(k-3)\frac{3\sqrt{k}}{3-\sqrt{k}}}{4\left[\frac{k-9}{27}\left(\frac{3\sqrt{k}}{3-\sqrt{k}}\right)^3+k\right]}} \tag{2.30}$$

2.6.3. Modified Cam-Clay (MCC) Model

As discussed in Section 2.5.1, special attention has to be paid when determining the shear strength of undrained soil. The Mohr-Coulomb model which has been briefly described is not very suitable to analyse undrained behaviour, since it does not capture the shear induced pore pressures. Therefore other constitutive models should be considered for this research as well.

Before the maximum strength of a soil has been reached, some irreversible straining can have occurred in the soil. Thus, plastic deformations already occur in the early stages of loading. To capture this behaviour in a constitutive model, the typical elastic-perfectly plastic model such as Mohr-Coulomb does not suffice anymore. To represent this hardening behaviour of soil, a constitutive model which utilises a hardening law after initial yielding is needed. Therefore researches have looked into the possibility of modelling soil as a strain hardening material. Roscoe et al. [60] use the strain hardening theory of plasticity to formulate a complete stress-strain model for normally or lightly over-consolidated clay, which will later be used by Schofield and Wroth [67] to formulate the Cam-Clay model. A modified version of the Cam-Clay model is suggested by Roscoe and Burland [59] and this Modified Cam-Clay model is extended to a general three-dimensional stress state. In this section the Modified Cam-Clay model will be described, where from now on this model will be referred to as just the Cam-Clay model. The description of this model is based on the work of Wood [74]. This model is an elastic-plastic strain hardening model that is based on the critical state theory and the assumption that there is a logarithmic relationship between the mean effective stress p' and specific volume v, where $v = 1+e$ in which e is the void ratio.

The Cam-Clay model is of interest for this research because it gives the possibility to determine the undrained shear strength of the soil. Therefore, the response of soil in an conventional drained analysis is not elaborated in this section. In this section only the parts of the model are discussed which are relevant to the undrained analysis. For the complete description of the model the reader is referred to Appendix A.2 and the book of Wood [74] (in particular Section 5.3 of the book for the conventional drained analysis).

The Cam-Clay model assumes that recoverable changes in volume are accompanied by a change in the mean effective stress p'. It implies that in the compression plane a linear relation can be found between the specific volume v and logarithm of p' for elastic un- and reloading of the soil. Figure 2.12 shows the yield locus of the Cam-Clay model in the $p':q$ plane and the compression plane $p':v$. This yield locus is given as:

$$\frac{p'}{p'_0} = \frac{M^2}{M^2+\eta^2} \tag{2.31}$$

where $\eta = q/p'$, which is the stress ratio.

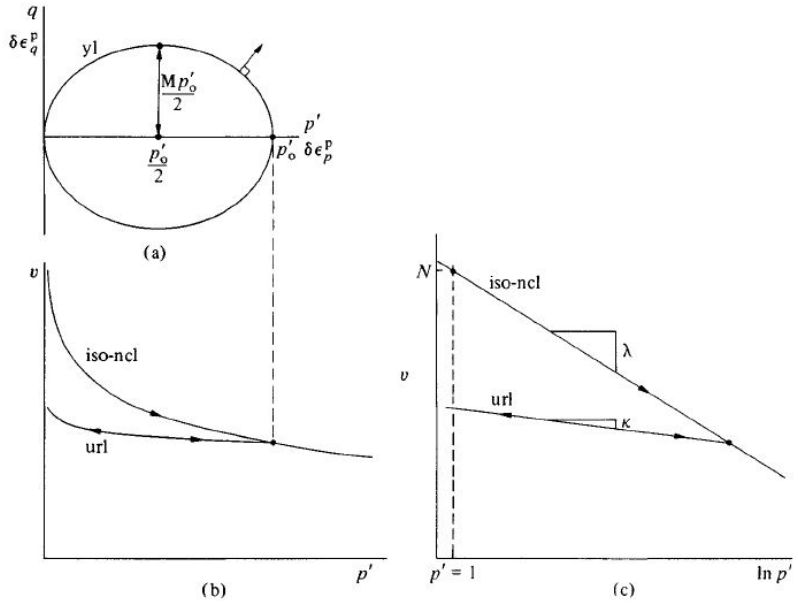

Figure 2.12: Elliptical Yield Locus for Cam-Clay Model (Wood [74])

In case the soil starts to yield in an undrained test, the volume change of the soil will be equal to zero. This means that the elastic and plastic contributions are exactly equal and opposite such that the total volumetric strain is zero. In an undrained test the mean effective stress reduces due to the build up of pore pressure, hence elastic volumetric expansion occurs. It is necessary for the yield curve to expand and produce plastic volumetric compression to balance the elastic expansion. The condition that the summation of the expansion and summation are equal to zero is given as:

$$\frac{p'_i}{p'} = \left(\frac{M^2 + \eta^2}{M^2 + \eta_i^2} \right)^{\Lambda} \tag{2.32}$$

where $\Lambda = (\lambda - \kappa)/\lambda$. Equation 2.32 gives the shape of the undrained effective stress path in the $p' : q$ plane, as shown in Figure 2.13, which is of interest in this research.

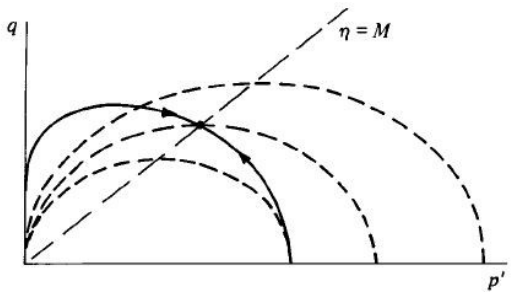

Figure 2.13: Equation 2.32 (Wood [74])

In Figure 2.14 three different tests are shown: an initially normally compressed, lightly overconsolidated and highly consolidated sample. The different stress states in the tests are indicated with points and each point lies on a new yield locus. For both the normally consolidated and lightly overconsolidated case holds that $\eta < M$. Yielding takes place with a strain increment vector directed to the right, which implies that plastic volumetric compression is occurring. The soil wants to harden plastically, and therefore the current yield locus has to expand. To balance the plastic compression, the mean effective stress must decrease (positive pore pressures occur) such that elastic expansion occurs. This is called the wet side. The difference between these two cases is that the lightly overconsolidated case begins with an elastic phase AB until the stress state reaches the initial yield locus.

For the heavily overconsolidated sample, $\eta > M$, yielding takes place with the plastic strain increment vector directed to the left, which implies that plastic volumetric expansion is occurring. The soil wants to soften plastically, thus the yield locus has to shrink. To balance the plastic expansion, the mean effective stress must increase (negative pore pressures occur) such that elastic compression occurs. This is called the dry side.

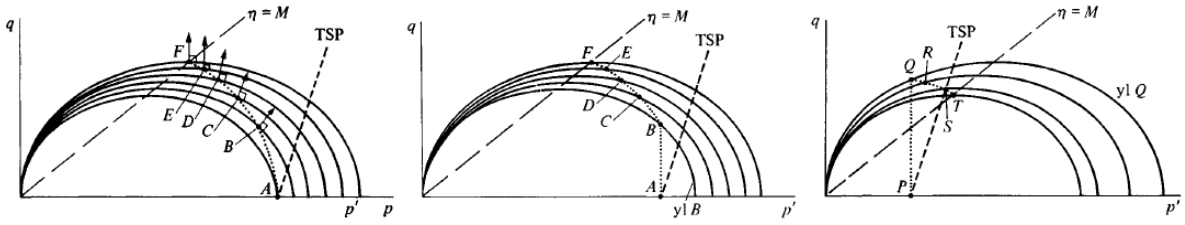

Figure 2.14: Stress Increments in Undrained Analysis (Wood [74])

Critical States

In the normally consolidated case in Figure 2.14, the direction of the plastic strain increment is plotted. The ratio plastic shear strain increment to plastic volumetric strain increment can thus be determined. This ratio increases when the normal to the yield locus becomes more parallel to the q axis. At point F this ratio becomes infinite, where unlimited plastic shear strains can develop without any extra plastic volumetric strain or effective stresses. Since no plastic volumetric strain occurs, the yield locus remains the same size. This condition of perfect plasticity is the critical state. In Figure 2.14 a line is drawn which joins the tops of the yield loci at $\eta = M$, this is called the critical state line (csl).

Undrained Shear Strength in Cam-Clay Framework

In the framework of critical state, a distinction is made between the shear strength of normally consolidated and overconsolidated soils. The ultimate shear strength is defined at the critical state. Literature has shown that using the shear strength at critical state is suitable for the calculation of slope stability (Van Duinen [72].)

A soil with a specific volume v (as shown in Figure 2.15), tested in undrained triaxial compression, will end up on the critical state line at the mean effective stress p'_f. The expression for this mean effective stress is:

$$p'_f = \exp\left(\frac{\Gamma - v}{\lambda}\right) \tag{2.33}$$

where, $\Gamma = N - (\lambda - \kappa)\ln 2$, which is the location of the critical state line in the compression plane as shown in Figure 2.16. With the following expressions for the ultimate value of deviator stress q_f and s_u:

$$q_f = M p'_f \qquad s_u = \frac{q_f}{2}, \tag{2.34}$$

the undrained shear strength can be given as:

$$s_u = \frac{q_f}{2} = \frac{M p'_f}{2} = \frac{M}{2}\exp\left(\frac{\Gamma - v}{\lambda}\right). \tag{2.35}$$

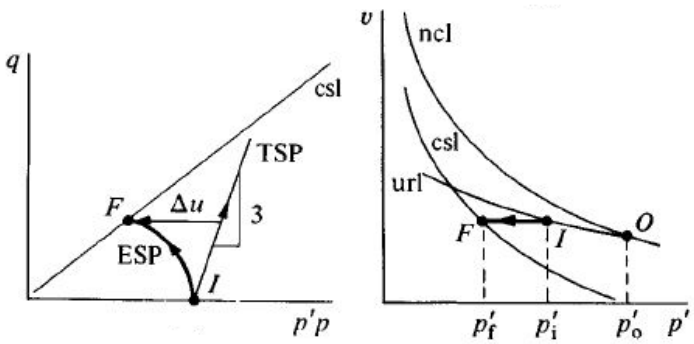

Figure 2.15: Effective Stress Plane and Compression Plane (Wood [74])

The undrained shear strength can be linked with consolidation history. Figure 2.16 shows that the normal compression line and critical state line are parallel in the compression plane. The critical state line can be formalised as:

$$v = \Gamma - \lambda \ln p' \tag{2.36}$$

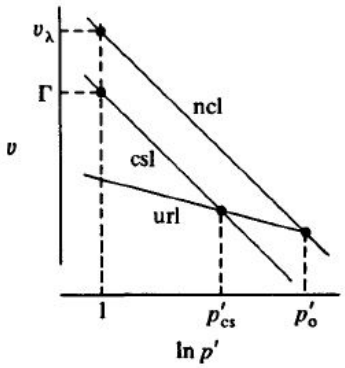

Figure 2.16: Normal Compression Line, Unloading-Reloading Line and Critical State Line (Wood [74])

The volume separation between the normal compression and critical state lines is $v_\lambda - \Gamma$. This separation can also be expressed in terms of pressures. The pressure ratio r is an extra soil parameter and defined as:

$$r = \exp\left(\frac{v_\lambda - \Gamma}{\lambda - \kappa}\right) \tag{2.37}$$

Again, having a look at Figure 2.15, the specific volume of the sample at point I is given by:

$$v_i = v_\lambda - \lambda p'_0 + \kappa \ln n_p, \tag{2.38}$$

where n_p is the isotropic overconsolidation ratio. Using Equation 2.35, the undrained shear strength at point F is on the critical state line is:

$$s_u = \frac{M}{2} \exp\left[\frac{\Gamma - v_\lambda}{\lambda} + \ln p'_0 - \left(\frac{\kappa}{\lambda}\right) \ln n_p\right], \tag{2.39}$$

which can be rewritten to:

$$\frac{s_u}{p_i} = \frac{M}{2}\left(\frac{n_p}{r}\right)^\Lambda, \tag{2.40}$$

where

$$\Lambda = \frac{\lambda - \kappa}{\lambda}. \tag{2.41}$$

This definition for the shear strength will be used in this research in the undrained analysis. In terms of vertical effective stress, the undrained shear strength can be expressed as:

$$\frac{s_u/\sigma'_{vi}}{(s_u/\sigma'_{vi})_{nc}} = \frac{n}{n_p} n_p^\Lambda \tag{2.42}$$

In Table 2.7 all symbols are given for the Modified Cam-Clay model. The model however only uses three parameters λ, κ and M.

Table 2.7: Parameters Modified Cam-Clay Model

λ	isotropic logarithmic compression index		[-]
κ	swelling index		[-]
M	friction constant	$M = \frac{6\sin(\phi')}{3-\sin(\phi')}$	[-]
η	stress ratio		[-]
e	initial void ratio	$\eta = q/p'$	[-]
p'	mean stress	$p' = \frac{\sigma'_{xx}+\sigma'_{yy}+\sigma'_{zz}}{3}$	[kN/m^2]
p'_f	mean effective stress at critical state line		[kN/m^2]
p'_0	mean effective stress during isotropic normal compression		[kN/m^2]
p'_i	initial mean effective stress		[kN/m^2]
q	deviator stress	$q = \left(\frac{(\sigma'_{yy}-\sigma'_{zz})^2+(\sigma'_{zz}-\sigma'_{xx})^2+(\sigma'_{xx}-\sigma'_{yy})^2}{2} + 3\left(\tau^2_{yz}+\tau^2_{zx}+\tau^2_{xy}\right)\right)$	[kN/m^2]
q_f	ultimate value of deviator stress		[kN/m^2]
n	overconsolidation ratio	$n = \frac{\sigma'_{vmax}}{\sigma'_v}$	[-]
n_p	isotropic overconsolidation ratio	$n_p = \frac{p'_{max}}{p'}$ or $\frac{p'_0}{p'_i}$	[-]
σ'_0	pre-consolidation pressure/initial vertical stress		[kN/m^2]
N	location of isotropic normal compression line in $v : \ln p'$ plane		[-]
r	pressure ratio	$r = \frac{p'_0}{p'_{cs}} = \exp\left(\frac{v_\lambda - \Lambda}{\lambda-\kappa}\right)$	[-]

The main advantages and limitations of the Modified Cam-Clay model are summarised in Table 2.8. For a more detailed description of the Modified Cam-Clay model the reader is referred to Section A.2 in the Appendix and the work of Schofield and Wroth [67], Roscoe and Burland [59] and Wood [74].

Table 2.8: Advantages and Limitations Modified Cam-Clay Model

Advantages	Limitations
Takes loading history and stress(path)-dependent stiffness differences into account	Less suitable for overconsolidated clay and in certain unloading stress paths; not suitable for sand
Reasonable model for primary loading of normally consolidated clays and soft soils, which means it is capable of modelling shear induced pore pressures	Critical state failure contour is 'only' Drucker-Prager (but can easily be adapted)
	Inaccurate horizontal/vertical stress ratio in 1D compression
	No secondary compression (creep)
	No anisotropy

2.6.4. SHANSEP Approach

The SHANSHEP (Stress History and Normalised Soil Engineering Properties) framework is introduced by Ladd and Foott [37] and is also described in the work of Ladd [36]. This approach can be used to determine the undrained shear strength of a soil. Rijkswaterstaat [58] currently advises to use this approach to analyse the strengths of impermeable clays. The derivation of this approach is in accordance with the Critical State Soil Mechanics model as introduced by Schofield and Wroth [67]. The concepts of the critical state are already explained in Section 2.5.1 and 2.6.3.

There has been important recognition that there is a close correlation between the normally consolidated undrained shear strength ratio $S = \left(s_u/\sigma'_y\right)_{nc}$ and the overconsolidation ratio $OCR\left(=\sigma'_y/\sigma'_v\right)$ of cohesive soils, according to Ladd [35], Ladd and Foott [37] and Ladd [36]. The shear strength of undrained layers can therefore be determined using the following formulation as described in Ladd [36]:

$$s_u = \sigma'_v \cdot S \cdot OCR^m, \tag{2.43}$$

In case the a material is in a normal consolidation state, OCR is equal to 1 and the maximum stress level previously experienced is not larger than the current stress level. An OCR value higher than 1 describes an overconsolidated state.

In Table 2.9 the parameters are given for the SHANSEP approach. The parameters S and m are soil dependent and testing is required to acquire these parameters. Information is required on the undrained shear strength at an overconsolidation ratio equal to 1 to determine the parameter S. σ_y in the overconsolidation ratio is the yield stress, which is the maximum experienced effective stress in the cohesive soil. Therefore the pre-consolidation pressure must be known very well; the user has to asses the in situ stress history for all stages construction stages, or these pressures have to be estimated. In the work of Ladd and Foott [37] the necessary steps to obtain the SHANSEP parameters are also presented. The interested reader is therefore referred to their work.

Table 2.9: Model Parameters SHANSEP

s_u	undrained shear strength		[kN/m^2]
σ'_y	yield stres		[kN/m^2]
σ'_v	in-situ effective vertical stress		[kN/m^2]
S	normally consolidated undrained shear strength ratio	$\left(\frac{s_u}{\sigma'_y}\right)_{nc}$	[-]
OCR	overconsolidation ratio	$\frac{\sigma'_y}{\sigma'_v}$	[-]
m	strength increase component		[-]

2.6.5. Hardening Soil Model

Another constitutive model which is capable of representing the hardening behaviour of soil, is the model introduced by Schanz et al. [65]: the Hardening Soil Model (HSM). This model is formulated in the framework of classical theory of plasticity. It is an advanced model for simulating the behaviour of different soil types, both for soft and stiff soils. The formulation of the HSM is based on the assumption of a hyperbolic relation between the vertical strain ϵ_1 and the deviatoric stress q. This relationship is shown in Figure 2.17. The soil is described much more accurately by using three different stiffness moduli, also shown in Figure 2.17.

Duncan and Chang [16] already introduced a nonlinear elastic criterion model to model the behaviour of soil as it approaches failure. Their nonlinear stress-strain relationship is also defined as a hyperbolic function. Nonetheless, the Hardening Soil Model has quite some advantages compared to the purely elastic Duncan-Chang model and the elastic-perfectly plastic model Mohr Coulomb. These advantages, but also the limitations of the model, are summarised in Table 2.10. This model will only be used to compare the results of the slope stability analysis based on a linear or nonlinear stress analysis. It will not be implemented in the maximum available shear strength determination, therefore the reader is referred to A.2.1 for the full description of this model. And for the complete derivation of the Hardening Soil model, the reader is referred to Schanz et al. [65].

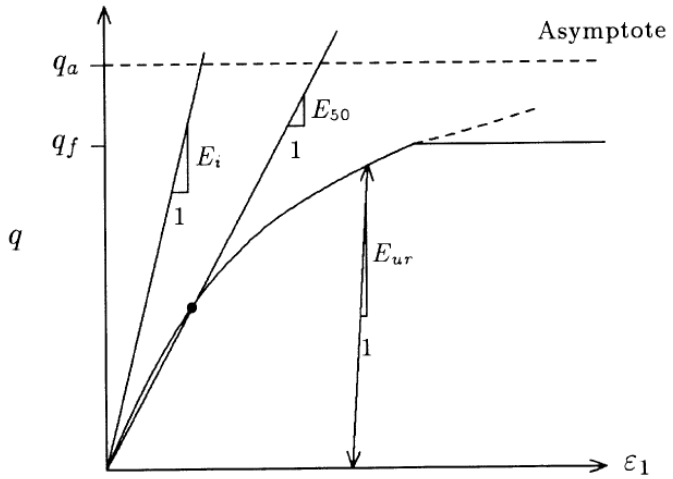

Figure 2.17: Hyperbolic Stress-Strain Relation in Primary Loading for a Standard Drained Triaxial Test (Schanz et al. [65])

Table 2.10: Advantages and Limitations Hardening Soil Model

Advantages	Limitations
Better non-linear formulation of soil behaviour in general	No peak strength and softening (immediate residual strength)
Distinction between primary loading and unloading/reloading	No accumulation of strain or pore pressure in cyclic loading
Memory of preconsolidation stress	No secondary compression (creep)
Different stiffnesses for different stress paths	No anisotropy
Well suited for unloading situations with simultaneous deviatoric loading	$E_{50}/E_{oed} > 2$ difficult to input
Takes into account soil dilatancy	
Yield surface can expand due to plastic straining	

2.7. Chapter Summary

In this chapter first an overview of the LEM and FEM are given. The main limitation of the limit equilibrium methods is that the analysis works with a static pore pressure field, in which the deformations in the soil are not coupled with the groundwater flow. Therefore no information on strains and deformations is given. Furthermore, the methods requires a predefined slip surface which has to be divided into slices. The most common reason for a LEM to be insufficient is when a correct display of the stresses is needed or if the slope stability in combination with a construction is examined. In contrary, the FEM is able to perform an adequate stress analysis. However, this methods uses the shear strength reduction method to find the critical slip surface. One limitation of the SSRM is that it can only give one critical slip surface. Another limitation is that the SSRM only reduces the shear strength parameters ϕ and c and no use is made of the shear strength expressions given by advanced constitutive models. The reason why LEM are applied more often than FEM is because FEM is more time-consuming. Another advantage of the LEM is that it gives the safety factor of every given slip surface, such that the stability of all relevant slip surfaces can be calculated.

Due to these limitations, a new type of method is proposed, namely the enhanced limit method. In this method a single finite element analysis is performed to obtain the occurring stresses in the soil. The method requires a safety factor definition, which can be of a strength, stress or strength-stress level approach. In this research a strength level approach will be implemented. The safety factor is defined as the sum of maximum available shear strength divided by the sum of mobilised shear stress along a slip surface. The ELM requires an optimisation method, such as dynamic programming, simplex or the genetic algorithm, to search for the most critical slip surface.

The second part of this chapter is focused on the soil mechanics. The differences between a drained and undrained analysis are highlighted. Special attention is given to the occurrence of the shear induced pore pressures, which are of interest in a stability analysis. These excess pore pressures reduce the effective stress of the soil, resulting in a strength decrease. An appropriate soil model should therefore be used to model these pore pressures. Multiple soil models and approaches are discussed, namely Mohr-Coulomb, Matsuoka-Nakai criterion, Modified Cam-Clay model, SHANSEP and the Hardening Soil model. The Coulomb criterion will be used to determine the shear strength of drained soils. The criterion of Matsuoka-Nakai will be included to examine the influence of the intermediate principal stress on the shear strength. The Modified Cam-Clay is considered, since this model is able to capture the shear induced pore pressures in an undrained analysis. The SHANSEP approach will be applied in the LEM program D-Stability and the Hardening Soil Model will be used to model a nonlinear stress-strain relationship in the finite element program PLAXIS. Both these programs will be introduced in the next chapters.

3
Methodology

In this chapter the methods are outlined which are used to reach the research goal.

3.1. Stress Analysis

The first step in the proposed method is the stress analysis. This stress analysis is performed in the program PLAXIS, Brinkgreve et al. [7]. PLAXIS can be used to perform finite element analyses within geotechnical engineering problems. The program is able to execute advanced finite element analysis of soil and rock deformation and is able to capture the groundwater and heat flow as well. Many advanced constitutive models for simulation of the (non)linear and time-dependent behaviour of soils are present in the programme. PLAXIS is also capable of performing a slope stability analysis, in which the factor of safety is determined using the shear strength reduction technique.

For this research PLAXIS will mainly be used for the stress analysis. The shear strength reduction method will also be used to compare the results with the proposed method. The dike profile of interest is used as input for the program. Soil characteristics, waterlevels, and possible loading stages have to be defined in the program as well. The soil model which is used to determine the maximum available shear strength does not have to coincide with the soil model used in PLAXIS to find the stresses. In the drained analysis in this research, the stress-strain relationship is assumed to be linear elastic. The SSRM uses the parameters of the Mohr-Coulomb model to obtain a safety factor.

3.1.1. Interpolation

PLAXIS divides the slope into triangular elements to calculate the displacements and stresses in the slope. The basic finite element in PLAXIS is a triangle, consisting of 6 or 15 nodes and 12 Gaussian integration points (stress points), as shown in Figure 3.1. The finite element calculation gives the values for the displacements at every node and the stresses at every stress point.

The output of the stress analysis has to be edited for further usage, such that the stresses can be used more conveniently in the slope stability analysis. In this research the x and y coordinates of the mesh obtained from PLAXIS are interpolated to a regularly-spaced grid of data on an interval which is chosen by the user. The values on the points of the new grid are interpolated values, or the point has to be present as a node or stress point in PLAXIS already. The used method to generate the grid with regularly-spaced points from the irregularly-spaced data obtained from PLAXIS is linear interpolation.

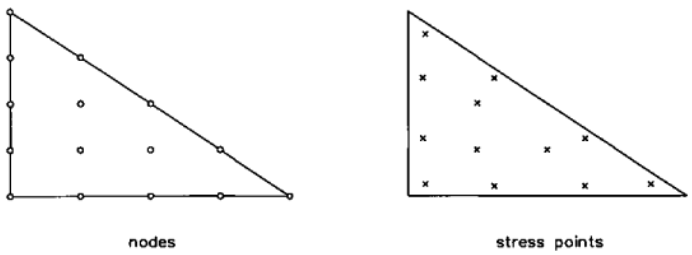

Figure 3.1: Location of Nodes and Stress Points in a Basic Finite Element in PLAXIS (Barneveld [3])

3.2. Strength Analysis

As discussed in Section 2.5, in this research the safety factor will be calculated by comparing the mobilised shear stress with the maximum available shear strength, using the following expression:

$$\text{FoS} = \frac{\sum_{i=1}^{n} \tau_{fi} \Delta L_i}{\sum_{i=1}^{n} \tau_i \Delta L_i}. \tag{3.1}$$

The advantages of using this definition are already discussed in Section 2.5 as well. To determine the maximum available shear strength, two definitions are used. Namely the Coulomb criterion and the shear strength expression of the Modified Cam-Clay model. The expressions are given as:

$$\tau_i = c' + \sigma' \tan\phi', \qquad \text{drained,} \tag{3.2}$$

$$\tau_i = s_u = \frac{M}{2}\left(\frac{n_p}{r}\right)^{\Lambda} p_i, \qquad \text{undrained.} \tag{3.3}$$

For the full description of the parameters the reader can go back to Sections 2.6.1 and 2.6.3.

3.3. Genetic Algorithm

As previously described in Section 2.3, there are multiple optimisation problems which can be used to find the critical slip surface. In this research the genetic algorithm, as already introduced in Section 2.3, is used to find the critical slip surface. Equation 3.1 is used to determine the safety factor and the genetic algorithm will search for the slip surface which gives the lowest safety factor. Li et al. [43] presents a real coded genetic algorithm to locate the critical slip surface and has used different methods to calculate the factor of safety, namely: Spencer, Morgenstern-Price and a finite-element based definition. They have investigated six different slope examples and it is found that the algorithm in combination with finite-element based definition as given in Equation 3.1 gives the lowest safety factor compared to the safety factors given by Morgenstern-Price or Spencer.

The genetic algorithm uses a pool of solutions in an iterative procedure to find the optimal solution. Each chromosome (solution) has a fitness value, which is found by evaluating the chromosome with the objective function. In this optimisation problem the fitness value is defined by the factor of safety. The aim of the optimisation tool is to find the chromosome (slip surface) which results in the lowest safety factor. The genetic algorithm works in two main stages: generating the initial population followed by reproducing a new (and better) population.

First the initial population is generated, in which every individual (or chromosome) is a slip surface. A slip surface is defined by the x- and y-coordinates of a number of nodes as illustrated in Figure 3.2. For every slip surface the safety factor is determined using the definition given by Equation 3.1. The population is then sorted based on the fitness value of the individuals. To ensure that the best solution (the slip surface with the lowest safety factor) is never lost, the individuals which give the lowest safety factor are always selected for the next population.

This selection of individuals is then used to generate the next population. From this initial population pairs are made randomly which will represent the parents. From all pairs of parents offspring will be generated in the crossover process. Hereafter, all the offspring will be modified in the mutation process. Both the crossover and mutation process will be described in more detail later in this section. After the completion of the mutation process, the generation of the new population is finalised. This new population is then combined with the 'parent' population. Based on the fitness ranking of these individuals a new selection will be made and used as the next 'parent' population. The process of reproduction, crossover, mutation and selection is repeated a couple of times or until convergence of the safety factor occurs. The processes of the genetic algorithm to optimise the safety factor are also shown in the flowchart in Figure 3.5.

All processes of the genetic algorithm which are described briefly above will be elaborated on separately in the following sections. The functions are based on the work of Cheng et al. [10] and Jurado-Piña and Jimenez [31].

3.3.1. Generation of Trial Slip Surfaces

The first step in the genetic algorithm is to create a population of initial slip surfaces. Cheng [9] presents an algorithm to find a trial slip surface which is admissible, which means that the slip surface is concave upward. In Figure 3.2 such an admissible slip surface is shown, generated by the proposed algorithm.

The ground surface is given by the function $y = y_1(x)$ and the lower bound surface is represented by $y = R(x)$. This lower bound can be given by the presence of a bed rock surface, or any other material or construction that is not expected to slide due to instability, or the engineer can give a good estimate of this lower bound.

The slip surface is represented by $N+1$ vertices $[V_1, V_2, ..., V_{N+1}]$, where N is the number of vertical sections. These vertices are defined by the coordinates $(x_1, y_1), (x_2, y_2), ..., (x_{N+1}, y_{N+1})$, and each section can be identified by two adjacent vertices. Every slip surface can be identified by the control variable vector $X = [x_1, y_1, x_2, y_2, ..., x_n, y_n, x_{N+1}, y_{N+1}]$. To find a realistic slip surface, the slip surface should be concave upward.

The variables x_1, y_1, x_{N+1} and y_{N+1} can be determined from the ground profile, therefore these are not independent control variables. For a slope with N sections, there will be $2N$ independent control variables. If the slip surface is divided equally in the horizontal directions, then the x-coordinates of the vertices can be found easily with the following equation:

$$x_i = x_1 + \frac{x_{N+1} - x_1}{N} \cdot (i-1) \qquad i = 2, ..., N \tag{3.4}$$

The following step is to determine the y-coordinates for the vertices $i = 2, ..., N$. After defining the values x_1 to x_{N+1}, the range $[y_{2\min}, y_{2\max}]$ can be determined from the geometry. The point y_2 can then be randomly generated within the range $[y_{2\min}, y_{2\max}]$. For the remaining $i = 3, ..., N$ points the y-coordinates can be determined using the following steps:

1. Draw a line between V_{i-1} and V_{i+1}, this line is called L_G.
2. Draw a vertical line at $x = x_i$.
3. The point of intersection of L_G and the line at x_i is called point y_G.
4. Draw a line between V_{i-2} and V_{i-1} and extend this line until x_i, this line is called L_H.
5. The point of intersection of line L_H and the line at x_i is called point y_H.
6. The bounds for point y_i can then be determined as:

$$y_{i,min} = \max\{y_H, R(x_i)\} \qquad y_{i,max} = \min\{y_G, y_1(x_i)\}. \tag{3.5}$$

With this procedure the remaining y-coordinates are found for the slip surface.

With these steps M_{init} trial slip surfaces are created for the initial population. The recommended value for M_{init} will be discussed later on, when the algorithm is applied to some examples. The slope profile is already specified in Python in the interpolation phase. The user only has to define the bounds in which the extreme nodes should be located. The extreme nodes V_1 and V_{N+1} are randomly generated within these allowable intervals.

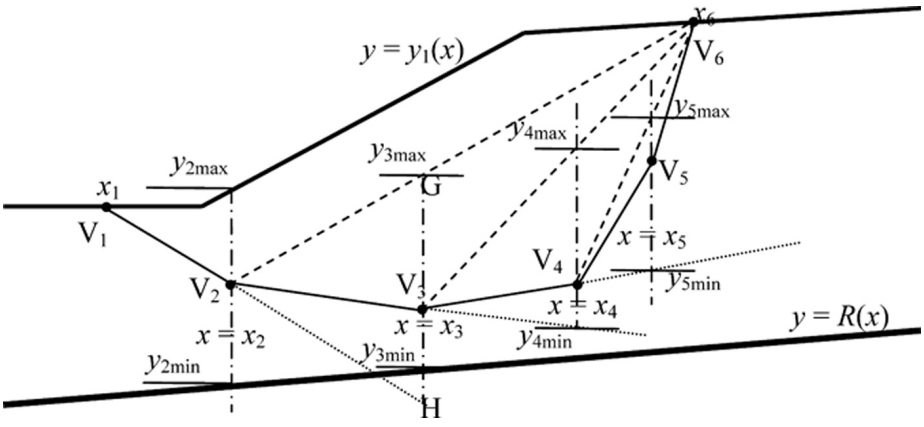

Figure 3.2: Procedure in Generating Admissible Slip Surface (Cheng [9])

3.3.2. Crossover

In the previous step a population of slip surfaces is created and within this population pairs are made randomly. There will be $M/2$ number of pairs. Each pair of individuals is seen as the parents of which two offspring will be created. A pair contains two slip surfaces S_i and S_j of which S_i gives the lowest safety factor. The heuristic crossover operator produces one new slip surface as offspring, defined as:

$$S'' = S_i + \zeta(S_i - S_j), \tag{3.6}$$

where ζ is a random number uniformly distributed between [0,1]. For every pair of corresponding nodes (the first node of the first parent and the first node of the second parent, and so on,) the difference is computed between the y-coordinates and x-coordinates of the nodes. These differences are multiplied with ζ and then added to slip surface S_i, such that the nodes of S_i will be shifted. This gives the resulting offspring. For every pair of parents the heuristic crossover is performed twice, such that every pair of parents creates two children. The x-coordinates of the extreme nodes of the newly created offspring should be in the predefined bounds and the y-coordinates should lie in the ground profile. To ensure that S'' fulfils these geometrical constraints some additional steps are required:

1. Check whether the extreme nodes V_1'' and V_{N+1}'' are within the allowable extreme intervals $e = 1, N+1$
   (a) If V_e'' lies within the extreme allowable interval, this will be taken as the extreme node of the offspring's slip surface
   (b) If V_e'' lies outside the extreme allowable interval, two cases can occur:
      i. If V_e'' lies on the left (more negative) side of the allowable interval, the minimum of the allowable interval is used as the coordinate for the extreme node
      ii. If V_e'' lies on the right (more positive) side of the allowable interval, the maximum of the allowable interval is used as the coordinate for the extreme node
2. Having obtained the new extreme vertices V_1'' and V_{N+1}'', the new slip surface is 'recoded' as will be described in Section 3.3.3. If the new slip surface is admissible, i.e. upwards-concave, it is taken as the offspring of the pair of parents. Otherwise it is rejected and the crossover procedure is carried out again to create a new offspring. If no valid offspring is found after a certain number of crossover trials, then the parent S_i is returned as the offspring.

3.3.3. Recoding of Individuals

When one or both of the extreme nodes are modified, the slip surface has to be recoded, such that the spacings between the x-coordinates of the nodes are still evenly divided. It is not strictly necessary for the algorithm to keep the nodes evenly spaced. However, by keeping the x-coordinates of the nodes evenly divided, only the first and last x-coordinate of the slip surface have to be saved to reconstruct the x-coordinates of all nodes. The new extreme nodes are used to produce equally-spaced lines L_i' ($i = 2, ..., N+1$), in which $N+1$ is the number of nodes. The recoded interior nodes $V_2', ..., V_N'$ are found at the intersection of the lines L_i' with the original slip surface as shown in Figure 3.3. This figure shows the example of the right extreme node (V_{N+1}) being modified in the negative x-direction (V_{N+1}'). This ensures that the rest of the nodes $V_2, ..., V_N$ are moved in the negative x-direction as well ($V_2', ..., V_N'$). Since the new locations of the recoded nodes are still on the same slip surface as before the extreme node was modified, the recoded slip surface is still admissible.

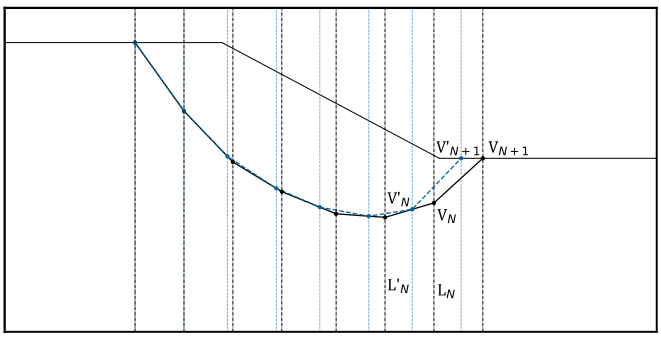

Figure 3.3: Recoding of Nodes

3.3.4. Mutation

The crossover process generates a new population 'the offspring'. All individuals in this generation will go through the process of mutation, however, it is possible that not every node, or not even a single node, will be mutated. A random variable r_1 is a uniformly distributed number between [0,1]. For every node in an individual this random variable is generated. If r_1 for a particular node is smaller than a predefined mutation rate ρ_m, then that node will be subjected to mutation, otherwise that node will not be mutated and remain at its location.

In this research uniform a mutation is applied, thus the random variable r_1 is uniformly distributed. The procedure is slightly different when the node is 'extreme' ($i = 1$ or $i = N+1$) or 'interior' ($i = 2,...N$). Both procedures will be described below.

- 'Interior' nodes. For every node V_i ($i = 2,...,N$) a feasible interval $[P_0, P_1]$ is computed. This interval can be seen in Figure 3.4. P_0 is found as the intersection between L_i, which is the x-coordinate of node V_i, and the line that connects the nodes V_{i-1} and V_{i+1}. To find P_1 two lines are created. First, the line between nodes V_{i-2} and V_{i-1} is extended until it intersects with the x-coordinate of node V_i (line L_i), this gives point P_{11}. Secondly, the line between nodes V_{i+1} and V_{i+2} is also extended until it intersects with L_i, this gives point P_{12}. P_1 is the point which is closer to V_i among P_{11} and P_{12}. Note that for node V_2 only point P_{12} exists and for node V_N only point P_{11} exists and automatically will be point P_1. Using P_0 and P_1, two lines are defined: l_0 is the vertical distance between point P_0 and V_i and l_1 the vertical distance between point P_1 and V_i. To choose the direction in which the node will be mutated to: in the positive y-direction (in the direction of P_0) or in the negative y-direction (in the direction of P_1), a probability of selection is defined proportional to the lengths of line l_0 and l_1. After a direction is chosen, the mutated node is computed as $V_i' = V_i + (P_j - V_i)\zeta$, where ζ is a uniformly distributed random number between [0,1]. Note that the mutation only changes the y-coordinate of the node.

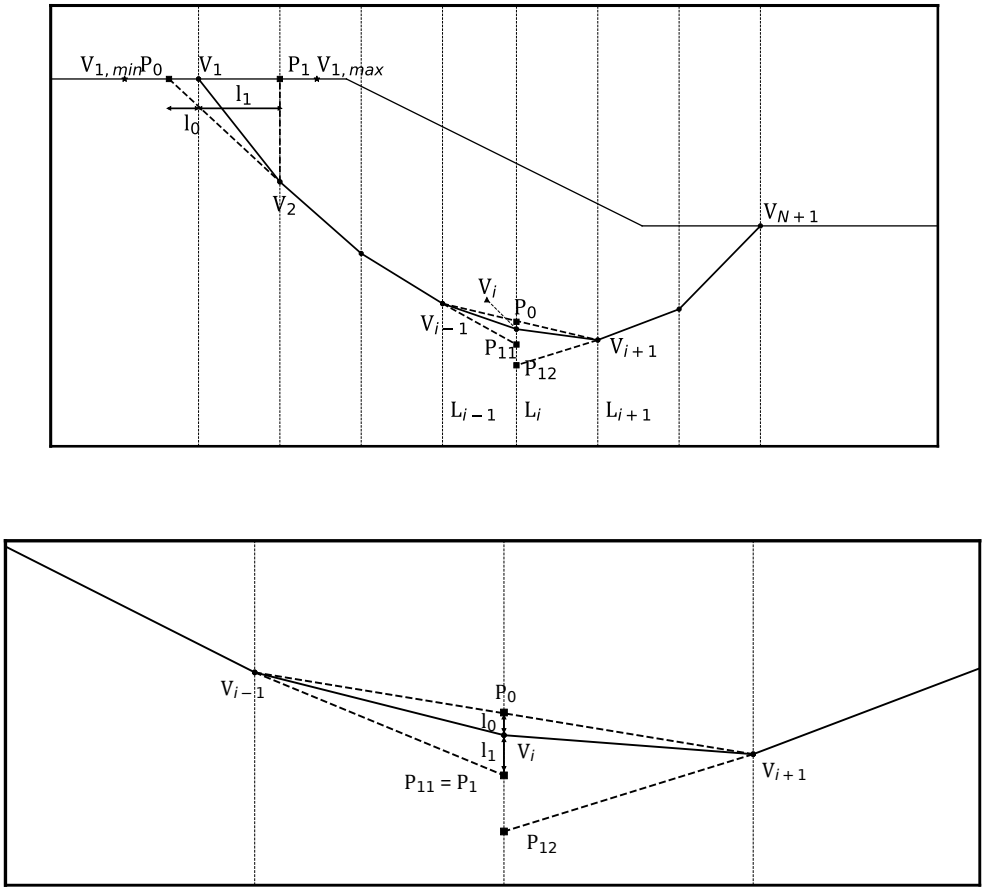

Figure 3.4: Uniform Mutation of Single Nodes based on Jurado-Piña and Jimenez [31]

- 'Extreme' nodes. For the extreme nodes also an interval $[P_0, P_1]$ is computed, but in a different manner than for the interior nodes. The procedure for the left extreme node V_1 will be discussed here, but the procedure is analogous for V_{N+1}. To find P_0 the line between nodes V_2 and V_3 is extended until it intersects with the ground surface, this gives P_0. P_1 is given by the intersection of the x-coordinate of node V_2 and the ground surface. Both are shown in Figure 3.4. If P_0 lies outside the allowable extreme interval, P_0 is moved to the minimum of the allowable interval. If P_1 lies outside the allowable extreme interval, P_1 is moved to the maximum of the allowable interval. Using the $[P_0, P_1]$ interval, lines l_0 and l_1 are defined again. A direction is chosen in the same matter as for the interior nodes and the extreme node is mutated as $V_i' = V_i + (P_j - V_i)\zeta$. If one or both of the extreme nodes have been mutated, the slip surface needs to be recoded again, as described in Section 3.3.3, such that the spacing between the nodes remains equal. This recoding is performed after both extreme nodes possibly have been mutated.

After the mutation procedure of one individual (where zero to all nodes might have been mutated), it is checked whether the mutated nodes lie inside the allowable search domain. This check ensures that the y-coordinates do not surpass the ground surface or pass below the lower bound (line $y = R(x)$ in Figure 3.2). A check is also performed to see if the new mutated slip surface is admissible, i.e. upwards-concave. In case the mutation process has made the slip surface inadmissible, then the original individual, before the mutation process, will be used as the final slip surface.

3.3.5. Fitness Computation and Selection

After the mutation process, the selection of the initial population (the parents) is combined with the generated population (the offspring). For every individual in this new population the safety factor is determined using the method as described in Section 2.5. The individuals are hereafter ranked based on their scores for the factor of safety. Based on this ranking, a selection of M individuals is made from this combined population. This selection is then used again as a parent generation in the next iteration of the optimisation problem. The complete process is shown in Figure 3.5. The optimisation process is stopped after a stopping criterion is met. In this study a stopping criterion is used which includes a maximum number of iterations (every iteration creates a new population) and convergence of the safety factor. If the maximum number of iterations is reached, but the safety factor is still decreasing more than a specified value ϵ (about 0.001), then the optimisation will not stop, but create a new generation again. Thus even when the maximum number of iterations is achieved, the optimisation will only stop when the safety factor is no longer optimised.

3.4. Comparison LEM and FEM

To examine the performance of the new approach, multiple case studies will be performed with the new approach, as well as with a LEM and FEM. The parameter of interest will be the safety factor. The safety factor of the finite element method is obtained with the $\phi - c$ reduction method, which is available in PLAXIS. The program D-Stability (Deltares [13]) will be used to acquire the safety factor with a limit equilibrium approach. The application D-Stability contains multiple limit equilibrium methods which can analyse slope stability, namely the method of slices, driving and resisting moments, Bishop, Uplift-Van and Spencer. The optimisation procedures to determine the slip surface contained in the application are grid search, genetic algorithm and Adaptive Particle Swarm Optimisation.

3.5. Chapter Summary

In this chapter the various methods are described, which are implemented in this research. It is explained that the finite element analysis program PLAXIS is used to perform the stress analysis. The stresses of interest are then exported into Python. The safety factor is calculated by comparing the mobilised shear stress with the maximum available shear strength along a slip surface. To calculate the maximum available shear strength, both the Coulomb criterion as Modified Cam-Clay model are applied. To find the most critical slip surface, the genetic algorithm is implemented. This algorithm contains multiple steps. The first step is to create an initial population of trial slip surfaces. From this initial population a new generation of slip surfaces is created in the crossover process. The new generation is hereafter mutated, such that enough diversity is present between the slip surfaces. Then the safety factor is calculated of all the slip surfaces and a selection of the best solutions is used in the next iteration. This process is performed a number of iterations, until the safety factor is converged. These steps are discussed elaborately in this chapter.

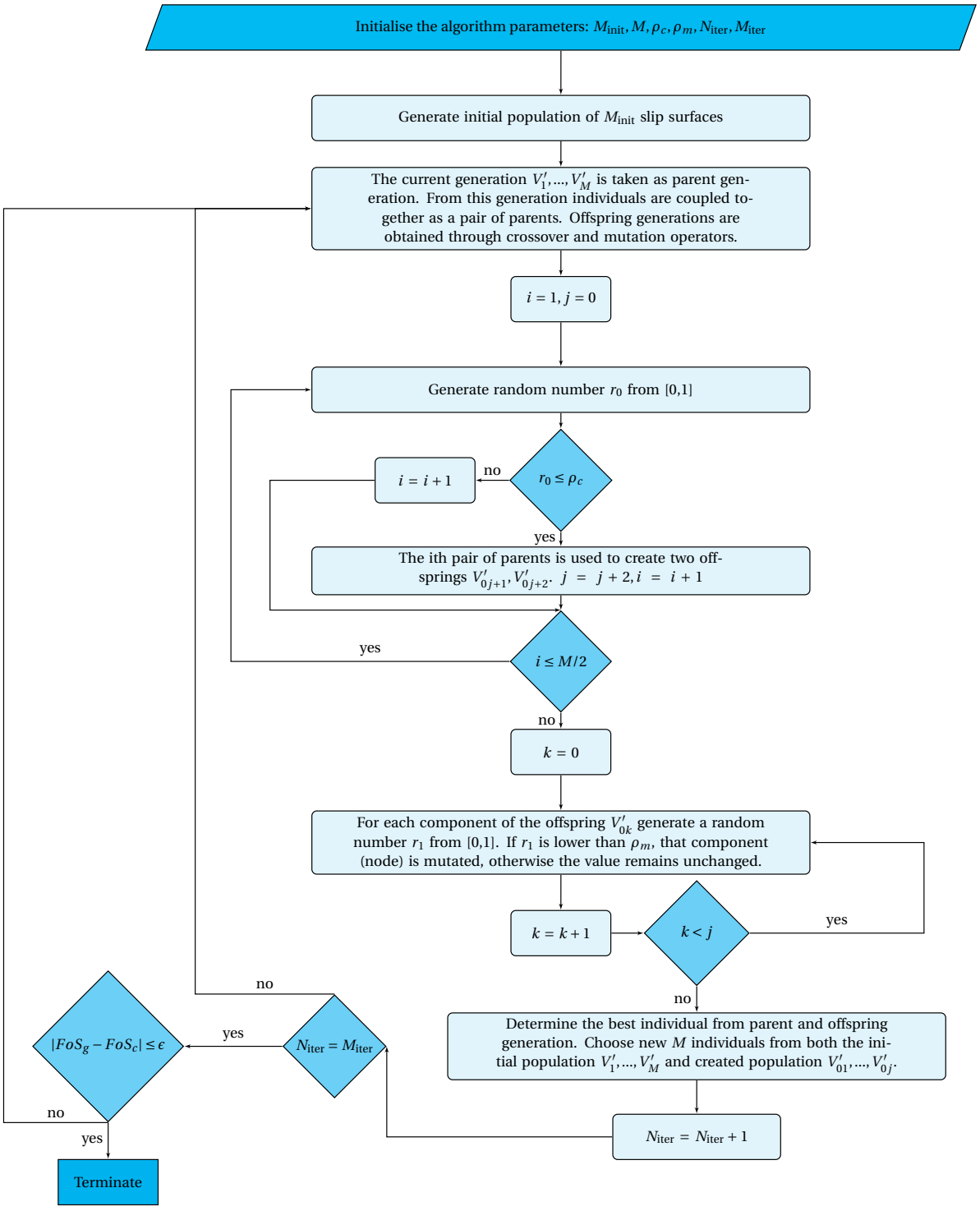

Figure 3.5: Genetic Algorithm to Determine the Optimal Slip Surface

4
Case Studies

In this chapter the results of a number of examples are reviewed, which demonstrate the proposed genetic algorithm to be efficient in finding accurate solutions to various slope stability problems. These examples, which are increasing in complexity, are obtained from literature, such that the results can be compared. For all examples holds that the stresses and pore-water pressures are computed using the finite element program PLAXIS. As mentioned before, the stress-strain relationship is assumed to be linear elastic in the stress analysis. PLAXIS is also used to determine the safety factor using the shear strength reduction method.

Some of the input parameters for the genetic algorithm have a big influence on the performance, and therefore also on the computation time of the algorithm. The sensitivity of these parameters will be discussed in the next chapter. To obtain the results presented in this chapter, the initial population size M_{init} is set at 100, the selection size M is 20 and the number of sections N is set at 7. These values are chosen based on the sensitivity analysis. Note that often a lower safety can be found than the ones shown in this chapter. However, finding these lower safety factors require a much longer computation time.

4.1. Example 1: Unbraced Vertical Cut in clay

In Duncan et al. [15] the failure of a vertical excavated slope is described. This slope is shown in Figure 4.1. The average confined compressive strength of the clay is reported to be 100.55 kPa (1.05 tsf) and the unit weight of the clay is given as 18.85 kN/m^3 (120 pcf). An analytical solution for a vertical slope in cohesive soil is given by Duncan et al. [15] as:

$$F = \frac{4c}{\gamma H} \tag{4.1}$$

For an undrained shear strength of s_u = 50.27 kPA (1050 psf) and a height of 9.61 meter the safety factor is calculated as 1.11. The critical slip surface found by the genetic algorithm has a safety factor of 1.099 and is shown in Figure 4.1. The resulting critical slip surface, with its corresponding safety factor indicates that the genetic algorithm is working properly. Hence, the following examples will be increasing in complexity.

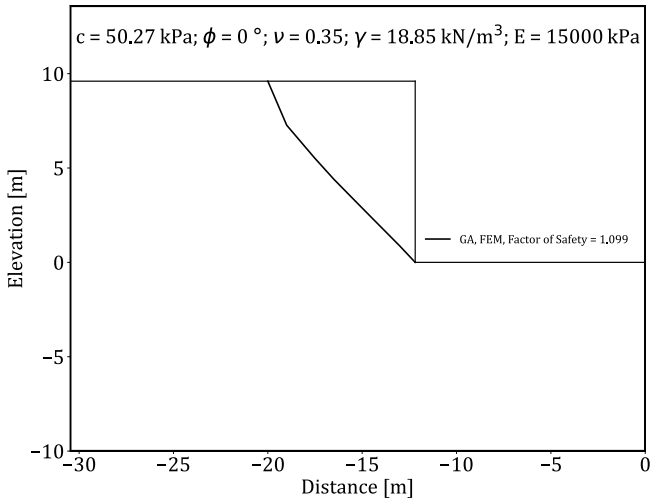

Figure 4.1: Critical Slip Surfaces obtained for Vertical Cut Slope

4.2. Example 2: Simple Homogeneous Wet Slope

In this section the results of the analysis of a simple homogeneous slope at 2:1 are presented. This example is retrieved from the paper of Pham and Fredlund [53]. In their research they have used a dynamic programming technique as the search algorithm and the calculation of the safety factor is similar to the definition used in this research, as described in Section 2.5. Differences with Pham and Fredlund [53] are expected, since their method to create slip surfaces is quite different compared to the method applied in this research. Optimisation is performed on segments of the slip surface, instead of on the complete slip surface as proposed in this report. This example is referred to as being in the wet condition, where the groundwater table passes through the toe of the slope. The results obtained with the genetic algorithm are compared to the safety factors found with the shear strength reduction method in the FEM, with the values produced by limit equilibrium methods Bishop and Spencer and with the safety factors found in literature. The resulting critical slip surface is shown in Figure 4.2 and all results of the safety factors are given in Table 4.1.

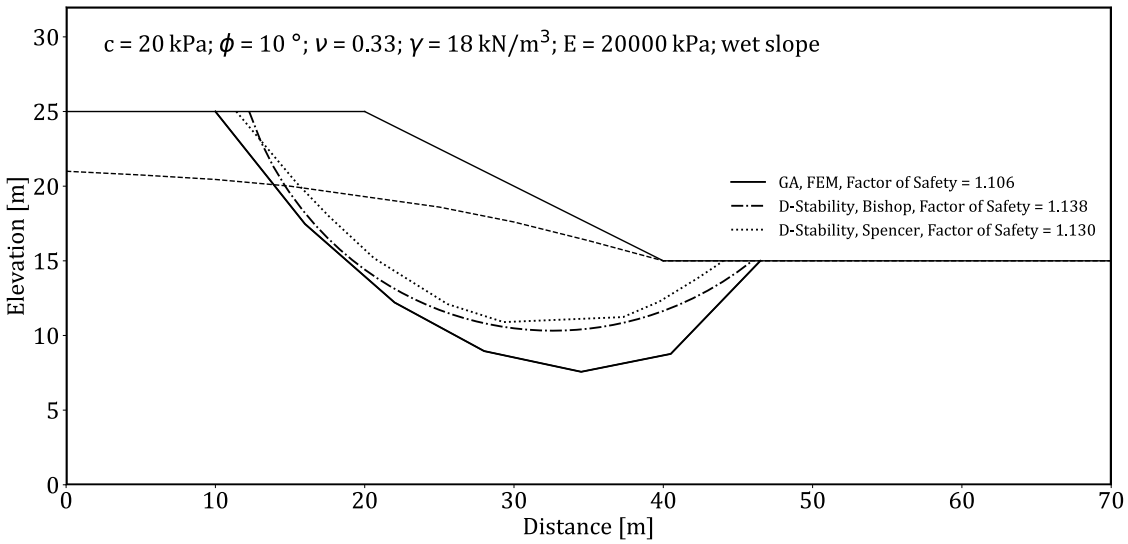

Figure 4.2: Critical Slip Surfaces obtained by Various Methods for Wet Condition

The critical slip surface determined by the GA tends to go slightly deeper than both critical slip surfaces found by D-Stability. This result is in accordance with the findings by Pham and Fredlund [53]. With their optimisation program DYNPROG they also found slip surfaces which were slightly deeper than the slip surfaces found by the limit equilibrium method.

The safety factor found with the genetic algorithm is a bit higher than the values found in literature, as shown in Table 4.1. This can have two causes. Firstly, the genetic algorithm is only performed a limited number of times using the parameters as described at the beginning of this chapter, due to the long computation time. Allowing the algorithm to run more iterations will result in a lower safety factor. Secondly, Pham and Fredlund [53] do not consider potential slip surfaces which contain negative shear stresses. In their research they state that the resisting force must always act in the direction opposite to the mass movement. This is used as the kinematical restriction applied to the shape of the slip surface in their study. Thus if the actuating force of a segment along the slip surface is in the contrary direction of the mass movement, then this segment is removed from the optimisation search. Consequently, the resulting critical slip surface will not hold any segments with a negative shear stress. In this study however, these segments are kept in the search algorithm. If a slip surface is created with many segments containing a negative shear stress, then the safety factor will be very high. This follows naturally from the definition of the safety factor. Since the genetic algorithm only uses a selection of the best solutions to generate the offspring, these slip surfaces will no longer be considered in the next generation. However, it is possible that the given critical slip surface can contain negative shear stresses, this is often at the beginning or end of the slip surface. This part will contribute as a resisting force, which will lead to the increase in the safety factor. The result as shown in Figure 4.2 contains a small segment at the top with resisting shear stresses. This can be the explanation for the slightly higher safety factor found by the genetic algorithm.

Table 4.1: Minimum Factors of Safety for the Examples Investigated

Search Approach	Method Calculation FoS	Minimum FoS	Computing Time [s]
Example 1			
Analytical (Duncan et al. [15])	Analytical	1.110	Unknown
PLAXIS (this research)	SSRM	1.069	21
GA (this research)	Finite-element-based	1.099	71
Example 2			
DP (Pham and Fredlund [53]	Finite-element-based	1.041	Unknown
SLOPE/W (Pham and Fredlund [53])	Bishop	1.167	Unknown
PLAXIS (this research)	SSRM	1.078	85
D-Stability (this research)	Bishop	1.138	Unknown
D-Stability (this research)	Spencer	1.130	Unknown
GA (this research)	Finite-element-based	1.106	1295
Example 3			
DP (Pham and Fredlund [53])	Finite-element-based	1.413	Unknown
SLOPE/W (Pham and Fredlund [53])	Morgenstern-Price	1.485	Unknown
SLOPE/W (Pham and Fredlund [53])	Janbu	1.293	Unknown
Real-coded GA (Li et al. [43])	Finite-element-based	1.393	3.47
Real-coded GA (Li et al. [43])	Morgenstern-Price	1.408	5.97
PLAXIS (this research)	SSRM	1.415	74
D-Stability (this research)	Bishop	1.364	Unknown
D-Stability (this research)	Spencer	1.372	Unknown
GA (this research)	Finite-element-based	1.326	1284
GA (this research)	Finite-element-based (M-N)	1.434	415
Example 4			
DP (Pham and Fredlund [53])	Finite-element-based	1.000	Unknown
SLOPE/W (Pham and Fredlund [53])	Morgenstern-Price	1.140	Unknown
Real-coded GA (Li et al. [43])	Finite-element-based	0.977	4.74
Real-coded GA (Li et al. [43])	Morgenstern-Price	1.017	9.42
PLAXIS (this research)	SSRM	1.007	54
D-Stability (this research)	Bishop	1.183	Unknown
D-Stability (this research)	Spencer	0.999	Unknown
GA (this research)	Finite-element-based	0.995	843
Example 5			
PLAXIS (this research)	SSRM	1.081	24
GA (this research)	Finite-element-based	1.067	1195
Example 6			
D-Stability (POVM [55])	Uplift-Van	0.883	Unknown
PLAXIS (POVM [55])	SSRM	0.9	Unknown
GA (this research)	Finite-element-based	0.675	1726

4.3. Example 3: Nonhomogeneous Slope

Examples 3 and 4 are presented by Pham and Fredlund [53] and are also analysed by Li et al. [43]. As mentioned before, Pham and Fredlund [53] use a dynamic programming technique as the search algorithm, whereas Li et al. [43] use a genetic algorithm. Li et al. [43] use multiple methods to calculate the safety factor including a finite-element-based definition as applied in this research, as well as the Morgernstern-Price method. Differences with Li et al. [43] are expected, since their genetic algorithm deviates from the genetic algorithm proposed in this research. In the mutation process, a dynamic bounding technique is used to find the new coordinates of the vertices. These bounds are different than the ones proposed in Section 3.3.4. Furthermore, Li et al. [43] add vertices during the optimisation process, whilst in this research the number of vertices is kept constant during the optimisation.

The first inhomogeneous slope which is analysed is shown in Figure 4.3. The two soil layers are slightly different and their properties are shown in the figure. The safety factor found in this research is substantially lower compared to the values found in literature, the FEM and LEM analysis, as shown in Table 4.1.

The critical slip surface computed with the genetic algorithm shows a slip surface which is deeper near the toe compared to the slip surface obtained from Bishop and Spencer. This is in accordance with the finding of Pham and Fredlund [53], who also found slip surfaces with a deeper toe.

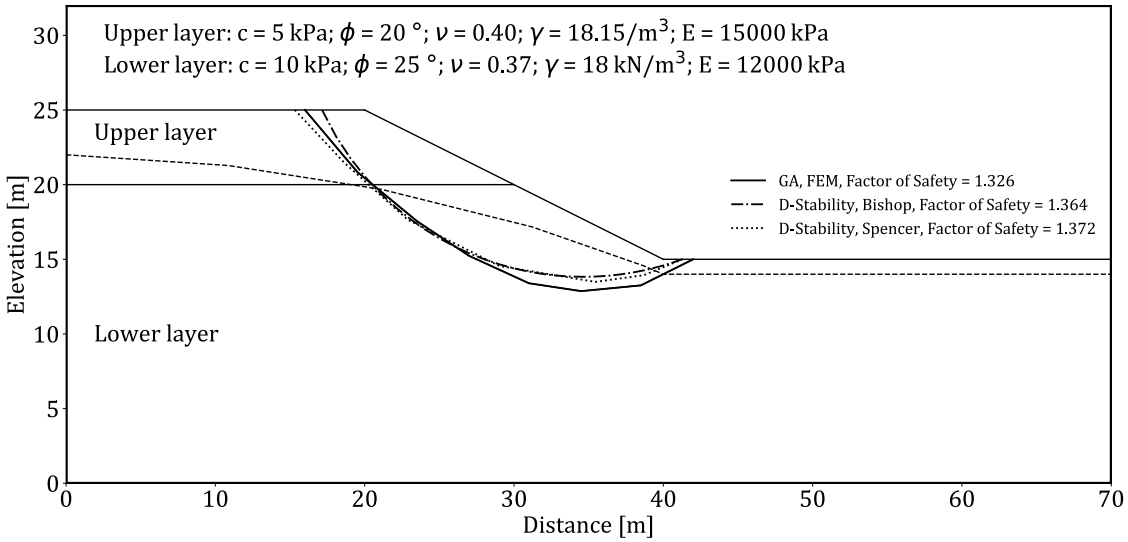

Figure 4.3: Critical Slip Surfaces obtained by Various Methods for Nonhomogeneous Slope 1

This example is also used to examine the effect of implementing a different failure criterion. In Section 2.6.2 the failure criterion of Matsuoka and Nakai is discussed. Figure 4.4 shows the results of the analysis using this criterion. The algorithm finds a critical slip surface which has a very similar shape as the one presented in Figure 4.3, but gives a higher safety factor of 1.434. If the safety factor of this critical slip surface is calculated with Coulomb's failure criterion, then the safety factor is only 1.323. This result is expected, since the formulation as proposed in Section 2.6.2 simply finds a greater value for the friction angle ϕ. This friction angle is directly used in Coulomb's criterion, therefore the maximum available shear strength will increase correspondingly. This figure also includes the slip surfaces obtained with Bishop and Spencer from D-Stability. With the stresses from PLAXIS and the criterion of Matsuoka and Nakai, a safety factor of 1.455 is found for Bishop's slip surface and a safety factor of 1.445 for Spencer, which are also about 0.1 higher than the values obtained from D-Stability.

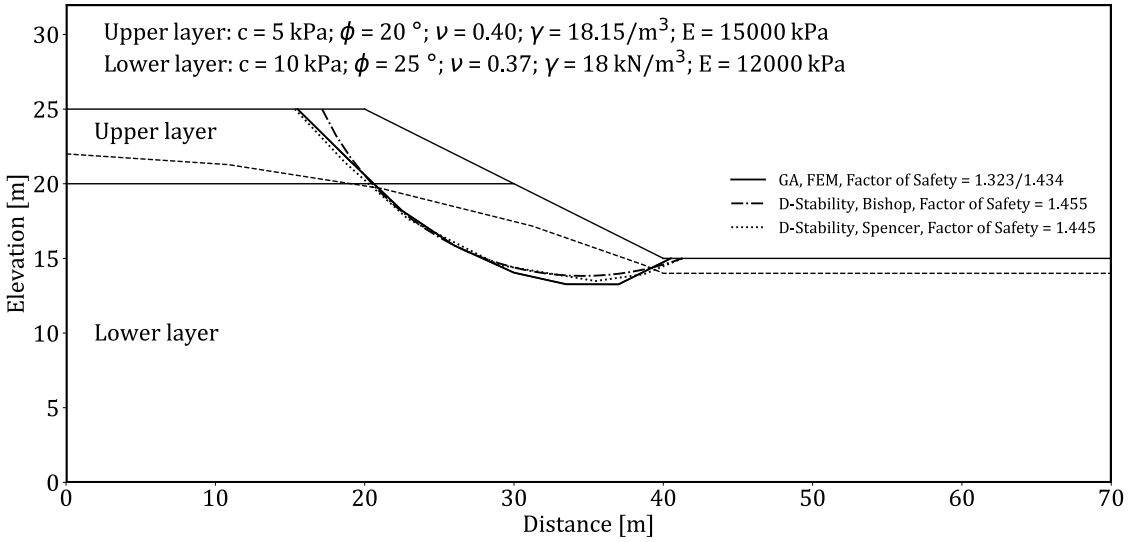

Figure 4.4: Critical Slip Surface obtained with Matsuoka-Nakai's Failure Criterion for Nonhomogeneous Slope 1

4.4. Example 4: Nonhomogeneous Slope with very Weak Layer

The results of the next inhomogeneous slope examined are shown in Figure 4.5. This slope is expected to fail since the safety factor is smaller than one. Li et al. [43] found a safety factor of 0.977, also indicating that the slope is failing. Once again, the factor of safety found in this research is similar to those found in literature and the safety factors obtained from PLAXIS and D-Stability. As can be expected, the Bishop method gives a substantially higher safety factor. Due to the weak layer in the dike profile, a non-circular slip surface is expected, which cannot be captured with Bishop. Contrarily, the analysis performed with Spencer's method is able to find a more critical non-circular slip surface, compared to the result of Bishop's method.

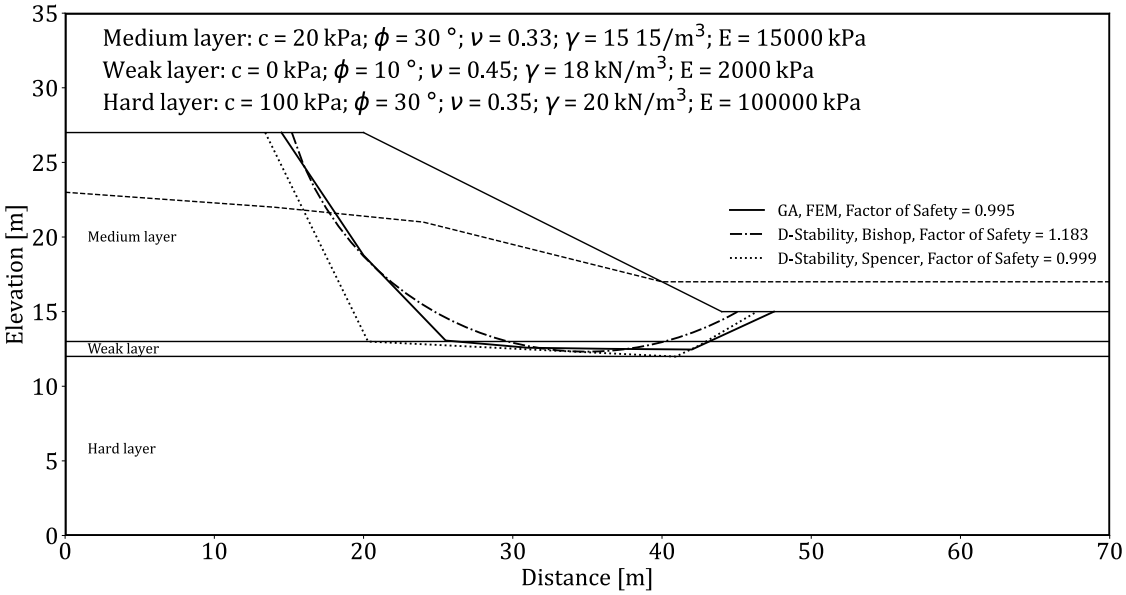

Figure 4.5: Critical Slip Surfaces obtained by Various Methods for Nonhomogeneous Slope 2

To demonstrate the optimisation process of the genetic algorithm, the convergence of the slip surfaces for Example 4 are shown in Figure 4.6 and 4.7. The x-coordinates for the extreme vertices range between $V_{1,\min}$ and $V_{1,\max}$ and between $V_{N+1,\min}$ and $V_{N+1,\max}$. These bounds are also indicated in the figure. In the first figure 20 slip surfaces are shown, which were generated for the initial population. These slip surfaces are not ranked yet, but merely the first 20 slip surfaces which were created are shown here. The second figure shows the 20 best slip surfaces from the initial generation, these are the 20 slip surfaces which gave the lowest safety factor. For this example 80 generations were produced. In the next figure only the best solution of every of the first 20 generations is shown and in the last figure only the best solutions of the last 20 generations are shown, therefore including the final critical slip surface.

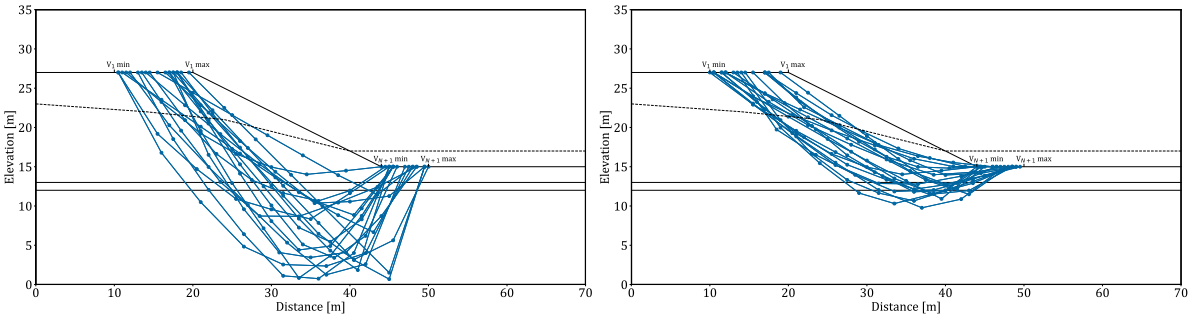

Figure 4.6: Convergence Process of Example 4 Part 1

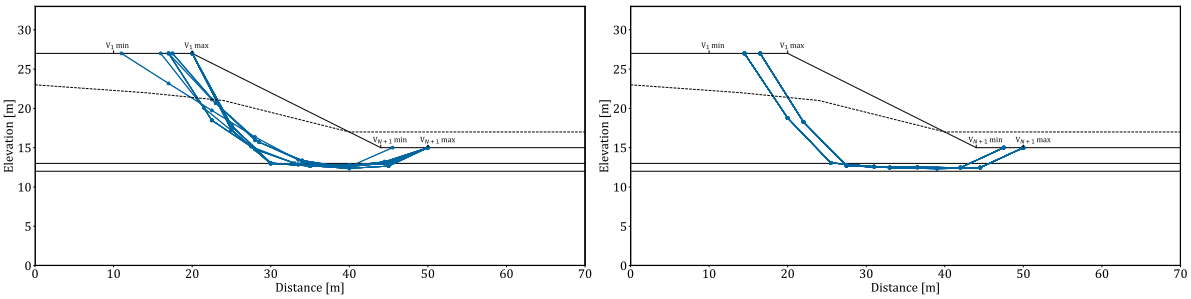

Figure 4.7: Convergence Process of Example 4 Part 2

The convergence curve of the safety factor of Example 4 is shown in Figure 4.8. Inherently, the number of generations is related to computation time, but both graphs are shown such that an impression is given on the total computation time. In this analysis the selection size M is set as 20, which means that after a new generation if produced, only 20 individuals will be chosen as parents to create the new generation. This figure shows that the safety factor is not decreased in every generation, or even in multiple consecutive generations. Therefore the stopping criterion is not based on the difference between the safety factors of two generations before a certain number of iterations has been performed, since such a criterion will stop the algorithm prematurely and prohibits finding the optimal safety factor. The safety factor drops dramatically in the first 35 generations and the minimum safety factor is almost reached after 80 generations.

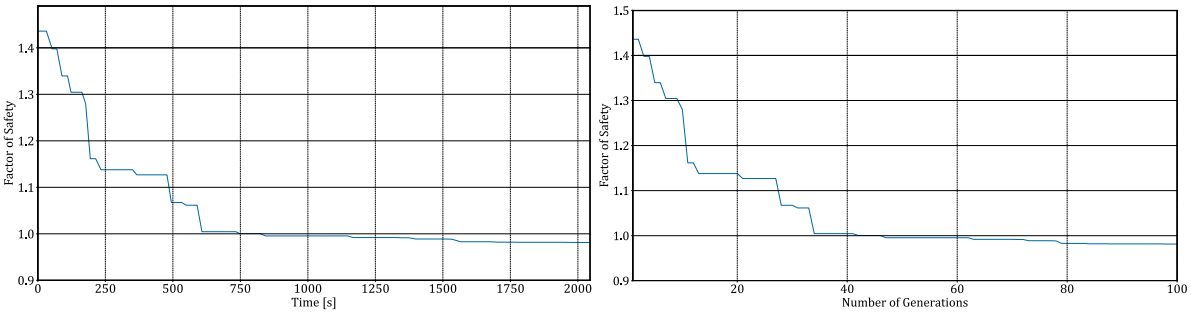

Figure 4.8: Convergence Process of Minimum Factor of Safety Example 4

The influence of the genetic algorithm parameters M_{init}, M and number of sections N will be further discussed in the next chapter.

4.5. Example 5: Undrained Analysis

In Section 2.5.1 the importance of including the undrained effect of impermeable soils is already highlighted. The proposed genetic algorithm is capable in performing the strength analysis for an undrained soil. A different definition should be applied in the genetic algorithm for the maximum available shear strength of the undrained soil and extra care should be taken when performing the stress analysis in the FEM. For this example the slope is constructed in different phases in PLAXIS. The soil is first consolidated, to obtain the overconsolidation ratio, before a rapid water increase is initiated. The stress distribution is captured at the moment the high water level is just reached, when the water has not been able to drain away quickly. The result of this slope is shown in Figure 4.9. PLAXIS gave a critical slip surface with a safety factor of 1.081 which is similar in shape to the result of the genetic algorithm. This result shows that the algorithm is able to find a more critical value.

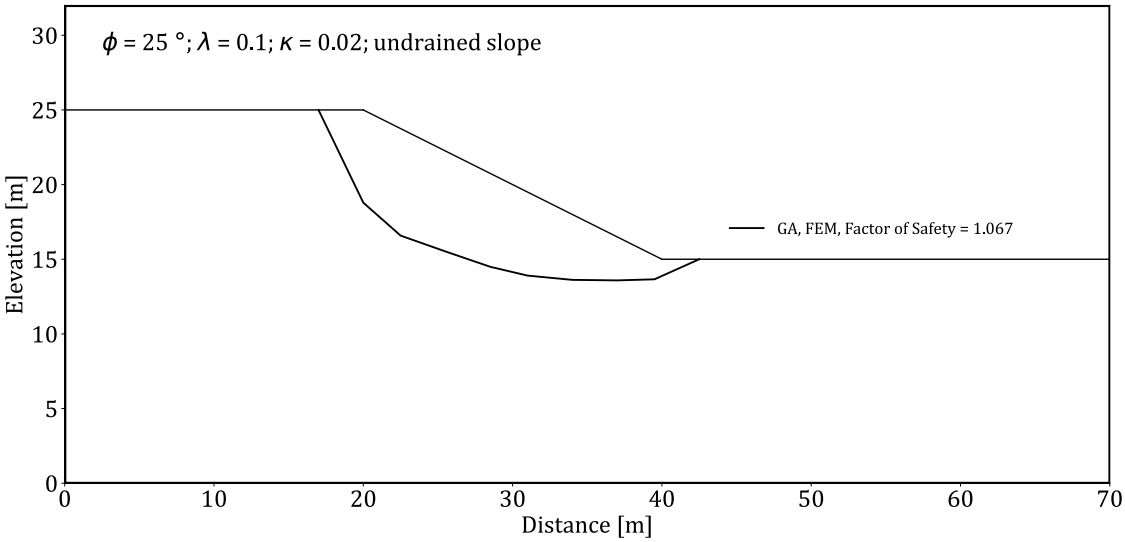

Figure 4.9: Critical Slip Surfaces obtained for Undrained Slope

4.6. Example 6: Bergambacht

The last example which is analysed with the proposed method is the dike Bergambacht. A geotechnical cross section of the dike is shown in Figure 4.10. The macrostability of this dike has been broadly analysed of which results are reported in POVM [55]. In this report multiple loading conditions are investigated and various measures have been presented to reinforce the failing dike. The calculations are based on the location of the old Lekdijk near Bergambacht, where in 2001 an experiment is performed to analyse the instability of the dike. For the complete description of the experiment the reader is referred to GeoDelft [21]. Extensive measurements of field tests and soil properties are available for this case, of which an overview can be found in the POVM [55] report.

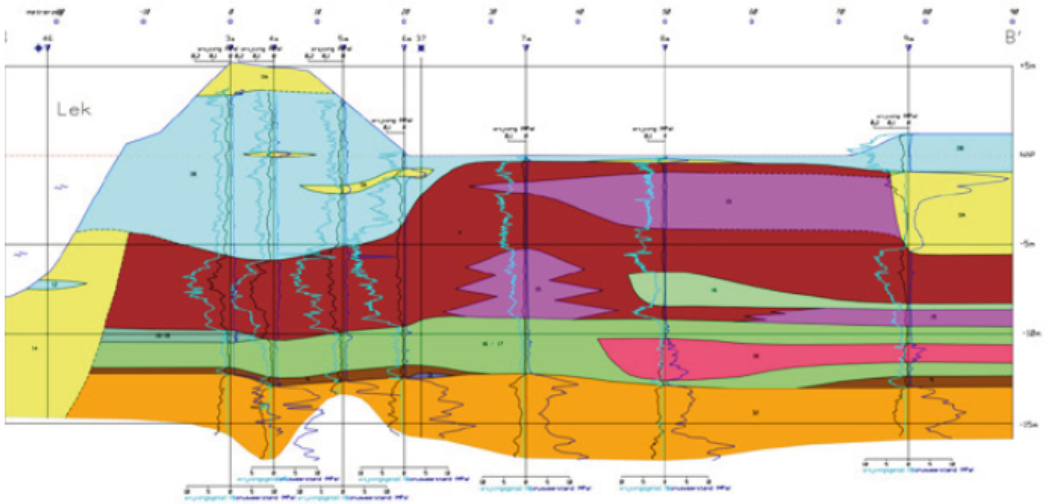

Figure 4.10: Cross Section Dike Bergambacht

The dike consists of nine different soil layers, of which the properties of interest for this research are summarised in Table 4.2. These soil properties are obtained from the POVM [55] report. The undrained behaviour of the clay and peat layers are analysed using the SHANSEP NGI-ADP-model in the POVM [55] report, whereas the Hardening Soil model is applied to the sand layers. In this research the strength of the sand layers are determined using the Coulomb criterion, whilst the undrained analysis is performed using the expressions of the Modified Cam-Clay model.

Table 4.2: Soil Properties Bergambacht

Layer	γ_{unsat} [kN/m^3]	γ_{sat} [kN/m^3]	ν	c' [kPa]	ϕ'	E [kPa]	λ^*[−]	κ^*[−]	S [-]	m [-]
Dijksmateriaal	18.45	18.45	-	2.0	27.2	-	0.0654	0.0077	0.25	0.76
Klei van Tiel	14.23	14.23	-	1.0	18.9	-	0.1270	0.0204	0.18	0.76
Hollandveen	10.35	10.35	-	1.0	29.8	-	0.2467	0.0307	0.29	0.76
Klei van Gorkum licht (humeus)	11.86	11.86	-	1.0	31.2	-	0.1783	0.0378	0.25	0.76
Klei van Gorkum	13.88	13.88	-	1.0	35.6	-	0.2176	0.0216	0.20	0.76
Klei van Gorkum zwaar	15.44	15.44	-	1.0	28.1	-	0.1065	0.0053	0.23	0.76
Basisveen	10.86	10.86	-	1.0	29.8	-	0.2467	0.0307	0.29	0.76
Zand siltig	19.00	19.00	-	0.1	30.0	-	-	-	-	-
Pleistoceen zand	18.00	20.00	-	0.1	32.5	-	-	-	-	-

The result of this slope is shown in Figure 4.11. The slip surface only passes through the clay and peat layers. A safety factor of 0.675 is found, indicating that the dike profile is very weak and expected to collapse.

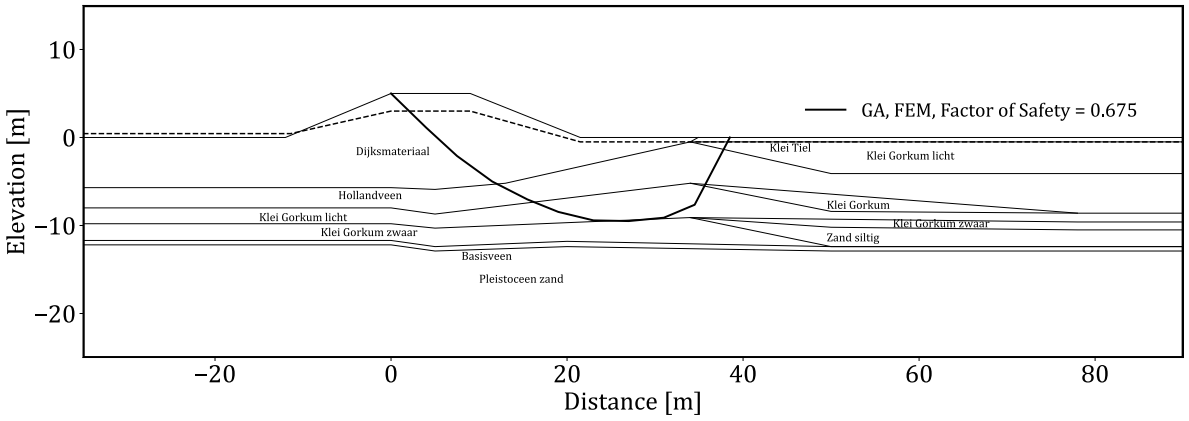

Figure 4.11: Critical Slip Surface for Bergambacht

As previously mentioned, this slope has also been thoroughly examined by various specialists. These results are presented in the POVM [55] report. For the same loading conditions as presented in Figure 4.11, they found a safety factor of 0.88 using the Uplift-Van model in D-Stability and a value of 0.9 with the shear strength reduction method in PLAXIS. The most critical slip surface obtained in D-Stability is shown in Figure 4.12. In their analysis, in both PLAXIS and D-Stability, the SHANSEP approach is used to determine the undrained shear strength. The obtained safety factors are very different compared to the result obtained with the genetic algorithm, nevertheless, the shape of the slip surfaces coincide adequately. Therefore this case study will be discussed in more detail in Chapter 6.

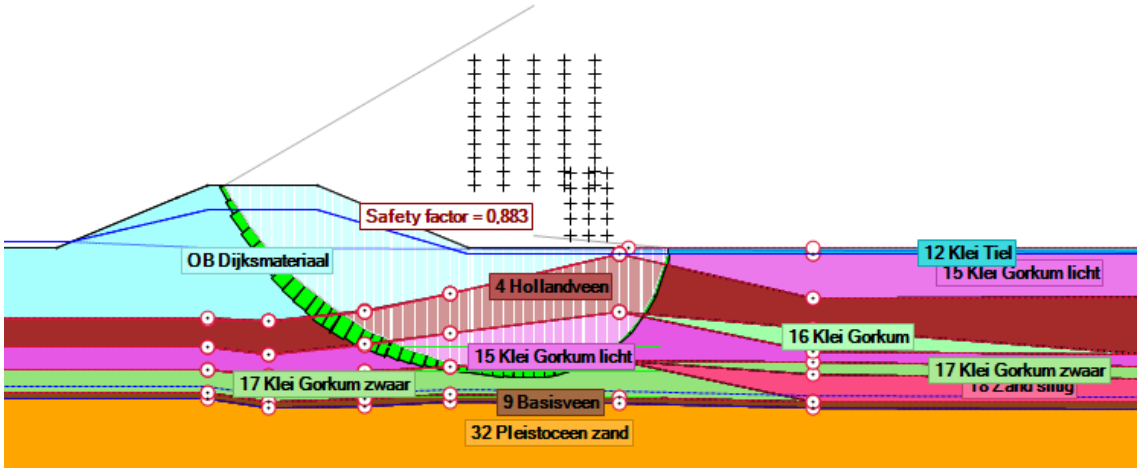

Figure 4.12: Critical Slip Surface Uplift-Van D-Stability

4.7. Chapter Summary

In this chapter the results of six different examples have been presented, which have shown that the proposed method is capable of finding adequate critical slip surfaces and safety factors. To determine the performance of the proposed method, the results obtained with the genetic algorithm are compared with the critical slip surfaces and safety factors acquired from D-Stability and PLAXIS. The proposed algorithm has proven to find correct shapes of the critical slip surfaces, even in an undrained analysis. The influence of using Matsuoka and Nakai's failure criterion is also examined in one example. This analysis has shown that applying Matsuoka-Nakai's criterion results in finding a higher safety factor. However, an associated flow rule is assumed in the derivation of the application based on this failure criterion. This limitation will be discussed in more detail in Chapter 6. As a final test the algorithm has been used to analyse a real dike profile, dike Bergambacht. The proposed method found a critical slip surface very similar to the shape obtained using Uplift-Van in D-Stability. However, the corresponding safety factor resulted to be much lower. This dike will therefore be inspected in more detail in Chapter 6 as well.

5
Sensitivity Analysis

In the previous chapter the results are given of different slope profiles. These results found with the genetic algorithm depend on several factors, such as the stress distribution, search grid density and input parameters of the algorithm. These factors can also influence the computation time. In this chapter the sensitivity of different factors are discussed. The 'Simple Homogeneous Wet' slope, as presented in Section 4.2 is used to perform the sensitivity analysis.

5.1. Initial Population Size

The first step in the genetic algorithm is the generation of M_{init} individuals, which is the initial population. In Figure 4.7 an example is shown of part of an initial population. This figure shows that the initial population is very diverse, which also results in a wide variety of safety factors. Creating a big initial population has the benefit that the chance of creating a slip surface which is similar to the critical slip surface increases. The disadvantage of a big initial population is a longer computation time.

Figure 5.1 shows the computation time of different sizes of the initial population, followed by a few optimisation generations, whilst keeping the selection size M constant at ten. The big dots show the ending time of the creation of an initial population, from which can be concluded that generating 100 individuals takes about 30 seconds. At the time that the initial population of size 500 is created (at around 160 seconds), the first population of size 100 has already created multiple generations resulting in a decrease in the safety factor. The figure also shows that the lowest safety factor found in the initial population of size 500 is lower compared to the best result in the population of size 100 (1.136 compared to 1.150). The algorithm fails to immediately decrease this safety factor, but the cause of this poor performance can simply be 'bad luck'. The algorithm depends on a lot of randomisation, therefore it could occur that the crossover and mutation process are not applied often enough because the crossover and/or mutation rate are not exceeded.

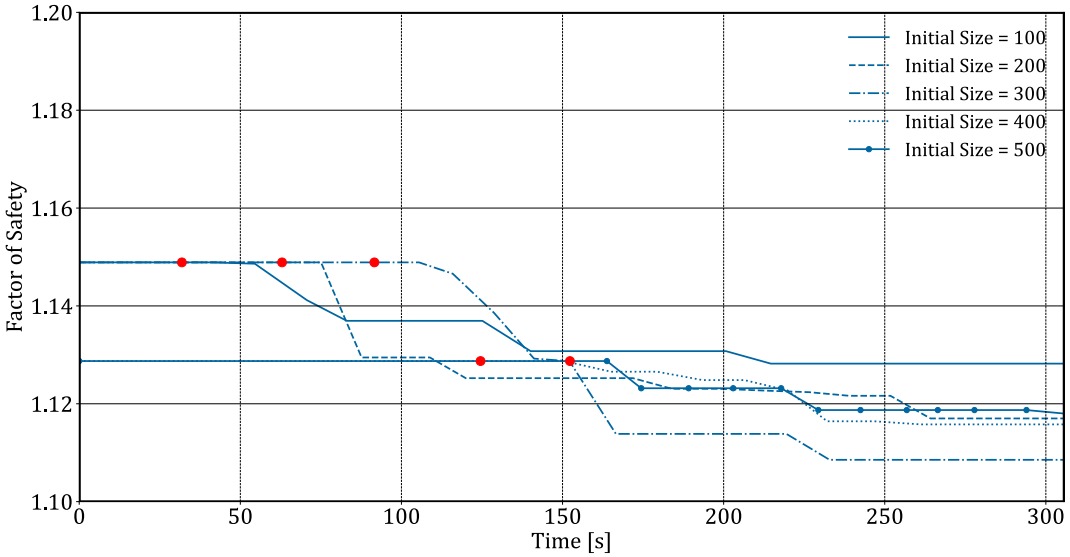

Figure 5.1: Sensitivity Initial Population Size

The comparison between the initial population sizes should be made as unbiased as possible. Therefore when creating the next population (e.g. of size 200), the previous population is copied and the remaining number of individuals (100) is created and added to that previous population. Figure 5.1 shows that when creating the population of size 200 and 300, no individual was found which gave a lower safety factor compared to the best result of the first initial population. This can also be seen from the left side of Figure 5.2. In this figure the most critical slip surface of the initial population is shown. It shows that the initial populations of size 100, 200 and 300 give the same slip surface. The same holds for the initial population sizes of 400 and 500. The right figure gives the most critical slip surface after the generation of new populations, which were created in 270 seconds. This figure shows that quickly after the generation of the initial population, the algorithm is capable of converging the slip surfaces. It therefore indicates that the initial population size is rather irrelevant when the algorithm is executed for enough iterations.

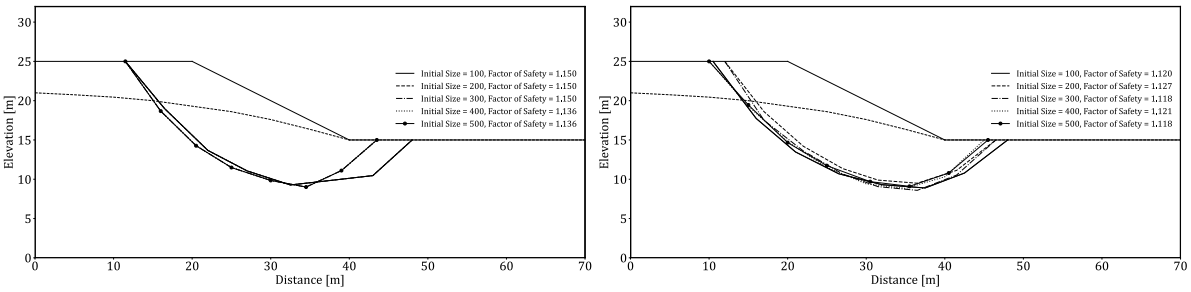

Figure 5.2: Slip Surfaces Comparing Sensitivity Initial Population Size

It is already mentioned that the final results of the genetic algorithm are very dependent on the randomisation process. Therefore, this analysis in which the initial population size is varied, whilst keeping the selection size constant, is performed multiple times. All results are shown Figure B.1 in Appendix B. These results are in accordance with the statements given in this section. From these findings the optimal initial population size M_{init} is set at 100. This ensures a short initial population computation time and allows for more time in the actual optimisation process.

5.2. Selection Size

The next factor of interest in this sensitivity analysis is the selection size M. In Figure 4.7 the slip surfaces are shown that got the best ranking in the initial population. The selection size is the amount of these slip surfaces which are used to create the offspring (the next population). Selecting very few slip surfaces can result in a limited optimisation process, considering that not enough variation is present between the parents. The genetic algorithm will then depend more on the mutation process instead of the crossover process to obtain enough diversity in the offspring. On the other hand, selecting many slip surfaces increases the computation time substantially.

From Figure 5.2 it was already concluded that after a couple of iterations, the solution of the genetic algorithm tends to convergence. The selection size has a big influence on the time until the solution converges. To consider the effect of the selection size on the computation time, multiple generations are created using the exact same initial population, but with varying selection sizes. The results of these analyses are shown in Figure 5.3. As expected, the safety factor decreases the fastest with the smallest selection size. However, after the first couple of iterations it fails to find a better solution quickly, since not enough variation is present anymore between the current solutions. The exact minimum number of sections which is required is not explored. On the contrary, the results of the biggest selection size show that even in the latest iterations, the algorithm is still able to improve.

This analysis is also performed multiple times and all results are shown in Figure B.2 in Appendix B. Pending all these results, no clear conclusion can be given on the optimal selection size. Especially considering the fact that all results tend to convergence after sufficient time. Only the smallest and biggest selection size are excluded from being the optimal value. For this research selection size is set to 20.

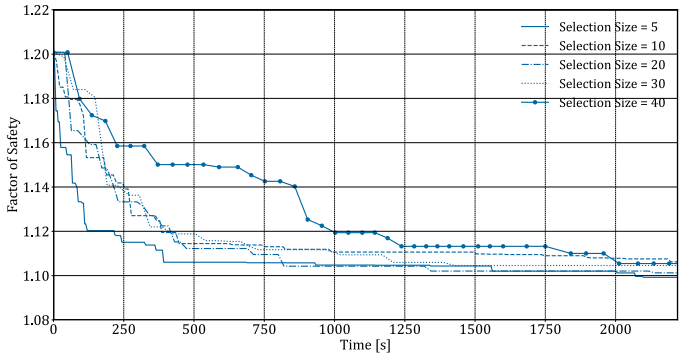

Figure 5.3: Sensitivity Selection Size

5.3. Number of Sections

The number of sections applied in the algorithm has no direct effect on the computation time, since the number of sections is only relevant in the generation of the initial population. In the strength analysis of a slip surface only the values of the nodes of the self-defined grid are considered which are close to the slip surface, as discussed in Section 3.1.1. The number of sections does not influence the number of nodes which are analysed per slip surface, only the total length of the slip surface affects this number. However, the density of the self-defined grid has a big influence on the computation time, as will be discussed in Section 5.5.

The number of sections has an effect on the shape of the slip surface. This shape has some influence on the performance of the algorithm, since it affects the mutation process. More sections will make the slip surface smoother. However, an exaggerated amount of sections will also make the mutation process more restricted. In Section 3.3.4 the mutation process is described, in which also the areas are shown in which a node can be mutated. When the slip surface becomes smoother, the size of these areas will reduce, which makes the mutation process less effective. In Figure 5.4 the safety factor is outlined against the number of generations for four different values for the number of sections, namely: five, six, seven and eight. For every number of sections the analysis is performed five times. These figures show that the slip surfaces with seven or eight sections achieve a lower safety factor in the same number of generations.

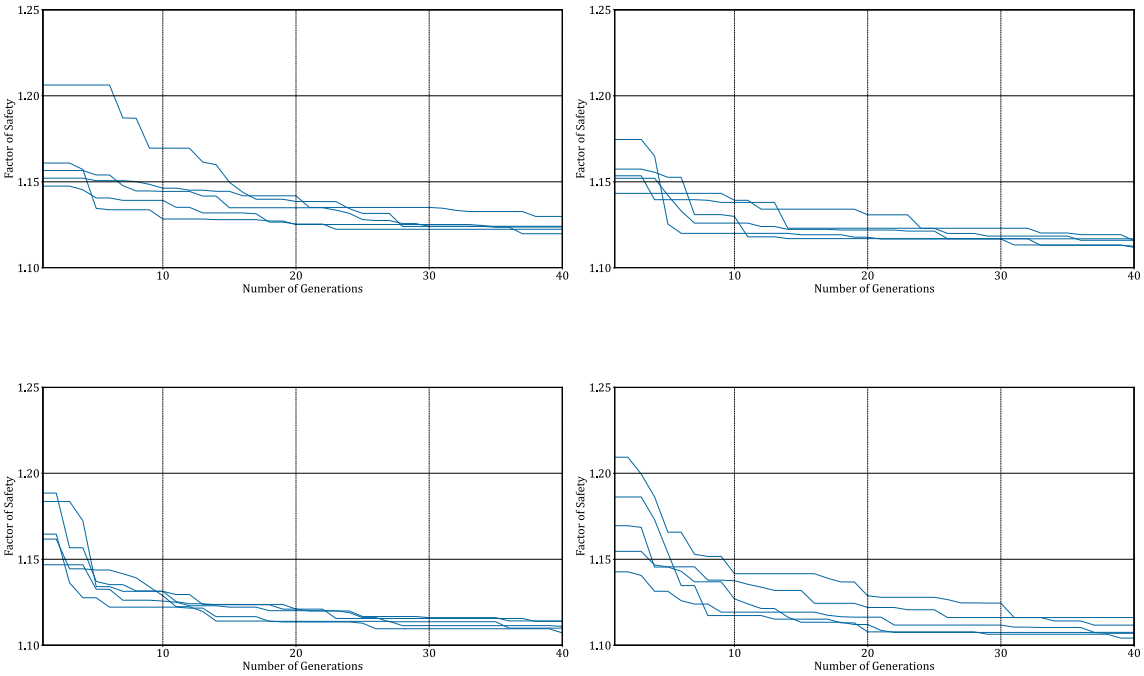

Figure 5.4: Sensitivity Number of Section

When increasing the number of sections to 12, the performance decreases again. This can be seen from Figure 5.5, which is in accordance with the reasoning given in this section. For this research the number of sections is set to seven.

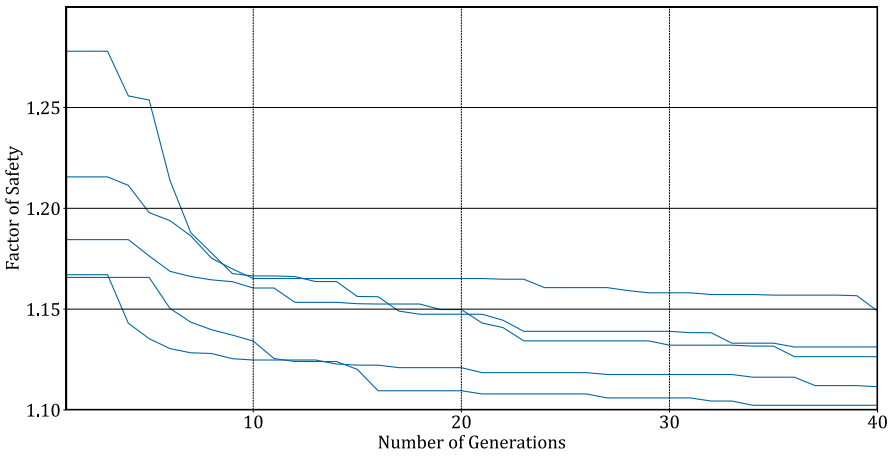

Figure 5.5: Sensitivity Number of Section

5.4. Stress Analysis

The chosen stress-strain relationship can have an effect on the shape of the critical slip surface, as well as on the critical safety factor. In this section the influence of the stress distribution as used in PLAXIS is analysed. Results of the genetic algorithm are presented, obtained from a linear and nonlinear stress-strain relationship. As stated before, for the linear stress analysis the linear elastic relationship is used in PLAXIS, whilst for the nonlinear stress analysis the hardening soil model (Schanz et al. [65]) is adopted. Figure 5.6 shows the critical slip surfaces determined from both analyses. The shape and location of the slip surfaces are quite similar, moreover, the difference in the safety factors is also minimal. The nonlinear stress distribution creates a critical slip surface which is only slightly wider. This indicates that there is little difference in the distribution of stresses between both analyses, or that the differences are too small to have a significant influence in the stability analysis. The analysis has been performed multiple times and the nonlinear analysis always gave a higher safety factor, although the observed differences were approximately 3.3%. However, it should be noted that in this example a very simple homogeneous slope is considered. To make a definite conclusion, the same analysis should be performed on a more complex dike profile.

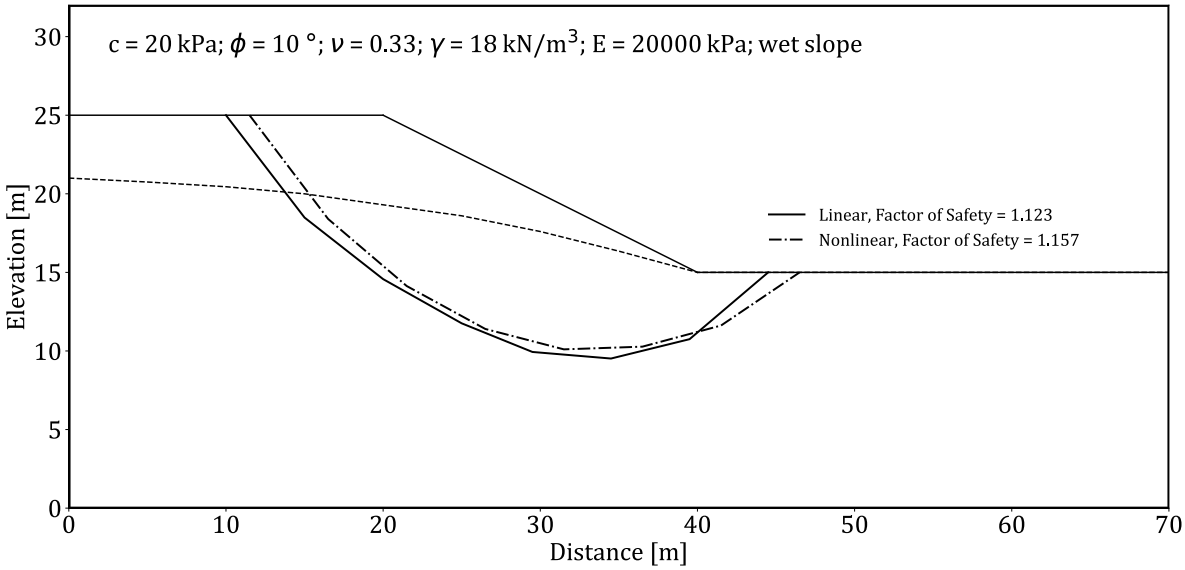

Figure 5.6: Sensitivity Stress Analysis

5.5. Grid Density

In Section 3.1.1 the interpolation process is described which is performed in Python. The values obtained from PLAXIS are interpolated to a regularly-spaced grid on a defined interval. Only the values on the nodes of this self-defined regularly-spaced grid will be used in the algorithm and consequently the mesh settings in PLAXIS have little influence on the outcome of the genetic algorithm. Instead, the interval size of the self-defined regularly-spaced grid does have a great impact on the performance of the algorithm.

The results as presented in Chapter 4 and in this chapter are obtained with a grid interval of 0.5 meter. This implies that the coordinates (vertices) of all the slip surfaces are rounded to half a meter. In this section different values for the interval in the grid are examined: a course grid with an interval of one meter, a medium grid with the interval of 0.5 meter and a fine grid with a 0.1 meter interval. The results are shown in Figure 5.7 and Table 5.1. The slip surfaces for all three densities are quite similar. The finest grid gives the lowest safety factor after the same number of iterations, but the computation time increases significantly in case this finer grid is applied. Overall, the interval of the grid does not heavily influence the results of the analysis in terms of the critical safety factor, since these values do not differ too much.

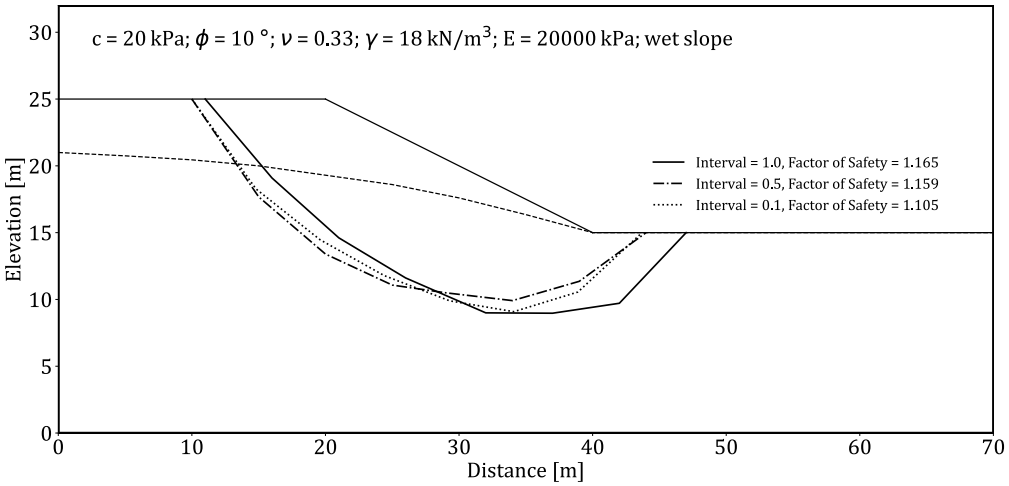

Figure 5.7: Sensitivity Grid Interval

Table 5.1: Performance Sensitivity Grid Interval

Interval	Safety Factor	Difference [%]	Computation Time [s]
1.0	1.165	5.43	138
0.5	1.159	4.88	246
0.1	1.105		2021

5.6. Chapter Summary

In this chapter a sensitivity analysis is performed on the stress distribution, search grid density and several input parameters of the genetic algorithm. Firstly, the influence of the input parameters of the genetic algorithm on the computation time are discussed. If the algorithm runs a great number of iterations, both the initial population size and selection size have little influence on the resulting safety factor, since the solution of the algorithm will convergence. Increasing the number of sections in the slip surface increases the smoothness, but reduces the performance of the algorithm. The sensitivity of the chosen stress-strain relationship in PLAXIS is also examined. For the example considered in this analysis, similar results were found with both the linear and nonlinear stress-strain relationship. However, this result could be due to the simple slope profile. Therefore a sensitivity study on the stress-strain relationship using a complex dike profile is recommended. Lastly, it is found that a finer grid density gives a lower safety factor after the same number of iterations in the genetic algorithm, compared to a coarser grid density. However, this lower safety factor is at a cost of an enormous increase in the computation time.

6
Discussion

In Chapter 4 the results of the different case studies are presented and the differences between the results of various methods are already mentioned. Some striking results were found, which will be discussed in more detail in this chapter. In the previous chapter the sensitivity of the proposed method is also already discussed, but there are other uncertainties which have not been taken into account in that chapter. These uncertainties will also be presented in this chapter.

6.1. Discussion Case Study Bergambacht

In Section 4.6 the results of dike Bergambacht have been presented. It is already pointed out that the safety factor found with the proposed approach is much smaller than the values found in other reports (with other methods). However, the shape of the slip surfaces coincide decently. In this section the results of this dike will be examined further.

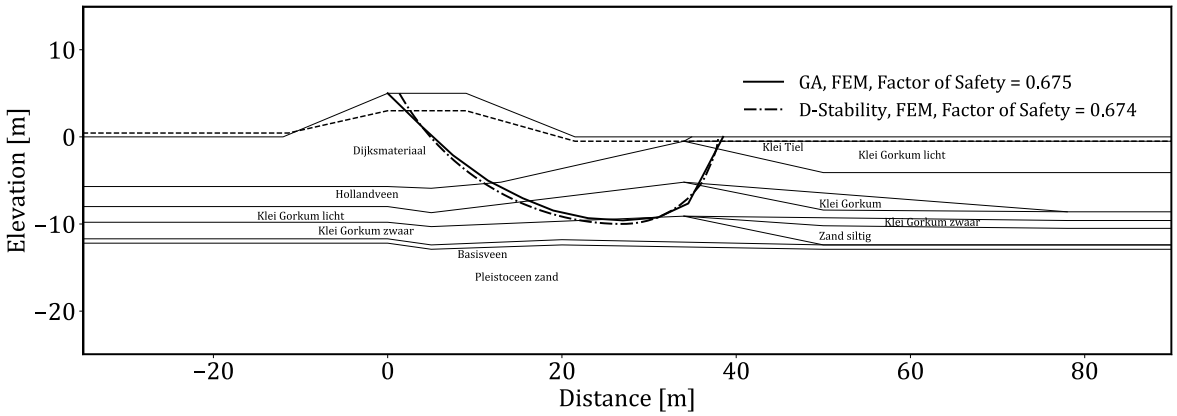

Figure 6.1: Critical Slip Surface GA Bergambacht

In Figure 6.1 the critical slip surface found with the genetic algorithm is shown as well as the slip surface obtained from D-Stability. This figure shows that the search method performs well and finds a critical slip surface with a shape that is expected. The slip surface found with D-Stability is also imported into the strength analysis as presented in this report. Thus instead of searching for this shape, it is directly inspected. Whenever the safety factor is calculated using the Modified Cam-Clay model expressions and the stresses from PLAXIS, the safety factor of the slip surface imported from D-Stability is about 0.2 lower than the value given by D-Stability using Uplift-Van (0.674 to 0.883).

To make a fair comparison between the results of the GA and D-Stability, the SHANSEP approach is implemented in the genetic algorithm. The undrained shear strength can be determined with the SHANSEP parameters and the expression as given in Section 2.6.4. Using this definition for the undrained shear strength, the safety factor is still defined as the ratio of the the total maximum available shear strength to the total mobilised shear stress along a slip surface. The results of the analysis of dike Bergambacht with the genetic algorithm using SHANSEP as well as the slip surface obtained from D-Stability are shown in Figure 6.2.

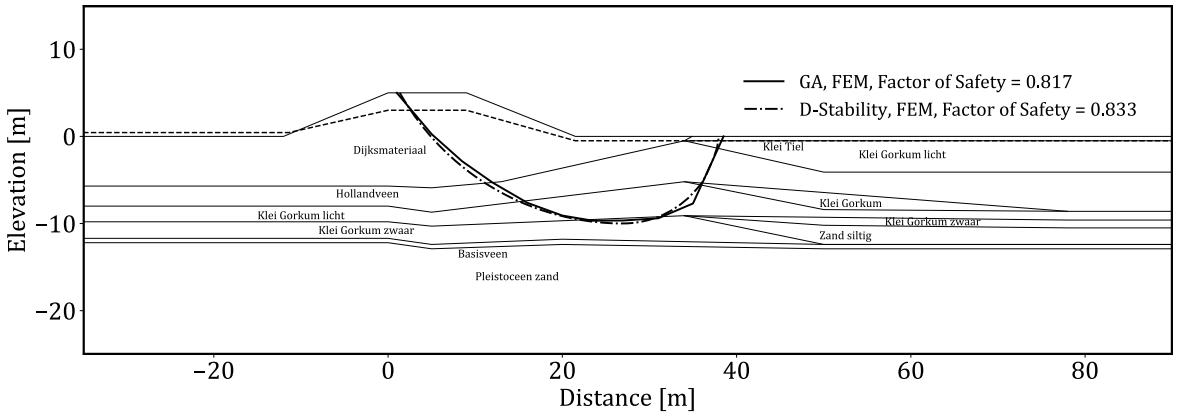

Figure 6.2: Critical Slip Surface GA Bergambacht SHANSEP

Again, the safety factor is calculated for the slip surface of D-Stability using the safety factor definition of this research, but this time using the expressions of the SHANSEP approach, which gives a value of 0.833. That is only slightly smaller than 0.883 (from D-Stability). There are only two variables of the SHANSEP formulation that can differ between the values from PLAXIS and D-Stability, which are the effective vertical stress σ'_y and overconsolidation ratio OCR. In the following figures, the values of these two variables are shown for every slice of the slip surface. The position of the slices can be seen in Figure 4.12.

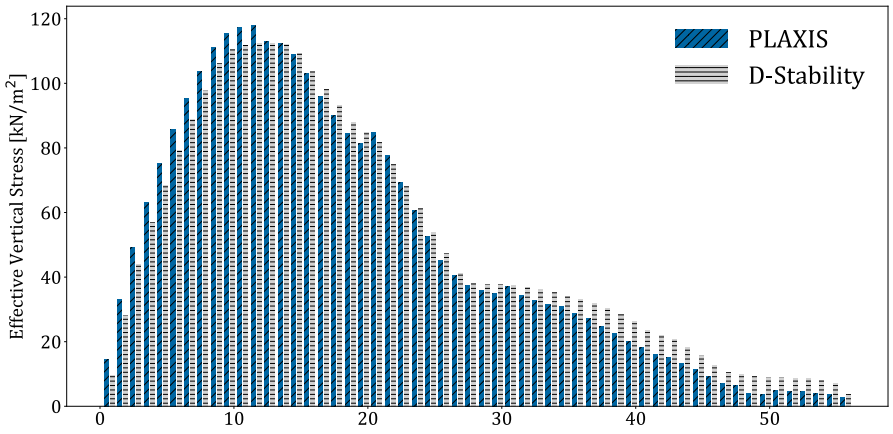

Figure 6.3: Comparison Effective Vertical Stress

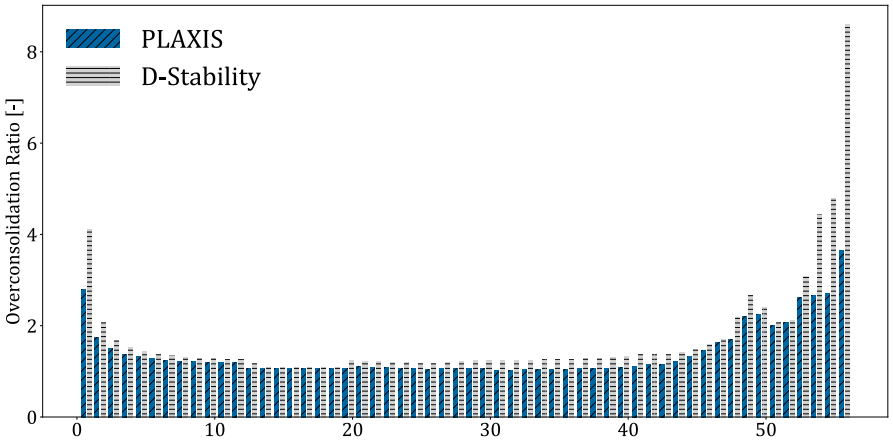

Figure 6.4: Comparison Overconsolidation Ratio

These figures show that the differences in the effective vertical stress are quite small. For the first 12 slices, PLAXIS finds a higher σ'_y whilst for the latter of the slip surface D-Stability gives a higher value. The over-consolidation ratio only differs a lot at the last couple of slices, whilst on overall D-Stability gives a higher OCR. Both the effective stress and OCR have a positive effect on the undrained shear strength. From these figures it can therefore be expected that D-Stability gives a higher undrained shear strength when applying SHANSEP, this is confirmed in Figure 6.5. This figure shows that for the greater part of the slip surface the values of D-Stability give a greater shear strength than PLAXIS, this demonstrates the higher safety factor found in D-Stability.

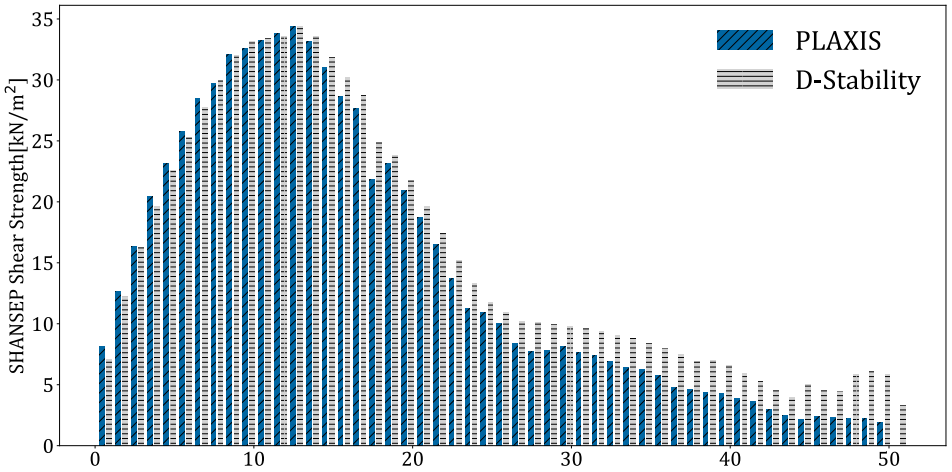

Figure 6.5: Comparison SHANSEP Shear Strength

With these results it can be concluded that the proposed method performs very properly. The genetic algorithm is able to locate the correct critical slip surface. If the same strength definition is used in both the GA and D-Stability, then the safety factors only differ slightly. This small difference can be explained by the differences between the stress analyses in PLAXIS and D-Stability. Form this analysis it can also be stated that the Modified Cam-Clay model determines an undrained shear strength which is much lower compared to the SHANSEP approach. This could be the effect of the inclusion of the shear induced pore pressures, which are captured accurately in the Modified Cam-Clay model.

6.2. Modified Cam-Clay Model

For the undrained strength analysis, the Modified Cam-Clay model has been used to find an expression for the undrained shear strength. The use of this model in a numerical analysis has some pitfalls. The most relevant limitation of the MCC model, for this research, is the shape of the yield surface in the $p-q$ plane. The yield surface in this model has a form of an ellipse in the $p-q$ plane, as shown in Figure 6.6. The size of the yield surface is not fixed, but is characterised by the preconsolidation pressure. Thus for every particular value of the consolidation pressure, a corresponding ellipse exists. The 'dry side' of the ellipse is associated with soil softening, which is also discussed in Section 2.6.3. In this region the stress paths cross the critical state line in the $p-q$ plane before reaching the failure surface, thus before plastic yielding occurs. Note that this crossing can only be observed when the yield surface is shown in a $p-q$ plane. The critical state line is actually a line in the $q-p-v$ plane. If the yield surface is extended to the $q-p-v$ plane, this crossing will not be detected. For soils which experience softening behaviour, the Modified Cam-Clay model can allow for unrealistically large shear stresses. Therefore this model should not be used to analyse heavily overconsolidated clays.

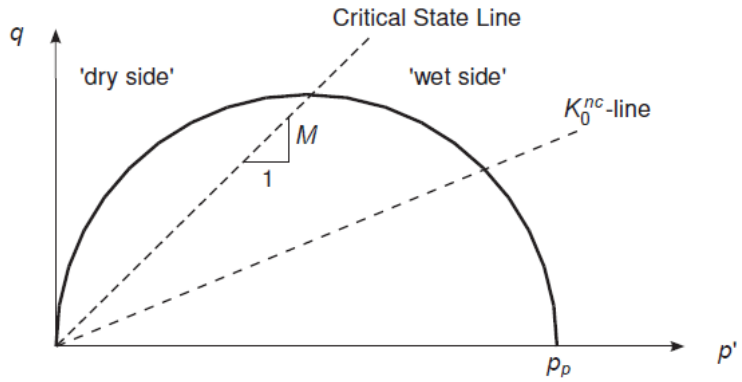

Figure 6.6: Yield Surface Modified Cam-Clay model (Brinkgreve et al. [7])

6.3. Matsuoka-Nakai Failure Criterion

One of the advantages of the proposed method is the possibility to change the definition of the maximum shear strength in the safety factor. To make use of this potential, another failure criterion was implemented besides Coulomb, namely Matsuoka-Nakai. The use of this failure criterion has to benefit that the influence of the intermediate principal stress is taken into account when determining the shear strength. In Section 4.3 the nonhomogenous dike profile is also analysed using Matsuoka-Nakai's failure criterion. This analysis showed that using this criterion instead of Coulomb's criterion results in finding a higher safety factor. This result could be expected from the approach described in Section 2.6.2, since literature has found that including the intermediate principal stress can result in a higher peak strength. However, one big remark should be made on the application of this failure criterion as well as on the description given in Section 2.6.2. The approach is derived under the assumption of an associated flow rule, meaning that the yield surface is equal to the plastic potential ($\Psi = \phi$). This can result in an overestimation of the shear strength and it is therefore recommended to include the effect of dilatancy in a further study.

6.4. Computation Time

Table 4.1 has shown that the computing time of the genetic algorithm is quite long compared to both LEM and FEM. However, the genetic algorithm is written in Python, which is an interpreted language. Computer languages are classified as high or low level, referring to how close they are to directly speaking with the computer in bits. A language which is closer to human communication and syntax is higher level. Python is designed to be more accessible for usage than most languages, making it a higher level than for example C or C++, which are compiled languages. The LEM and FEM programs which are used in this research are written in such a compiled language. A compiled language is the the lowest level of interaction with the computer such that it can directly be performed by the CPU. An interpreted code takes some extra steps of interpretation before it can be used by the computer. Therefore naturally an interpreted code is slower than a compiled code. Depending on the number of computations, a compiled language can outperform Python enormously. The results as given in Table 4.1 show a long computing time for the genetic algorithm, however, implementing this algorithm in a compiled language can decrease this computation time such that it can compete with the other compiled programs.

6.5. Spatial Variability

The stress analysis and the search for the critical slip surface in the genetic algorithm are both performed in a two-dimensional analysis. A two-dimensional analysis cannot take the variation of the soil characteristics in the slope perpendicular to the slip surface into account. Lim et al. [44] have indicated that their proposed three-dimension finite element analysis gave safety factors which were 10% lower compared to traditional two-dimensional limit equilibrium methods, indicating that the two-dimensional analysis can give unsafe results. The proposed method in this report can be extended to a three-dimensional analysis. PLAXIS is already able to perform a 3D stress analysis and in the genetic algorithm an extra variable can be included. But the determination of the safety factor should be done cautiously, extra attention should then be paid to the direction of the shear stresses as well.

The soil characteristics do not only have to vary perpendicular to the slip surface, but variation can also already be present in the flat slope which is considered right now. Some of the examples in Chapter 4 contain different soils, but within one soil layer, the parameters are assumed to be homogeneous for the complete layer. The effect of spatial variability in the soils on a two-dimensional slope stability analysis should also be considered.

6.6. Chapter Summary

In this chapter a closer look is taken on the case study Bergambacht. The result as given in Section 4.6 finds a lower safety factor than both D-Stability and PLAXIS, whilst the shape of the critical slip surface coincides quite well. Therefore, instead of using the Modified Cam-Clay model to determine the undrained shear strength, SHANSEP has been implemented as well. If the SHANSEP approach is used to determine the undrained shear strength, then the resulting safety factor is closer to the values obtained by other methods. The safety factor is slightly lower than the value found by D-Stability, this is a result of the differences in the stress analyses of both methods. This discussion has shown that the genetic algorithm is performing well, but that the Modified Cam-Clay model estimates a much lower undrained shear strength. The cause of the lower shear strength is the inclusion of the shear induced pore pressures. In this chapter it is also highlighted that the Modified Cam-Clay model is unable to analyse (very) overconsolidated clays. Therefore, if these types of soils are to be analysed, another soil model should be implemented. One advantage of the proposed method is the flexibility of the safety factor, it allows for different definitions of the maximum available shear strength. Example 3 is therefore also analysed with the failure criterion of Matsuoka and Nakai, which shows to give a higher estimation for the maximum available shear strength. However, the derivation of the application of this criterion in this report assumes an associated flow rule and it is therefore recommended to further investigate this criterion with a non-associated flow rule. Moreover, an explanation is given for the long computation time of the genetic algorithm compared to PLAXIS and D-Stability. The algorithm is written in Python, which is an interpreted language, whilst the FEM and LEM programs are written in a compiled language, which are by definition faster. Lastly, it is recommended to also include spatial variability in a further study.

7
Conclusion and Recommendations

The conclusions of this research are presented in this chapter. Firstly, the main findings of this research are stated. Secondly, some limitations of the models used in this research are mentioned. Thereafter, several recommendations are given for further research on this topic. At last, the chapter is finalised by evaluating the research objective which is stated in Section 1.5.

7.1. Conclusions

From the literature study it can be concluded that both the limit equilibrium methods and the finite element method have limitations regarding the analysis of slope stability. The biggest drawback of the FEM is the use of the shear strength reduction method to determine the safety factor. This method does not represent the behaviour of the soil, but simply decreases the soil strength parameters ϕ and c until the dike reaches failure. Consequently, the program does not make use of the expressions for the (undrained) shear strength from advanced soil models to determine the strength of the slip surface. Another limitation of the SSRM is that it only gives one critical slip surface, other slip surfaces of interest cannot be examined. Hence Deltares has initiated a study which investigates the possibility of combining both methods. The main goal of this research is to further investigate this method and verify its performance. Therefore the main research question for this study is formulated as:

How can a new approach use both LEM and FEM concepts to analyse the stability of slopes?

The main research question is split up in sub-questions that should be answered to reach the research goal. Answering these questions will be part of the conclusion.

How should a stress analysis be performed by a finite element approach in PLAXIS?
The finite element program PLAXIS is mainly used to obtain the stresses in the soil of the dike of interest. The analysis is performed using a linear elastic stress-strain relationship. Therefore no use has to be made of the available soil models. The shear strength reduction method present in PLAXIS is also used to obtain a reference safety factor. Since the optimisation method solely uses the obtained stresses from the finite element method, other programs than PLAXIS should be suitable for the proposed analysis method as well. Depending on the available constitutive models in the finite element program, the proposed method is also able to work with every other chosen stress-strain relationship.

How can the critical slip surface be determined using the stress analysis obtained from the FEM?
The proposed method consists of mainly three stages. First, the stress analysis is performed in a finite element program. Secondly, the definition of the safety factor, including an expression for the maximum shear strength, is formalised. At last, the optimisation method searches for the critical slip surface.

There are multiple optimisation methods which can be applied to find the most critical slip surface in the stress field obtained from the finite element analysis. In this research a genetic algorithm is proposed. The algorithm needs a definition for the safety factor to determine the score of a slip surface: a slip surface with a low safety factor scores well. A strength type safety factor is applied, which compares the total resisting strength along the slip surface with the total mobilised shear stress. This type of safety factor expression allows for the user to use their preferred shear strength definition. In this research the Coulomb criterion and Modified Cam-Clay model are used to express the maximum available shear strength in a drained and undrained soil respectively.

The possibility of importing the obtained stress field from the finite element analysis into a limit equilibrium method program is not explored. However, it is possible to apply safety factor definitions described by Bishop, Morgenstern-Price and of other limit equilibrium methods, in the proposed method. The algorithm will use this definition of the safety factor to score the slip surfaces and the optimisation will be carried out in the same manner as described in Section 3.3. This again shows the possibilities of the proposed method. It is capable of handling different safety factor definitions as preferred by the user.

How is the performance of the new method compared to other, more classical, methods in analysing the slope stability?
From the different examples considered in Chapter 4 it can be concluded that the proposed method is capable of finding a reasonable critical slip surface and corresponding safety factor. The biggest drawback of the method is the long computation time.

The safety factors found with the proposed method are very dependent on the number of generations created in the optimisation process. When the genetic algorithm is allowed to run for many iterations, it is able to find more critical safety factors than the FEM analysis as well as the methods proposed in literature. However, the results shown Table 4.1 do not support this statement, since the algorithm is stopped prematurely. Another reason for the slightly higher safety factors is also discussed in Section 4.2. The genetic algorithm allows for a slip surface to contain sections with a negative shear stress. The safety factor will naturally be higher when these negative sections are present, due to the definition of the safety factor.

The sensitivity analysis of the proposed method has also shown that the effect of the used stress distribution in the finite element stress analysis has little influence on the final critical slip surface. It is shown that a non-linear stress strain relationship gave a slightly higher safety factor. However, this result could be due to the simple slope profile. The interval of the self-defined grid has shown to have a great effect on the computation time, but little influence on the shape of the critical slip surface as well as the corresponding safety factor. The finest grid (with the smallest interval) gave the most critical value for the safety factor, but its computation time is about eight times longer than for the medium density.

The limitations of the shear strength reduction method is one of the greater motivations for the development of the proposed research. This SSRM in PLAXIS is used to compute the reference safety factor. In Section 1.4 the drawbacks of this method are already discussed and the proposed method surpasses the SSRM in multiple aspects. One disadvantage of the SSRM is that an irrelevant failure surface can be given. In the proposed method the user is asked to give boundaries for the entry point and exit point of the slip surface, therefore the algorithm will always give a relevant critical slip surface.

7.2. Limitations of the Method

The proposed method which has been presented in this research has some limitations, these are stated in this section.

Limitations on soils and strength definitions. In this research only a select number of constitutive models is used to determine the shear strength of the soil. The Modified Cam-Clay model is used to determine the maximum undrained shear strength of an impermeable soil. In Chapter 6 it is already mentioned that this is not a correct expression for the shear strength of heavily overconsolidated clays. To apply the proposed method on these type of soils, a different constitutive model should be implemented, which is capable of modelling the behaviour of these heavily overconsolidated clays.

Limitations on mechanisms in dike profile. The proposed method has only been applied to a few dike profiles. In only one case a profile is examined which consisted of many different soil layers. This example showed that the proposed method is able to represent the strength of these different layers. However, other mechanisms which could occur in dike profiles, such as uplift, have not been considered yet. Therefore no conclusion can yet be given on the performance of the proposed method when the dike has sections where the effective stresses are reduced to zero.

7.3. Recommendations for Further Research

During this study some recommendations have been found for further research, these are addressed in this section. The limitations as stated above can also be seen as recommendations to improve the study. In Chapter 6 some uncertainties of the proposed method have been discussed, including some recommendations. These will be restated in this section.

Genetic algorithm on sections. The genetic algorithm as proposed in this research optimises the slip surface as a whole. The algorithm does not allow for increasing the number of sections during the optimisation process. Literature has presented different optimisation processes which do not optimise the complete slip surface, but score every section separately. Sections which get a low score are taken outside the search space of the search algorithm, such that it will never be a part of a slip surface anymore. This can be a more efficient way of employing the genetic algorithm, since the search space is reduced during the optimisation process.

Improve crossover and mutation process. The computation time of the proposed method is quite long. A substantial part of this computation time is a result of the crossover and mutation process. These processes can be improved in multiple manners. First of all, in the current implementation, the best solution is immediately put into a pair to create offspring with the crossover process. This can result in a completely different slip surface, which gives a higher safety factor and scores lower. This way the 'best' solution will be lost. An alternative can be to always keep the best solution as it is in the next generation, or immediately apply mutation on it, instead of using it as a parent in the crossover process. Secondly, in the proposed method only uniform mutation is applied. There are plenty more mutation processes possible, but the performance of these alternatives have not been examined.

Interpolation process. The results of the stress analysis obtained from PLAXIS are interpolated to a self-defined grid in Python as described in Section 3.1.1. From that point on only the values present on these interpolation points are considered in the algorithm. Another possibility is to allow the algorithm to use all positions in the dike profile to create the slip surface and then interpolate the values from the finite element analysis to find the stresses along the slip surface. This might result in a smaller accuracy loss.

Include non-associated flow rule. The failure criteria as used in this research should be extended to a non-associated flow rule, in which dilatancy is accurately modelled.

Include spatial variability. The proposed method could be extended to a 3D analysis in which the variability of the soil parameters inside one dike layer can be included as well.

7.4. Conclusion on the Research Objective

In Section 1.5 some hypotheses are formulated concerning the research which is carried out in this study. The conclusions on these hypotheses are stated below.

The new approach is able to give a reasonable factor of safety in accordance with classical methods.
The different examples as presented in Chapter 4 have shown that the new approach is capable in finding safety factors which are in accordance with the results of other slope stability analysis methods, including the classical LEM and FEM.

The new approach gives a better representation of the soil mechanics and is able to use non-linear assumptions to determine the (critical) soil strength and slip surface.
The stress analysis is performed in a finite element analysis, which gives a good representation of the behaviour of the soil. The expression of the safety factor is also straightforward, which only uses the occurring mobilised shear stresses (obtained from the finite element analysis) and a definition for the maximum available shear strength from available constitutive models. The proposed method only applies one kinematical constraint to produce the slip surfaces. It forces the slip surfaces to be upward concave. No other assumptions or restrictions are applied on the shape of the slip surface.

The new approach can be applied to different (complex) geometries to capture different loading conditions of embankments.
The results of the case studies as presented in Chapter 4 have shown that the proposed genetic algorithm is able to handle different soil conditions and shear strength definitions. The results of Example 4 indicate that the method is capable of locating an extremely weak layer and Example 5 shows the proper performance of analysing an undrained soil. The result of the case study of dike Bergambacht shows that the proposed method is capable of analysing a real and complex dike.

From these conclusions it can be determined that the research objective has been reached, which is stated as:

Improve the analysis of slope stability by developing a new method which combines concepts of both the Limit Equilibrium Method and Finite Element Method.

The method shows promising results, but its performance in even more complicated cases, such as the occurrence of uplift or the presence of a sheet pile, should still be demonstrated. And more use could be made of its potential to incorporate all constitutive models.

Bibliography

[1] K. P. Aryal. Slope stability evaluations by limit equilibrium and finite element methods. 2006.

[2] R. Baker. Determination of the critical slip surface in slope stability computations. *International Journal for Numerical and Analytical Methods in Geomechanics*, 4(4):333–359, 1980.

[3] A. Barneveld. *FEM based soil stress and strain analyses aimed at plant growth factors.* 2000.

[4] N. A. Barricelli. *Symbiogenetic evolution processes realized by artificial methods.* 1957.

[5] A. W. Bishop. The use of the slip circle in the stability analysis of slopes. *Geotechnique*, 5(1):7–17, 1955.

[6] R. B. J. Brinkgreve. Selection of soil models and parameters for geotechnical engineering application. In *Soil constitutive models: Evaluation, selection, and calibration*, pages 69–98. 2005.

[7] R. B. J. Brinkgreve, W. Broere, and D. Waterman. Plaxis 2d-version 8 reference manual. *Delft University of Technology&Plaxis bv, The Netherlands*, 2002.

[8] Z. Y. Chen and C. M. Shao. Evaluation of minimum factor of safety in slope stability analysis. *Canadian Geotechnical Journal*, 25(4):735–748, 1988.

[9] Y. M. Cheng. Location of critical failure surface and some further studies on slope stability analysis. *Computers and geotechnics*, 30(3):255–267, 2003.

[10] Y. M. Cheng, L. Li, and S. C. Chi. Performance studies on six heuristic global optimization methods in the location of critical slip surface. *Computers and Geotechnics*, 34(6):462–484, 2007.

[11] Y. M. Cheng, L. Li, S. C. Chi, and W. B. Wei. Particle swarm optimization algorithm for the location of the critical non-circular failure surface in two-dimensional slope stability analysis. *Computers and Geotechnics*, 34(2):92–103, 2007.

[12] A. K. Chugh. Variable interslice force inclination in slope stability analysis. *Soils and Foundations*, 26(1): 115–121, 1986.

[13] Deltares. D-stability. Technical report, Deltares, 2019.

[14] J. M. Duncan. State of the art: limit equilibrium and finite-element analysis of slopes. *Journal of Geotechnical engineering*, 122(7):577–596, 1996.

[15] J. M. Duncan, S. G. Wright, and T. L. Brandon. *Soil strength and slope stability.* John Wiley & Sons, 2014.

[16] J.M. Duncan and C. Chang. Nonlinear analysis of stress and strain in soils. *Journal of Soil Mechanics & Foundations Div*, 1970.

[17] M. M. Farias and D. J. Naylor. Safety analysis using finite elements. *Computers and Geotechnics*, 22(2): 165–181, 1998.

[18] W. Fellenius. Calculation of stability of earth dam. In *Transactions. 2nd Congress Large Dams, Washington, DC, 1936*, volume 4, pages 445–462, 1936.

[19] D. G. Fredlund, R. E. G. Scoular, and N. Zakerzadeh. Using a finite element stress analysis to compute the factor of safety. In *52nd Canadian Geotechnical Conf*, pages 73–80, 1999.

[20] A. H. Gandomi, A. R. Kashani, M. Mousavi, and M. Jalalvandi. Slope stability analysis using evolutionary optimization techniques. *International Journal for Numerical and Analytical Methods in Geomechanics*, 41(2):251–264, 2017.

[21] GeoDelft. Evaluatie rapport praktijkproef bergambacht. Technical report, GeoDelft, 2002.

[22] K. Georgiadis, D. M. Potts, and L. Zdravkovic. Modelling the shear strength of soils in the general stress space. *Computers and Geotechnics*, 31(5):357–364, 2004.

[23] A.C. Goh. Search for critical slip circle using genetic algorithms. *Civil Engineering Systems*, 17(3):181–211, 2000.

[24] D. V. Griffiths and P. A. Lane. Slope stability analysis by finite elements. *Geotechnique*, 49(3):387–403, 1999.

[25] N. A. Hammouri, A. I. H. Malkawi, and M. M. A. Yamin. Stability analysis of slopes using the finite element method and limiting equilibrium approach. *Bulletin of Engineering Geology and the Environment*, 67(4):471, 2008.

[26] J. Heyman and C. A. Coulomb. *Coulomb's memoir on statics: an essay in the history of civil engineering*. CUP Archive, 1972.

[27] J. H. Holland. *Adaptation in natural and artificial systems: an introductory analysis with applications to biology, control, and artificial intelligence*. MIT press, 1992.

[28] N. Janbu. Application of composite slip surface for stability analysis. In *Proceedings of European Conference on Stability of Earth Slopes, Sweden, 1954*, volume 3, pages 43–49, 1954.

[29] N. Janbu. Slope stability computations. *Publication of: Wiley (John) and Sons, Incorporated*, 1973.

[30] S. N. Jonkman, R. E. Jorissen, T. Schweckendiek, and J. P. van den Bos. *Flood Defences Lecture Notes*. TU Delft, 2018.

[31] R. Jurado-Piña and R. Jimenez. A genetic algorithm for slope stability analyses with concave slip surfaces using custom operators. *Engineering Optimization*, 47(4):453–472, 2015.

[32] J. Y. Kim and S. R. Lee. An improved search strategy for the critical slip surface using finite element stress fields. *Computers and Geotechnics*, 21(4):295–313, 1997.

[33] J. Krahn. The 2001 rm hardy lecture: The limits of limit equilibrium analyses. *Canadian geotechnical journal*, 40(3):643–660, 2003.

[34] F. H. Kulhawy. *Finite element analysis of the behavior of embankments*. PhD thesis, Library Photographic Service, University of California, 1969.

[35] C. C. Ladd. The prediction of in situ strees-strain behaviour of soft saturated clay during undrained shear. In *Proc. NGI Bolkesjo Symp.*, pages 14–20, 1969.

[36] C. C. Ladd. Stability evaluation during staged construction. *Journal of geotechnical engineering*, 117(4): 540–615, 1991.

[37] C. C. Ladd and R. Foott. New design procedure for stability of soft clays. *Journal of Geotechnical and Geoenvironmental Engineering*, 100(Proc Paper 10064), 1974.

[38] P. V. Lade. Overview of constitutive models for soils. In *Soil constitutive models: Evaluation, selection, and calibration*, pages 1–34. 2005.

[39] P. V. Lade and J.M. Duncan. Elastoplastic stress-strain theory for cohesionless soil. *Journal of the Geotechnical Engineering Division*, 101(10):1037–1053, 1975.

[40] R. Lagioia and A. Panteghini. On the existence of a unique class of yield and failure criteria comprising tresca, von mises, drucker–prager, mohr–coulomb, galileo–rankine, matsuoka–nakai and lade–duncan. *Proceedings of the Royal Society A: Mathematical, Physical and Engineering Sciences*, 472(2185):20150713, 2016.

[41] R. Lagioia and A. Panteghini. Accounting for specific failure criteria in the slip-line method for plane strain problems. *Géotechnique Letters*, 7(2):184–189, 2017.

[42] P. A. Lane and D. V. Griffiths. Assessment of stability of slopes under drawdown conditions. *Journal of geotechnical and geoenvironmental engineering*, 126(5):443–450, 2000.

[43] Y. C. Li, Y. M. Chen, T. L. Zhan, D. S. Ling, and P. J. Cleall. An efficient approach for locating the critical slip surface in slope stability analyses using a real-coded genetic algorithm. *Canadian Geotechnical Journal*, 47(7):806–820, 2010.

[44] K. Lim, A. J. Li, and A. V. Lyamin. Three-dimensional slope stability assessment of two-layered undrained clay. *Computers and Geotechnics*, 70:1–17, 2015.

[45] S. Y. Liu, L. T. Shao, and H. J. Li. Slope stability analysis using the limit equilibrium method and two finite element methods. *Computers and Geotechnics*, 63:291–298, 2015.

[46] A. I. H. Malkawi, W. F. Hassan, and S. K. Sarma. Global search method for locating general slip surface using monte carlo techniques. *Journal of geotechnical and geoenvironmental engineering*, 127(8):688–698, 2001.

[47] H. Matsuoka and T. Nakai. Stress-deformation and strength characteristics of soil under three different principal stresses. In *Proceedings of the Japan Society of Civil Engineers*, volume 1974, pages 59–70. Japan Society of Civil Engineers, 1974.

[48] O. Mohr. Ueber die darstellung des spannungszustandes und des deformationszustandes eines körperelementes und über die anwendung derselben in der festigkeitslehre. *Civilingenieur*, 28:113–156, 1882.

[49] M. M. Moni and M. M. Sazzad. Stability analysis of slopes with surcharge by lem and fem. *International Journal of Advances in Structural and Geotechnical Engineering*, 4(4):216–225, 2015.

[50] N. U. Morgenstern and V. E. Price. The analysis of the stability of general slip surfaces. *Geotechnique*, 15 (1):79–93, 1965.

[51] V. U. Nguyen. Determination of critical slope failure surfaces. *Journal of Geotechnical Engineering*, 111 (2):238–250, 1985.

[52] T. Pasik and R. van der Meij. Locating critical circular and unconstrained failure surface in slope stability analysis with tailored genetic algorithm. *Studia Geotechnica et Mechanica*, 39(4):87–98, 2017.

[53] H. T. V. Pham and D. G. Fredlund. The application of dynamic programming to slope stability analysis. *Canadian Geotechnical Journal*, 40(4):830–847, 2003.

[54] D. M. Potts and A. Gens. The effect of the plastic potential in boundary value problems involving plane strain deformation. *International Journal for Numerical and Analytical Methods in Geomechanics*, 8(3): 259–286, 1984.

[55] POVM. Povm eindige-elementenmethode. Technical report, POVM, 2020.

[56] N. Prasad and K. Sai. Applicability of mohr-coulomb drucker-prager models for assessment of undrained shear behaviour of clayey soils. 2014.

[57] M. Rabie. Comparison study between traditional and finite element methods for slopes under heavy rainfall. *HBRC Journal*, 10(2):160–168, 2014.

[58] Rijkswaterstaat. Wbi2017 code calibration. Technical report, Rijkswaterstaat, 2017.

[59] K. H. Roscoe and J. B. Burland. On the generalized stress-strain behaviour of wet clay. 1968.

[60] K. H. Roscoe, A. Schofield, and A. Thurairajah. Yielding of clays in states wetter than critical. *Geotechnique*, 13(3):211–240, 1963.

[61] P. W. Rowe. The stress-dilatancy relation for static equilibrium of an assembly of particles in contact. *Proceedings of the Royal Society of London. Series A. Mathematical and Physical Sciences*, 269(1339):500–527, 1962.

[62] N. Sabhahit, S. Jacob, and M. R. Madhav. Genetic algorithms in searching the critical slip surface. *Indian Geotechnical Journal*, 32(2):86–101, 2002.

[63] S. K. Sarma. Stability analysis of embankments and slopes. *Geotechnique*, 23(3):423–433, 1973.

[64] M. Satake. On equivalent mohr circle in granular materials. Technical report, 1982.

[65] T. Schanz, P. A. Vermeer, and P. G. Bonnier. The hardening soil model: formulation and verification. *Beyond 2000 in computational geotechnics*, pages 281–296, 1999.

[66] G. J. Schiereck. Fundamentals on water defences. *TAW-ENW report*, 1998.

[67] A. Schofield and P. Wroth. *Critical state soil mechanics*. McGraw-hill, 1968.

[68] A. W. Skempton. The pore-pressure coefficients a and b. *Geotechnique*, 4(4):143–147, 1954.

[69] E. Spencer. A method of analysis of the stability of embankments assuming parallel inter-slice forces. *Geotechnique*, 17(1):11–26, 1967.

[70] C. Surarak, S. Likitlersuang, D. Wanatowski, A. Balasubramaniam, E. Oh, and H. Guan. Stiffness and strength parameters for hardening soil model of soft and stiff bangkok clays. *Soils and foundations*, 52 (4):682–697, 2012.

[71] M. A. Van. New approach for uplift induced slope failure. pages 2285–2288, 2001.

[72] T. A. Van Duinen. Grensverleggend onderzoek macrostabiliteit bij opdrijven-fase 2.c. *Deltares rapport 419230–0040*, 2008.

[73] A. Verruijt. *Soil mechanics*. Delft University of Technology Delft, 2001.

[74] D. M. Wood. *Soil behaviour and critical state soil mechanics*. Cambridge university press, 1990.

[75] C. P. Wroth. The interpretation of in situ soil tests. *Geotechnique*, 34(4):449–489, 1984.

[76] T. Yamagami and T. Veta. Search for noncircular slip surfaces by the morgenstern-price method. In *Proc. 6th Int. Conf. Numer. Methods in Geomech.*, pages 1335–1340, 1988.

[77] J. F. Zhu and C. F. Chen. Search for circular and noncircular critical slip surfaces in slope stability analysis by hybrid genetic algorithm. *Journal of Central South University*, 21(1):387–397, 2014.

[78] O. C. Zienkiewicz, C. Humpheson, and R.W. Lewis. Associated and non-associated visco-plasticity and plasticity in soil mechanics. *Geotechnique*, 25(4):671–689, 1975.

[79] A. R. Zolfaghari, A. C. Heath, and P. F. McCombie. Simple genetic algorithm search for critical non-circular failure surface in slope stability analysis. *Computers and geotechnics*, 32(3):139–152, 2005.

A
Soil Models

A.1. Mohr-Coulomb Model

To model the drained shear strength of soils, the Mohr-Coulomb model can be used. Introduced by Otto Mohr in 1882 (Mohr [48]), Mohr's circle illustrates principal stresses and stress transformations via a graphical format as presented in Figure A.1.

The two principal stresses are σ_1 and σ_3. In case that the inspected plane is aligned with the principal direction, the normal stresses are equal to the principal stresses. Each point on Mohr's circle represents the normal and shear stress on a certain plane. All planes together form the circle, since as the inspected plane is rotated away from the principal directions, the stress points traverse the circle. The ratio of shear stress to normal stress varies along the circle, as this ratio is different for different planes. For the derivation of Mohr's circle the reader is referred to Verruijt [73].

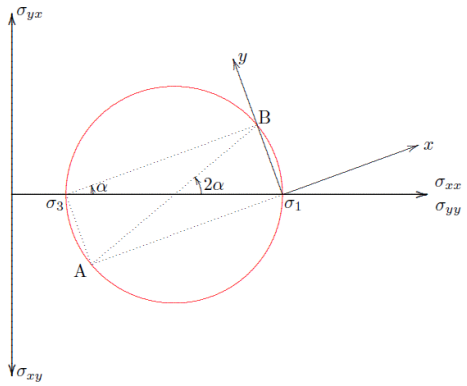

Figure A.1: Mohr's Circle (Verruijt [73])

Charles-Augustin de Coulomb used the analogy of a sliding block to propose a relationship of the maximum possible shear stress in a soil body, according to Heyman and Coulomb [26]. This criterion can be written as

$$\tau_f = c' + \sigma' \tan\phi', \tag{A.1}$$

where c' is the cohesion, σ' the effective stress and ϕ the angle of shearing resistance.

For a certain plane in Mohr's circle, the criterion in Equation A.1 can be met. In Figure A.2 these critical planes are indicated by C and D. On all other planes the shear stress remains below the critical value. The ratio between τ/σ is maximal when Mohr's circle touches the Coulomb envelope, this is where failure will start to occur. This is called the Mohr-Coulomb failure criterion. For this criterion the mathematical formulation is given as:

$$f = \frac{1}{2}\left|\sigma'_1 - \sigma'_3\right| + \frac{1}{2}\left(\sigma'_1 + \sigma'_3\right)\sin(\phi) - c\cos(\phi) \tag{A.2}$$

In case a third plasticity parameter, the dilatancy angle Ψ, is included, the plastic potential function is given as:

$$g = \frac{1}{2}\left|\sigma'_1 - \sigma'_3\right| + \frac{1}{2}\left(\sigma'_1 + \sigma'_3\right)\sin(\Psi) \tag{A.3}$$

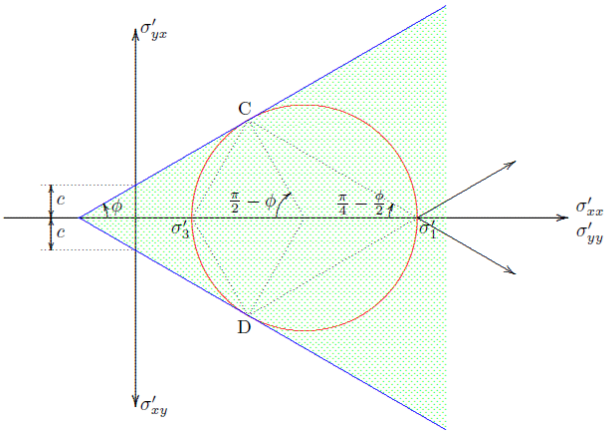

Figure A.2: Mohr Coulomb (Verruijt [73])

The Mohr-Coulomb model is an elastic-perfectly plastic model as shown in Figure A.3. The linear elastic part is based on Hooke's law of isotropic elasticity, whilst the perfectly plastic part is based on the Mohr-Coulomb failure criterion. When implementing the Mohr-Coulomb model, attention has to be given to the transition between the yield surfaces as shown in Figure A.4. The yield surface is shaped as a hexagon which consists of six contours. In PLAXIS the exact form of the model is implemented, using a sharp transition between the yield surfaces. The parameters required by the Mohr-Coulomb model are listed in Table A.1.

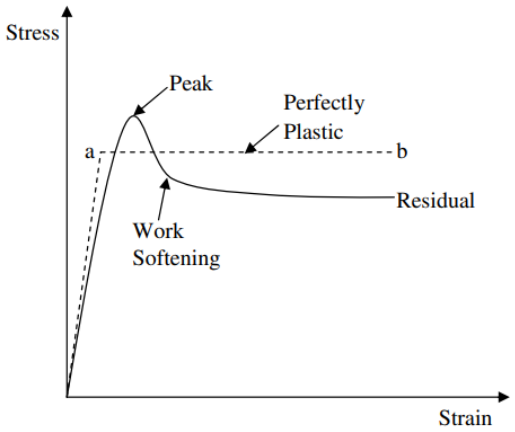

Figure A.3: Elastic-perfectly plastic assumption of Mohr-Coulomb model (Prasad and Sai [56])

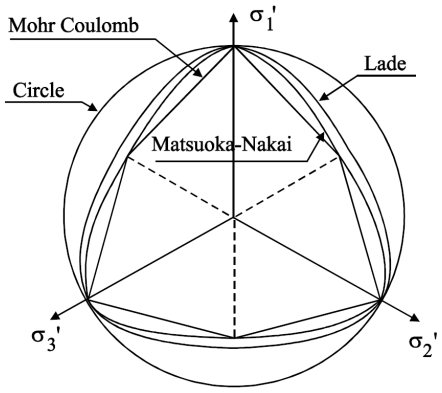

Figure A.4: Failure Surfaces in the Deviatoric Plane (Georgiadis et al. [22])

Table A.1: Model Parameters Mohr-Coulomb Model

c'	(effective) cohesion	$[kN/m^2]$
ϕ'	(effective) internal friction angle	[°]
Ψ	Dilatancy angle	[°]
E	Elasticity modulus	$[kN/m^2]$
ν	Poisson's ratio	[-]
γ	Volumetric weight of the soil	$[kN/m^2]$

The dilation angle Ψ controls the amount of strain developed during shearing. If $\Psi = \phi$, the plasticity flow is called associated, in case $\Psi \neq \phi$ the plasticity flow is called non-associated. Ψ is maximal when reaching the peak strength and decreases till the critical state strength.

A summary on the main characteristics of the Mohr-Coulomb model are given in A.2.

Table A.2: Advantages and Limitations Mohr-Coulomb Model

Advantages	Limitations
Simple and clear	Isotropic and homogeneous behaviour
Limited number and well defined parameters	Until failure linear elastic behaviour
Dilatancy can be included	No stress-dependent stiffness
Good representation of drained failure behaviour	Dilatancy continues forever (no critical state)
	No distinction between primary loading, unloading or reloading
	Undrained behaviour not always realistic
	Not able to model shear induced pore pressure
	No time-dependency (creep)
	No anisotropy

A.2. Modified Cam-Clay (MCC) Model

Before the maximum stress of a soil has been reached, some irreversible straining has occurred in the soil. Thus, plastic deformations already occr in the early stages of loading. To capture this behaviour in a constitutive model, the typical elastic-perfectly plastic model such as Mohr-Coulomb does not suffice anymore. To represent this hardening behaviour of soil, a constitutive model which utilizes a hardening law after initial yielding is needed. Therefore researches have looked into the possibility of modelling soil as a strain hardening material. Roscoe et al. [60] use the strain hardening theory of plasticity to formulate a complete stress-strain model for normally or lightly over-consolidated clay, known as the Cam-Clay model, which is formulated by Schofield and Wroth [67]. A modified version of the Cam-Clay model is suggested by Roscoe and Burland [59] and this modified Cam-Clay model is extended to a general three-dimensional stress state. In this section the modified Cam-Clay model will be described, where from now on this model will be referred to as just the Cam-Clay model. The description of this model is based on the work of Wood [74]. This model is an elastic-plastic strain hardening model that is based on the critical state theory and the assumption that there is a logarithmic relationship between the mean effective stress p' and specific volume v, where $v = 1 + e$ in which e is the void ratio.

To specify an elastic-plastic model, the following properties have to be defined:

1. Elastic properties: the recoverable deformation
2. Yield surface: occurrence of plastic deformation
3. Plastic potential: the mechanism of plastic deformations
4. Hardening rule: the magnitudes of the plastic deformations and the change in size of the yield surface

This model assumes that recoverable changes in volume are accompanied by a change in the mean effective stress p' following the expression:

$$\delta\epsilon_p^e = \kappa \frac{\delta p'}{\upsilon p'}. \tag{A.4}$$

This expression implies that in the compression plane a linear relation can be found between the specific volume υ and logarithm of p' for elastic unloading-reloading of the soil. The recoverable shear strains are assumed to follow the changes in deviator stress q:

$$\delta\epsilon_q^e = \frac{\delta q}{3G'}, \tag{A.5}$$

with a constant shear modulus G'. Figure A.5 shows the yield locus of the Cam Clay model in the $p' : q$ plane and the compression plane $p' : \upsilon$. This yield locus is given by the following equation:

$$\frac{p'}{p'_0} = \frac{M^2}{M^2 + \eta^2} \tag{A.6}$$

where $\eta = q/p'$. The yield locus can also be rewritten as:

$$f = q^2 - M^2[p'(p'_0 - p')] = 0 \tag{A.7}$$

In this model it is assumed that the soil conforms the normality condition, therefore the plastic potentials are given in the same for as the yield function: $g = f$. The plastic strain increments are given as:

$$\frac{\delta\epsilon_p^P}{\delta\epsilon_q^P} = \frac{M^2 - \eta^2}{2\eta} \tag{A.8}$$

It is assumed that the yield loci expand at constant shape, thus all have the form as given by Equation A.7, where the size is controlled by the stress p'_0. The expansion of the yield loci is linked with the normal compression of the soil: a linear relationship is assumed between the specific volume υ and logarithm of p'_0 during isotropic normal compression of the soil as can be seen in Figure A.5,

$$\upsilon = N - \lambda \ln p'_0 \tag{A.9}$$

where N is a soil constant which specifies the position of the normal compression line in the compression plane as shown in Figure A.5. It is the specific volume obtained by unloading the current configuration (p, υ) to the initial pressure (p_0). The plastic volumetric strains can be found with:

$$\delta\epsilon_p^P = [(\lambda - \kappa)/\upsilon] \frac{\delta p'_0}{p'_0} \tag{A.10}$$

and the hardening rule is given as:

$$\frac{\delta p'_0}{\delta\epsilon_p^P} = \frac{\upsilon p'_0}{\lambda - \kappa} \qquad \frac{\delta p'_0}{\delta\epsilon_q^P} = 0 \tag{A.11}$$

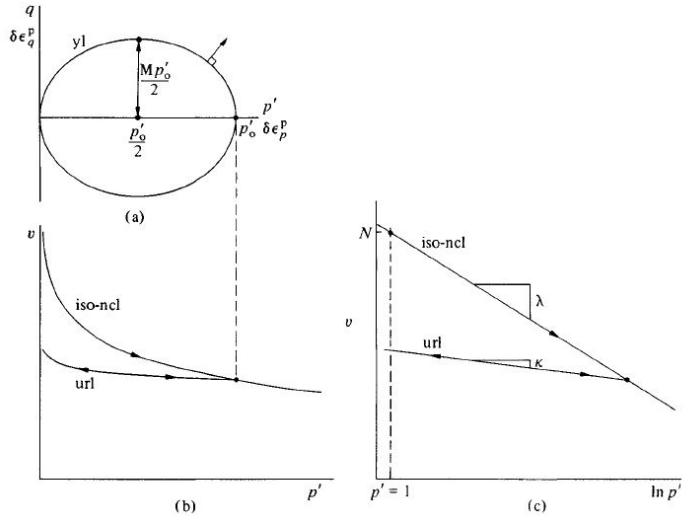

Figure A.5: Elliptical Yield Locus for Cam-Clay Model (Wood [74])

In case the soil starts to yield in an undrained test, the volume change of the soil will be equal to zero. This means that the elastic and plastic contributions are exactly equal and opposite such that the total volumetric strain is zero. In an undrained test the mean effective stress reduces due to the build up of pore pressure, hence elastic volumetric expansion occurs. It is necessary for the yield curve to expand and produce plastic volumetric compression to balance the elastic expansion. (It will be showed later on that the reverse situation can also occur in an undrained situation where plastic volumetric expansion occurs, balanced by elastic volumetric compression. This however, does not oppose the statement that the total volumetric strain is equal to zero.) The condition that the summation of these are equal to zero is given as

$$\delta\epsilon_p^e + \delta\epsilon_p^P = 0 \rightarrow \kappa \frac{\delta p'}{\upsilon p'} = -(\lambda - \kappa)\frac{\delta p_0'}{\upsilon p_0'} \tag{A.12}$$

which forces a link between the mean effective stress p' and changes in the size of the yield locus, given by p_0'. The expression can be rewritten as:

$$\frac{p_i'}{p'} = \left(\frac{M^2 + \eta^2}{M^2 + \eta_i^2}\right)^{\Lambda} \tag{A.13}$$

where $\Lambda = (\lambda - \kappa)/\lambda$. Equation A.13 gives the shape of the undrained effective stress path in the $p' : q$ plane, as shown in Figure A.6.

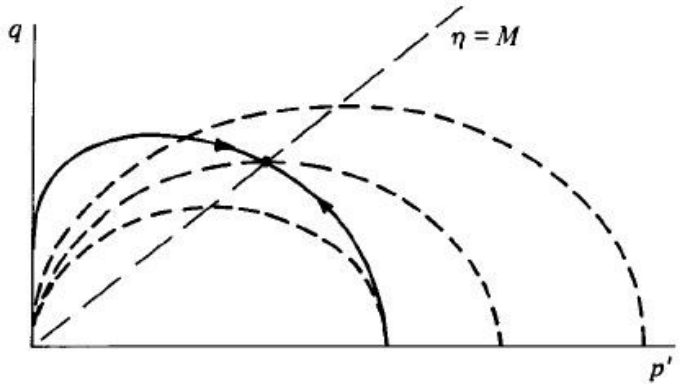

Figure A.6: Equation A.13 (Wood [74])

In Figure A.7 three different tests are shown: an initially normally compressed, lightly overconsolidated and highly consolidated sample. Each point lies on a new yield locus.

For both the normally consolidated and lighly overconsolidated case holds that $\eta < M$. Yielding takes place with a strain increment vector directed to the right, which implies that plastic volumetric compression is occurring. The soil wants to harden plastically, and therefore the current yield locus has to expand. To balance the plastic compression, the mean effective stress must decrease (positive pore pressures) such that elastic expansion occurs. This is called the wet side. The difference between these two cases is that the lightly overconsolidated case begins with an elastic phase AB until the stress state reaches the initial yield locus.

For the heavily overconsolidated sample $\eta > M$, yielding takes place with plastic strain increment vector directed to the left, which implies that plastic volumetric expansion is occurring. The soil wants to soften plastically, and therefore the yield locus has to shrink. To balance the plastic expansion, the mean effective stress must increase (negative pore pressures) such that elastic compression occurs. This is called the dry side.

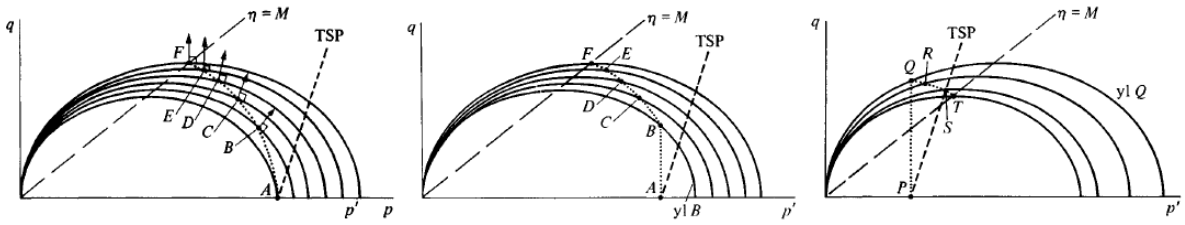

Figure A.7: Stress Increments in Undrained Analysis (Wood [74])

Critical States

In the normally consolidated case in Figure A.7, the direction of the plastic strain increment is plotted. The ratio plastic shear strain increment to plastic volumetric strain increment can thus be determined, this ratio increases when the normal to the yield locus becomes more parallel to the q axis. At point F this ratio becomes infinite, where unlimited plastic shear strains can develop without any extra plastic volumetric strain or effective stresses. Since no plastic volumetric strain occurs, the yield locus remains the same size. This condition of perfect plasticity is the critical state. In Figure A.7 a line is drawn which joins the tops of the yield loci at $\eta = M$, this is called the critical state line (csl). In the framework of critical state, a distinction is made between the shear strength of normally consolidated and overconsolidated soils. The ultimate shear strength is defined at the critical state. Literature has shown that using the shear strength at critical state is suitable for the calculation of slope stability Van Duinen [72].

Undrained Shear Strength in Cam-Clay Framework

Figure A.8 shows Mohr's circles. If a soil sample is undrained, then this circle of effective stress at failure (point E) can be represented by infinite number of these total stress circles. The ultimate value of deviator stress q_f is the diameter of the Mohr circle of effective or total stress, as shown in this figure, and is twice the undrained shear strength s_u.

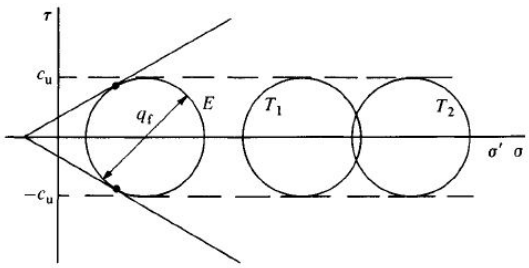

Figure A.8: Mohr's Circle of Total and Effective Stress (Wood [74])

A soil with a specific volume v (as shown in Figure A.9) will end up on the critical state line at the mean effective stress p'_f when tested in undrained triaxial compression. The expression for this mean effective stress is:

$$p'_f = \exp\left(\frac{\Gamma - v}{\lambda}\right) \tag{A.14}$$

where, $\Gamma = N - (\lambda - \kappa)\ln 2$, which is the location of the critical state line in the compression plane as shown in Figure A.10. With the following expressions for q_f and c_u:

$$q_f = Mp'_f \qquad s_u = \frac{q_f}{2} \tag{A.15}$$

the undrained shear strength is given as:

$$s_u = \frac{q_f}{2} = \frac{Mp'_f}{2} = \frac{M}{2}\exp\left(\frac{\Gamma - v}{\lambda}\right). \tag{A.16}$$

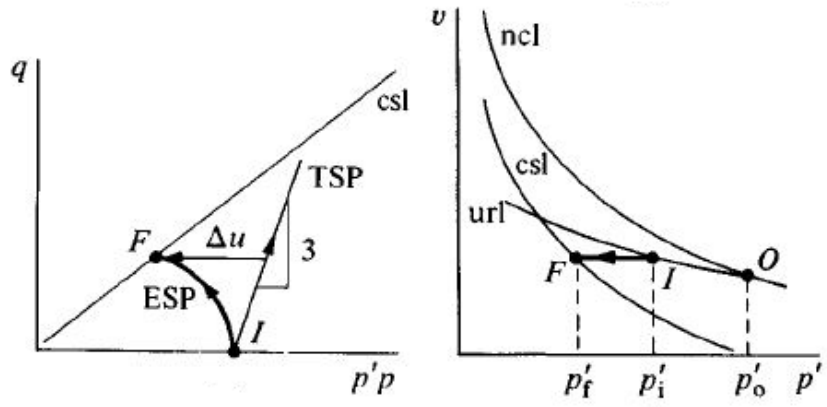

Figure A.9: Effective Stress Plane and Compression Plane (Wood [74])

This undrained shear strength can be linked with consolidation history. In Figure A.10 it is shown that the normal compression line and critical state line are parallel in the compression plane. Expressions for the normal compression line and unloading-reloading line are given by Equations **??**, **??** respectively. The critical state line can be written as:

$$v = \Gamma - \lambda \ln p' \tag{A.17}$$

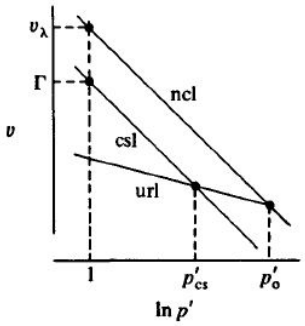

Figure A.10: Normal compression line, unloading-reloading line and critical state line(Wood [74])

The volume separation between the normal compression and critical state lines is $v_\lambda - \Gamma$. This separation can also be expressed in terms of pressures. The pressure ratio r is an extra soil parameter and defined as:

$$r = \exp\left(\frac{v_\lambda - \Gamma}{\lambda - \kappa}\right) \tag{A.18}$$

Again, having a look at Figure A.9, the specific volume of the sample at point I is given by:

$$v_i = v_\lambda - \lambda p'_0 + \kappa \ln n_p, \tag{A.19}$$

where n_p is the isotropic overconsolidation ratio. Using Equation A.16, the undrained shear strength at point F is on the critical state line is:

$$s_u = \frac{M}{2} \exp\left[\frac{\Gamma - v_\lambda}{\lambda} + \ln p'_0 - \left(\frac{\kappa}{\lambda}\right) \ln n_p\right], \tag{A.20}$$

which can be rewritten to:

$$\frac{s_u}{p_i} = \frac{M}{2}\left(\frac{n_p}{r}\right)^\Lambda, \tag{A.21}$$

where

$$\Lambda = \frac{\lambda - \kappa}{\lambda} \tag{A.22}$$

In terms of vertical effective stress, the undrained shear strength can be expressed as:

$$\frac{s_u/\sigma'_{vi}}{(s_u/\sigma'_{vi})_{nc}} = \frac{n}{n_p} n_p^\Lambda \tag{A.23}$$

In Table A.1 all symbols are given for the Cam-Clay Model. The model however only uses three parameters λ, κ and M.

Table A.3: Parameters Modified Cam-Clay

λ	isotropic logarithmic compression index		[-]
κ	swelling index		[-]
M	friction constant	$M = \frac{6\sin\phi'}{3-\sin\phi'}$	[-]
e	initial void ratio		[-]
p'	mean stress	$p' = \frac{\sigma'_1+\sigma'_2+\sigma'_3}{3}$	$[kN/m^2]$
p'_f	mean effective stress at critical state line		$[kN/m^2]$
p'_0	mean effective stress during isotropic normal compression		$[kN/m^2]$
p'_i	initial mean effective stress		$[kN/m^2]$
q	deviator stress	$q = \left(\frac{(\sigma'_2-\sigma'_3)^2+(\sigma'_3-\sigma'_1)^2+(\sigma'_1-\sigma'_2)^2}{2}\right)$	$[kN/m^2]$
q_f	ultimate value of deviator stress		$[kN/m^2]$
n	overconsolidation ratio	$n = \frac{\sigma'_{vmax}}{\sigma'_v}$	[-]
n_p	isotropic overconsolidation ratio	$n_p = \frac{p'_{max}}{p'}$ or $\frac{p'_0}{p'_i}$	[-]
σ'_0	pre-consolidation pressure/initial vertical stress		$[kN/m^2]$
N	location of isotropic normal compression line in $v : \ln p'$ plane		[-]
r	pressure ratio	$r = \frac{p'_0}{p'_{cs}} = \exp\left(\frac{v_\lambda - \Lambda}{\lambda - \kappa}\right)$	[-]

The main advantages and limitations of the modified Cam Clay model are summarised in Table A.4.

Table A.4: Advantages and Limitations Modified Cam-Clay Model

Advantages	Limitations
Takes loading history and stress(path)-dependent stiffness differences into account	Less suitable for overconsolidated clay and in certain unloading stress paths; not suitable for sand
Reasonable model for primary loading of normally consolidated clays and soft soils, which means it is capable of modelling shear induced pore pressures	Critical state failure contour is 'only' Drucker-Prager (but can easily be adapted)
	Inaccurate horizontal/vertical stress ratio in 1D compression
	No secondary compression (creep)
	No anisotropy

A.2.1. Hardening Soil Model

Schanz et al. [65] have introduced a new constitutive model, the Hardening Soil Model, which is formulated in the framework of classical theory of plasticity. It is an advanced model for simulating the behaviour of different soil types, both for soft and stiff soils. The formulation of the Hardening Soil Model is based on the assumption of a hyperbolic relation between the vertical strain ϵ_1 and the deviatoric stress q. This relationship is shown in Figure A.11.

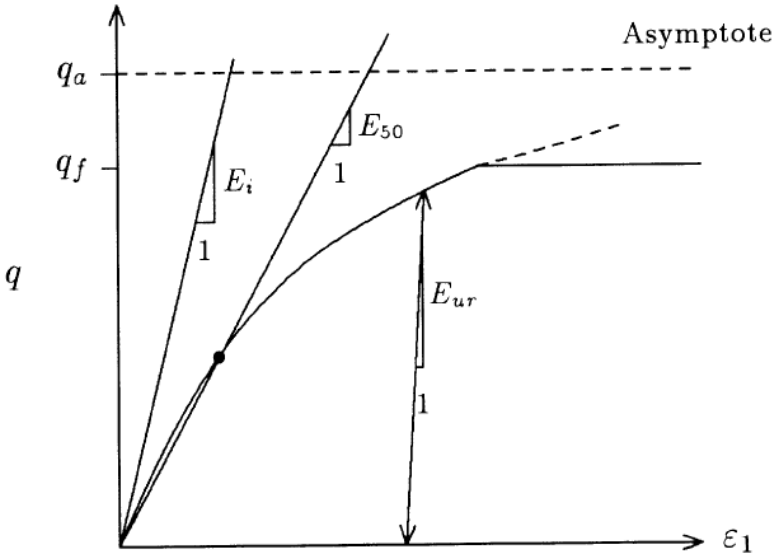

Figure A.11: Hyperbolic Stress-Strain Relation in Primary Loading for a Standard Drained Triaxial Test (Schanz et al. [65])

Stiffness for Primary Loading

The stiffness of soil decreases when subjected to primary deviatoric loading. At the same time plastic strains develop in the soil which are irreversible. In case of a drained triaxial test, the relationship between the axial strain ϵ_1 and the deviatoric stress q can be approximated by a hyperbola (Schanz et al. [65]). Standard drained triaxial tests give yield curves given by the following equation:

$$\epsilon_1 = \frac{q_a}{2E_{50}} \frac{(\sigma_1 - \sigma_3)}{q_a - (\sigma_1 - \sigma_3)} \qquad \text{for } q < q_f, \tag{A.24}$$

q_f is the ultimate deviatoric stress and q_a the asymptotic value of the shear strength. These are defined as:

$$q_f = \frac{6\sin\phi_p}{3 - \sin\phi_p}(p + c\cot\phi_p) \qquad q_a = \frac{q_f}{R_f}. \tag{A.25}$$

In case the observed deviatoric stress q equals q_f, the failure criterion is met and perfectly plastic yielding occurs.

From Figure A.11 it can be seen that three different stiffness moduli are plotted, these coincide with different loading conditions. For primary loading the stress strain behaviour is highly nonlinear. The parameter E_{50} is used which is the confining stress dependent stiffness modules for primary loading. The expression for E_{50} is given as follows:

$$E_{50} = E_{50}^{ref} \left(\frac{\sigma_3 + c\cot\phi_p}{\sigma^{ref} + c\cot\phi_p} \right)^m. \tag{A.26}$$

where E_{50}^{ref} is the reference stiffness modulus corresponding to the reference stress p^{ref}. It can be determined from a triaxial stress-strain-curve for a mobilisation of 50% of the maximum shear strength q_f.

Stiffness for Un-/Reloadig

For the unloading and reloading case, the stiffness modulus is formulated as:

$$E_{ur} = E_{ur}^{ref} \left(\frac{\sigma_3 + c\cot\phi_p}{\sigma^{ref} + c\cot\phi_p} \right)^m . \tag{A.27}$$

where E_{ur}^{ref} is the reference Young's modulus for unloading and reloading, corresponding to the reference pressure σ^{ref}. The elastic components of the strain are calculated using this expression for the stiffness modulus:

$$\epsilon_1^e = \frac{q}{E_{ur}} \quad , \quad \epsilon_2^e = \epsilon_3^e = \nu_{ur} \frac{q}{E_{ur}} \tag{A.28}$$

The expression for the elastic strains are the strains that develop during deviatoric loading, fully elastic volume changes are not included in this equation.

Yield Surface

The yield function in the Hardening Soil Model is given as:

$$f_{12} = \frac{q_a}{E_{50}} \frac{(\sigma_1 - \sigma_2)}{q_a - (\sigma_1 - \sigma_2)} - \frac{2(\sigma_1 - \sigma_2)}{E_{ur}} - \gamma^p \tag{A.29}$$

$$f_{13} = \frac{q_a}{E_{50}} \frac{(\sigma_1 - \sigma_3)}{q_a - (\sigma_1 - \sigma_3)} - \frac{2(\sigma_1 - \sigma_3)}{E_{ur}} - \gamma^p \tag{A.30}$$

where the plastic shear strain γ_p is given as:

$$\gamma^p = \epsilon_1^p - \epsilon_2^p - \epsilon_3^p = 2\epsilon_1^p - \epsilon_v^p \approx 2\epsilon_1^p . \tag{A.31}$$

This plastic shear strain γ^p is used as the relevant parameter for frictional hardening. Equation A.31 shows that the definition for the plastic shear strain is actually an approximation, since ϵ_v^p is not taken into account. The plastic volumetric strains ϵ_v^p will never be exactly zero. However, for hard soils plastic volume changes ten to be small when compared with the axial strain, making the approximation appropriate (Schanz et al. [65]).

Flow Rule

Just like other plasticity models, the Hardening-Soil model involves a relationship between the rates of plastic strain: between $\dot{\epsilon}_v^p$ and $\dot{\gamma}^p$. This flow rule has the form:

$$\dot{\epsilon}_v^p = \sin\Psi_m \dot{\gamma}^p , \tag{A.32}$$

where the mobilised dilatancy angle Ψ_m is given as:

$$\sin\Psi_m = \frac{\sin\phi_m - \sin\phi_{cv}}{1 - \sin\phi_m \sin\phi_{cv}} , \tag{A.33}$$

where ϕ_{cv} is the critical state friction angle and ϕ_m the mobilised friction angle:

$$\sin\phi_m = \frac{\sigma_1 - \sigma_3}{\sigma_1 + \sigma_3 - 2c\cot\phi_p} \tag{A.34}$$

These equations correspond to the stress-dilatancy theory as described by Rowe [61]. This theory states that when the stress ratios is small ($\phi_m < \phi_{cv}$), the material contracts. Whereas dilatancy occurs for high stress ratios ($\phi_m > \phi_{cv}$). When the soil fails, the mobilised friction angle equals the failure angle, such that Equation A.33 can be rewritten to:

$$\sin\Psi_{cv} = \frac{\sin\phi_p - \sin\Psi_p}{1 - \sin\phi_p \sin\Psi_p} . \tag{A.35}$$

Thus the critical state angle can be computed from the failure angels ϕ_p and Ψ_p. This flow rule is equivalent to the definition of the plastic potential functions, given as:

$$g_{12} = (\sigma_1 - \sigma_2)/2 - (\sigma_1 + \sigma_2)/2 \cdot \sin\Psi_m \tag{A.36}$$

$$g_{13} = (\sigma_1 - \sigma_3)/2 - (\sigma_1 + \sigma_3)/2 \cdot \sin\Psi_m \tag{A.37}$$

Cap Yield Surface

The stiffness moduli E_{50}^{ref} and E_{ur}^{ref} are parameters that control the shear yield surfaces. These shear hardening surfaces, as shown in Figure A.12 do not explain the plastic volume strain that is measured in isotropic compression. A second type of yield surface is introduced, which is called the cap type yield surface. These cap yield surfaces are also shown in Figure A.12 for soil with no cohesion. From this figure it can be seen that the cap yield surface is needed to close of the region in the direction of the p-axis.

Earlier it has already been mentioned that E_{50}^{ref} largely controls the magnitude of the plastic strains, which are again associated with the shear yield surface. Likewise, the oedometer modulus E_{oed}^{ref} controls the magnitude of the plastic strains that originate from the cap yield surface and is formulated as follows:

$$E_{oed} = E_{oed}^{ref}\left(\frac{\sigma_3 + c\cot\phi_p}{\sigma^{ref} + c\cot\phi_p}\right)^m \tag{A.38}$$

The cap yield surface is given as:

$$f_c = \frac{\tilde{q}^2}{M^2} + (p+a)^2 - (p_c+a)^2 \tag{A.39}$$

where $a = c\cot\phi$, $p = \sigma_1 + \sigma_2 + \sigma_3$ and

$$\tilde{q} = \sigma_1 + (\alpha-1)\sigma_2 - \alpha\sigma_3, \qquad \text{with } \alpha = \frac{3\sin\phi}{3-\sin\phi} \tag{A.40}$$

An associated flow rule is used for yielding on the cap surface, such that the plastic potential g_c is found as $g_c = f_c$. In addition to the parameters σ_{ref} and m, an extra model parameter M is added. However, there is a relationship between K_0^{NC} and M, such that it can be used as an input parameter that determines the magnitude of M.

For further derivation of the Hardening Soil model, the reader is referred to Schanz et al. [65].

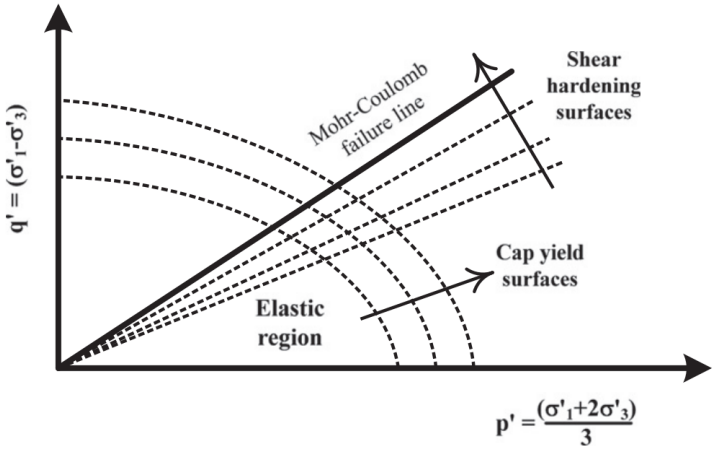

Figure A.12: Shear and cap yield surfaces in the Hardening Soil Model (Surarak et al. [70])

Undrained Shear Strength

The undrained shear strength can be found as $s_u = q_f/2$, with

$$q_f = \frac{6\sin\phi_p}{3-\sin\phi_p}(p + c\cot\phi_p). \tag{A.41}$$

In Table A.5 the model parameters are given used in the Hardening Soil Model.

Table A.5: Model Parameters Hardening Soil Model

c'	(effective) cohesion	$[kN/m^2]$
ϕ'_p	(effective) internal friction angle	[°]
Ψ	Dilatancy angle	[°]
E_{50}^{ref}	Secant stiffness in standard drained triaxial test	$[kN/m^2]$
E_{oed}^{ref}	Tangent stiffness for primary oedometer loading	$[kN/m^2]$
E_{ur}^{ref}	Stiffness for unloading and reloading	$[kN/m^2]$
m	Power for stress-level dependency of stiffness	[-]
p_{ref}	Reference stress for stiffness	$[kN/m^2]$
ν_{ur}	Unloading/reloading Poisson's ratio	$[kN/m^2]$
K_0^{nc}	CK_0 value for normal consolidation	$[kN/m^2]$
R_f	Failure ratio	[-]

$$K_0^{NC} = 1 - \sin\phi_p \tag{A.42}$$

For soft clays m = 1.

The main advantages and limitations of the hardening soil model are summarised in Table A.6.

Table A.6: Advantages and Limitations Hardening Soil Model

Advantages	Limitations
Better non-linear formulation of soil behaviour in general	No peak strength and softening (immediate residual strength)
Distinction between primary loading and unloading/reloading	No accumulation of strain or pore pressure in cyclic loading
Memory of preconsolidation stress	No secondary compression (creep)
Different stiffnesses for different stress paths	No anisotropy
Well suited for unloading situations with simultaneous deviatoric loading	$E_{50}/E_{oed} > 2$ difficult to input
Takes into account soil dilatancy	
Yield surface can expand due to plastic straining	

B

Sensitivity Analysis

B.1. Initial Population Size

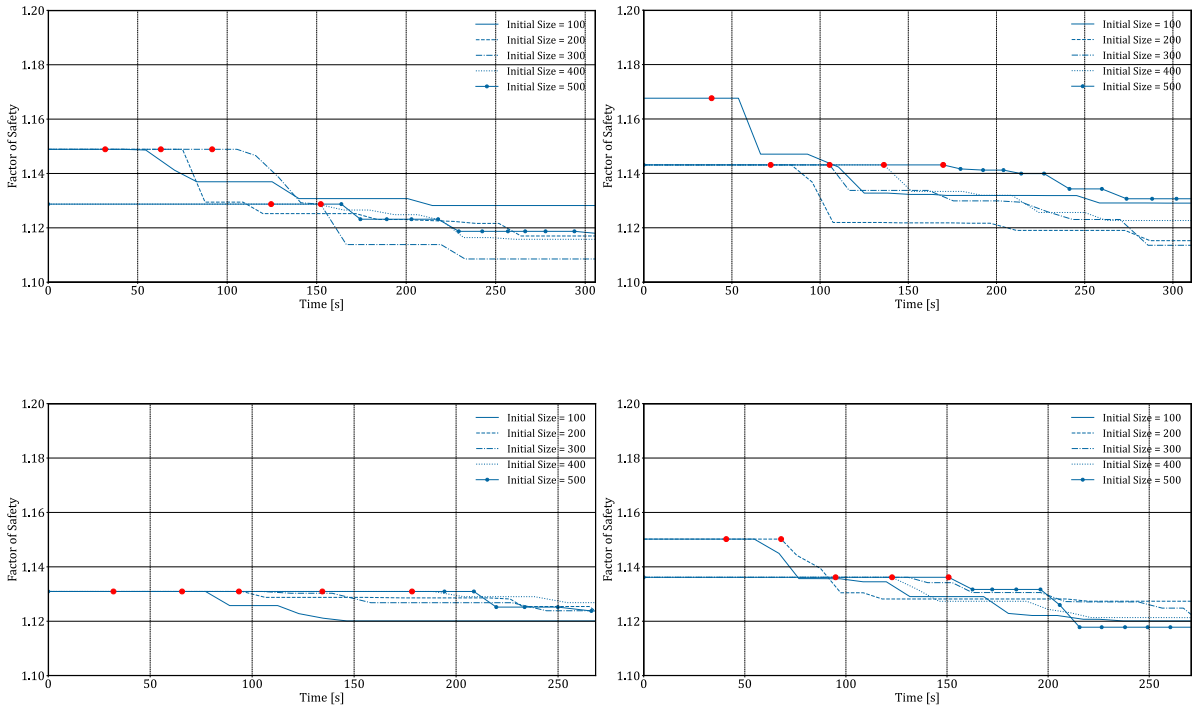

Figure B.1: Sensitivity of Initial Population Size

B.2. Selection Size

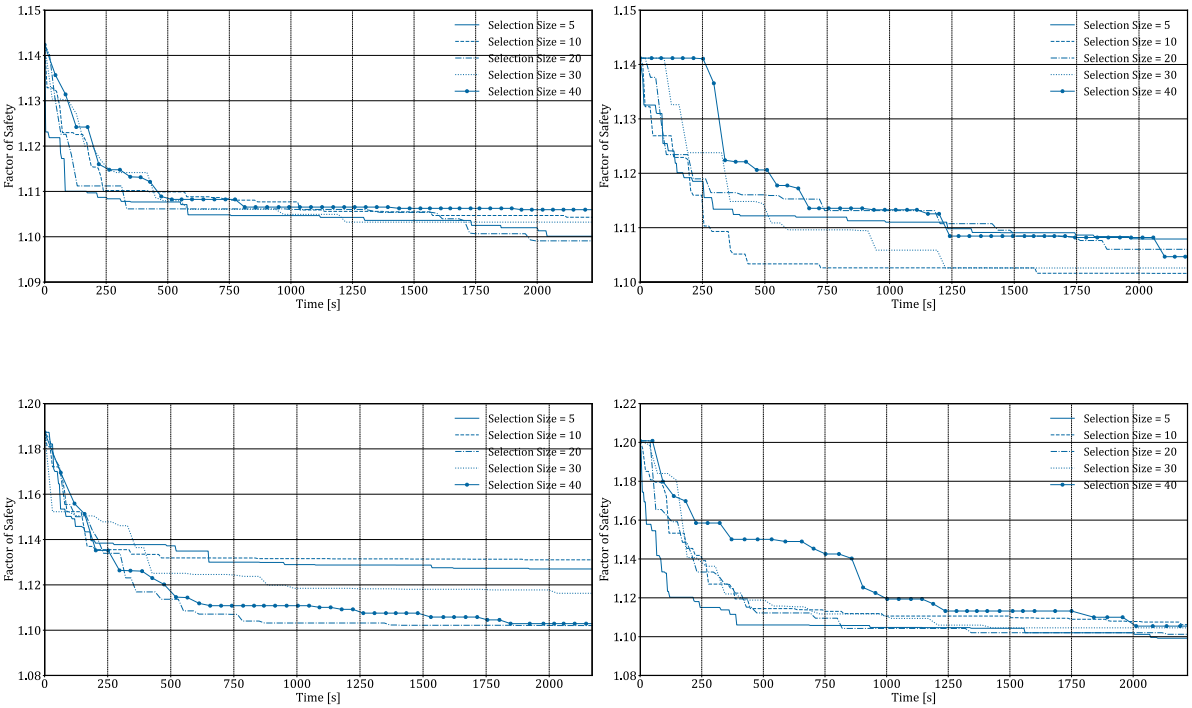

Figure B.2: Sensitivity of Selection Size